Tesi Doctoral

Transitions at the mesoscale: morphological changes in thin solid films and magnetic filaments

Tesi presentada per Pedro A. Sánchez al Departament de Física de la Universitat de les Illes Balears per optar al grau de Doctor en Física

Pedro A. Sánchez

Palma de Mallorca, Desembre de 2010

Transitions at the mesoscale: morphological changes in thin solid films and magnetic filaments

Pedro A. Sánchez
Instituto de Fisica Interdisciplinar y Sistemas Complejos
IFISC (UIB-CSIC)

Els directors de tesi Oreste Piro Perusín i Tomás M. Sintes Olives, Professors Titulars d'Universitat de la Universitat de les Illes Balears, certifiquen que aquesta tesi doctoral ha estat realitzada pel Sr. Pedro A. Sánchez Romero sota la seva direcció a l'Institut de Física Interdisciplinària i Sistemes Complexes, i per a què quedi constància escrita firmen

Oreste Piro Perusín   Tomás M. Sintes Olives

Palma de Mallorca, 2 de Desembre de 2010

a Carmen y Estrella

I checked it very thoroughly and that quite
definitely is the answer. I think the problem,
to be quite honest with you, is that you've
never actually known what the question is.

(Deep Thought computer,
The Hitchhiker's Guide to the Galaxy)

Resumen

Una de las cualidades más notables de la Física es su capacidad para estudiar la Naturaleza en un enorme rango de dimensiones y energías, que se amplía constantemente a medida que se acumulan conocimientos y progresa la tecnología. Sin embargo, todas las teorías físicas ideadas hasta el momento tienen un alcance limitado, perdiendo su sentido o todo poder predictivo más allá de determinados límites, en algunos casos muy estrechos en comparación con el vasto dominio de lo observable. En consecuencia, la aplicabilidad de las distintas teorías físicas establece dominios parciales de escala, con solapamientos más o menos amplios denominados *fronteras* que constituyen ámbitos particularmente interesantes para el estudio científico. Es decir, el avance científico y técnico no sólo permite ampliar los extremos del rango total de dimensiones y velocidades accesibles a nuestro afán de comprensión, sino que también conlleva el estudio de nuevos fenómenos físicos en las fronteras entre distintos dominios típicos definidos por teorías bien establecidas.

Salvo en excepcionales casos paradigmáticos, la "nueva física" que surge de los estudios en fronteras se ajusta a las teorías propias de los correspondientes dominios en contacto. Sin embargo, como es comprensible, lo más frecuente es que tales teorías se desarrollaran inicialmente para modelar sistemas bajo condiciones bastante alejadas de las que se dan en la frontera. Es precisamente el cambio de escala en las dimensiones y velocidades características del sistema lo que puede permitir la observación de nuevos fenómenos, al cambiar con ellas la jerarquía de las interacciones relevantes. Por otra parte, es frecuente que los estudios en la frontera requieran, más allá de las leyes fundamentales que resulten aplicables, el desarrollo de nuevas técnicas y aproximaciones para la obtención de modelos específicos con una adecuada capacidad predictiva. Este tipo de modelos para fenómenos propios de una frontera entre distintos dominios o escalas recibe la denominación genérica de *modelos de mesoescala*.

Una de las fronteras que ha recibido gran atención en las últimas décadas en el ámbito de la Física de la Materia Condensada ha sido la de los *sistemas mesoscópicos*. El adjetivo hace referencia a la frontera entre los *sistemas microscópicos*, compuestos típicamente por una pequeña cantidad de átomos, y los *sistemas macroscópicos*, constituidos por una

gran cantidad. Se trata por tanto de la frontera entre los que habitualmente se consideran dominios típicos de la Mecánica Cuántica y de la Mecánica Clásica, con dimensiones características comprendidas aproximadamente entre 10 nm y 1 mm. Los estudios en esta frontera han experimentado un crecimiento que puede calificarse como vertiginoso gracias a uno de sus principales atractivos: ofrecer un enorme potencial de desarrollo de nuevas tecnologías de alto impacto. Esta expectativa ha propiciado una gran inversión de recursos para la investigación básica y aplicada de sistemas mesoscópicos, especialmente en la escala más pequeña (típicamente nanométrica) bajo las etiquetas genéricas de *nanociencia* y *nanotecnología*. El impacto económico y social de las tecnologías que ya se han beneficiado de tales estudios, como la microelectrónica, es evidente y considerable. El de futuras tecnologías como las máquinas nanométricas, la medicina a nivel celular o en general la síntesis de materiales modelados a escala molecular puede resultar, previsiblemente, mucho más profundo. Sin embargo, el aspecto tecnológico no es el único atractivo de los sistemas mesoscópicos: tanto el hecho de ser un campo de estudio relativamente joven, con escasas áreas verdaderamente maduras, como los grandes y novedosos retos científicos que plantea hacen de esta frontera una de las más interesantes desde un punto de vista puramente intelectual y académico.

El desarrollo de modelos mesoscópicos presenta una serie de complicaciones muy específicas, dada la especial naturaleza de esta frontera, que obliga a usar estrategias y aproximaciones muy diversas dependiendo del tipo de sistema y de las propiedades que se pretendan modelar. En cualquier caso el objetivo principal es obtener una representación más o menos abstracta que recoja lo esencial de las propiedades y el comportamiento del sistema, evitando en la medida de lo posible tratar directamente los detalles microscópicos ya que, salvo en los sistemas más pequeños, éstos tienden a convertir los modelos en problemas demasiado complejos e intratables. Entre las principales estrategias se encuentran la aplicación de los métodos de la Mecánica Estadística y las aproximaciones estocásticas, la determinación de interacciones mesoscópicas efectivas generalizadas a partir de las interacciones microscópicas estudiadas en sistemas más simples a pequeña escala o, como estrategia particularmente atractiva, la búsqueda de *propiedades universales*, que son aquellas esencialmente independientes de los detalles microscópicos y que idealmente pueden presentarse en diferentes escalas. Como ejemplo paradigmático de propiedades universales cabe destacar la formación de patrones o morfologías características en multitud de sistemas físicos, tanto en condiciones de equilibrio como lejos del equilibrio, cuyas propiedades se ajustan a la geometría fractal o poseen relaciones de

escala bien definidas.

El objeto central de esta tesis es el estudio teórico de morfologías características y propiedades universales de dos sistemas mesoscópicos distintos mediante el desarrollo de modelos computacionales sencillos de tipo atomístico y su aplicación a la realización intensiva de simulaciones.

En primer lugar se estudian las morfologías surgidas de procesos de crecimiento fuera del equilibrio de *materiales en lámina delgada*, sintetizados a partir de técnicas de deposición de vapor, en el contexto de los modelos cualitativos que clasifican las distintas morfologías mesoscópicas de estos materiales, en buena medida independientes de sus propiedades microscópicas, llamados Modelos de Zonas de Estructura. El estudio se ha realizado mediante el desarrollo de un modelo estocástico que incorpora por primera vez la definición de distintas simetrías de enlace a los mecanismos fundamentales del proceso de crecimiento, permitiendo determinar los efectos de la limitación del número de coordinación máximo en las morfologías resultantes y la simulación de la imposición de determinadas simetrías por parte de la microestructura del sustrato. Los materiales en lámina delgada constituyen uno de los sistemas con propiedades mesoscópicas de gran interés tecnológico estudiados durante más tiempo y con mayor intensidad, con numerosas aplicaciones en múltiples campos de la ingeniería de materiales.

Por otra parte se caracterizan por primera vez las morfologías de equilibrio propias de un sistema mesoscópico apenas estudiado hasta el momento: los llamados *filamentos magnéticos*. Éstos consisten en ensamblajes supramoleculares formados por cadenas unidimensionales de partículas nanométricas con un momento magnético neto permanente, unidas mediante un enlace semiflexible formado por macromoléculas. Este novedoso tipo de sistemas posee un gran potencial inexplorado de aplicaciones nanotecnológicas en campos como la biofísica o la microfluídica, ya que su dinámica y sus conformaciones pueden ser controladas mediante campos magnéticos externos, presumiblemente con gran precisión, sin que éstos afecten directamente a cualquier otra sustancia no magnética presente en el sistema. En concreto, se ha definido un modelo de simulación sencillo con el que se han estudiado, mediante simulaciones de dinámica molecular, las morfologías de equilibrio y la criticalidad que presentaría un filamento magnético en las proximidades de una superficie plana adsorbente.

Abstract

One of the most striking features of Physics studying the behavior of Nature is that it covers an impressively wide range of sizes and energy scales. These ranges are continuously expanding as new knowledge is acquired and new technologies are developed. However, all the physical theories devised so far have a limited coverage, losing all its meaning or predictive power beyond certain limits which are in some cases quite narrow in front of the vast realm of the known and observable phenomena. The applicability of the different physical theories establishes partial scale domains which may overlap to different extents. The overlap regions between domains, called *frontiers*, are particularly interesting areas for scientific study. Therefore, the scientific and technical progress not only broadens the full range of lengths and speeds of physical phenomena under study, but also involves research of new physical phenomena at the frontiers between different domains defined by well-established theories.

Except for uncommon paradigmatic cases, the "new physics" arising from a frontier research can be described by the models which apply to the eventually overlapping domains. However, by definition physical theories are originally developed to model systems under conditions far from those found at the frontiers. In fact, the change in lengths and speed scales is the leading factor in the emergence of new phenomena in the frontiers, since a change in the scales may lead to a change in the hierarchy of relevant physical interactions. Moreover, frontier research frequently requires the development of new techniques and approaches in order to obtain specific models with a reasonable predictive power. Specific models for phenomena found at the frontier of different scale domains are generically called *mesoscale models*.

One of the frontiers which has attracted a wide interest in the last decades within the field of Condensed Matter Physics has been that of the *mesoscopic systems*. The adjective mesoscopic refers to the boundary between *microscopic systems*, typically composed by a small number of atoms, and *macroscopic systems*, consisting of a large amount. Therefore, it is the frontier between the typical domains of Quantum Mechanics and Classical Mechanics, with characteristic dimensions ranging from approximately 10 nm to 1 mm.

Studies in this frontier have experienced a considerable growth thanks to one of its most attractive features: it is a field with a great potential for development of new technologies with a presumably high impact. This expectation has led to a significant investment of resources in basic and applied research on mesoscopic systems, especially at the nanometric scale under the generic labels of *nanoscience* and *nanotechnology*. The economic and social impact of the first technologies which have benefited from such studies, such as microelectronics, is obvious and considerable. Potential future applications such as different types of engineered nano-machines, medicine at the cellular level or, in general, the synthesis of materials modeled at the molecular scale might produce a much deeper impact. However, the technological aspect is not the only appeal of mesoscopic systems: the fact of being a relatively new and unexplored field, with few mature studies, and the scientific challenges imposed by the specific characteristics of this frontier makes it one of the most interesting research fields from a purely intellectual and academic point of view.

The development of mesoscopic models presents specific challenges which require very different strategies and approaches depending on the considered system and the particular properties to be modeled. In practice, the main objective of any approach is to obtain a more or less abstract model able to reproduce the main properties of the system by avoiding, as far as possible, to address directly the microscopic details which tend to convert the models in too complex and intractable problems. The leading strategies include the application of Statistical Mechanics methods and different stochastic approaches, the determination of generalized effective mesoscopic interactions from microscopic interactions studied at smaller scales and, as a particularly attractive strategy, the search for *universal properties* in the system. Universal properties are defined as essentially independent of the microscopic details and observed persistently at different scales. For instance, a paradigmatic example of universal properties is the formation of patterns or morphological characteristics in many physical systems, either at equilibrium or far from equilibrium, whose properties are consistent with the fractal geometry or have well-defined scaling relations.

The main purpose of this thesis is the theoretical study of morphological characteristics and universal properties of two different mesoscopic systems by developing simple discrete computational models and performing extensive numerical simulations.

The first result to be presented is a study of the mesoscopic structures of thin solid films synthetized from non-equilibrium growth processes of physical vapor deposition. The study has been performed within the context of the qualitative models, known as

Structure Zone models, which classify the different mesoscopic morphologies of these materials. Structure Zone models are coarse classifications based on the phenomenological universality of these morphologies, which are found to be largely independent of the microscopic details. A minimal stochastic computational model has been developed for this study using a discrete —or atomistic— approach. This model, for the first time incorporates to the fundamental growth mechanisms usually found in this type of computational representations, well defined bonding symmetries for the deposited species in order to determine the effect of a limited maximum coordination on the resulting morphologies, as well as to reproduce the imposition of specific bonding symmetries by the substrate microstructure. Thin solid films are one of the systems with relevant mesoscopic properties studied for a longer time and with a greater intensity, as corresponds to a mature technology with a wide range of applications in many fields of materials engineering. However, until recent years these studies have been mainly biased toward the properties of metallic and semiconductor materials. The increasing interest for novel applications of thin films grown from very different material types has led to new modeling challenges to address.

The second part of the thesis is devoted to the first theoretical characterization of the equilibrium morphologies of a novel mesoscopic system barely studied: the so-called *magnetic filaments*. These are supramolecular assemblies consisting of one-dimensional chains of nanometric particles with a permanent magnetic moment, linked by semiflexible bonds of macromolecules. This new type of system has a great prospective potential for nanotechnology applications in fields such as biophysics and microfluidics, since its dynamics and conformations can be controlled by external magnetic fields, presumably with high accuracy, without directly affecting any other non-magnetic substance in the system. In particular, the equilibrium morphologies and the critical behavior of a single filament near an adsorbent flat surface have been studied by extensive Langevin molecular dynamics simulations with a novel minimal model.

Agradecimientos

Esta tesis es el fruto de casi cinco años de trabajo y —como en toda actividad humana no trivial— de una singular combinación de casualidades inesperadas, voluntades personales[1] y todo tipo de aciertos y errores.

El primer reconocimiento debo dedicarlo, por supuesto, a los principales responsables académicos de ese trabajo, mis directores de tesis Oreste Piro y Tomás Sintes. En particular, a Oreste Piro debo agradecerle su confianza por adoptarme como becario del proyecto HIELOCRIS, facilitándome una oportunidad única de realizar una tesis doctoral[2]. A Tomás Sintes le debo agradecer especialmente el haber soportado la principal carga diaria que supone dirigir a un estudiante atípico y con ideas propias[3].

Colaboradores indispensables en este proyecto académico han sido Julyan H. E. Cartwright y Joan J. Cerdà. Julyan ha sido uno de los artífices del proyecto HIELOCRIS y me ha brindado estímulo en numerosas ocasiones. Joan[4], además de aportar el impulso necesario que dio lugar al segundo estudio incluído en esta tesis, me ha ofecido increíbles cantidades de apoyo moral durante la última etapa.

I want to give a special thanks to Christian Holm for his support to the study of magnetic filaments and for offering me an opportunity to have a stimulating and fruitful stay abroad.

A lo largo de toda la investigación, los recursos computacionales y en general los medios materiales necesarios para su desarrollo han sido proporcionados por el IFISC. Durante los últimos tres años, el Instituto también ha facilitado la financiación de mis investigaciones mediante la actividad docente en el Departamento de Física de la UIB. Por todo ello expreso mi sincero agradecimiento al máximo responsable del Instituto,

---

[1]Tal vez aquí el término "terquedades" hubiera sido más preciso, pero suena fatal.

[2]Puede decirse que única en todos los sentidos. En particular, como única vía de realizarla sin correr el riesgo de morir de inanición o de senectud en el intento, lo cual no deja de suponer cierto aliciente para dedicar unos años de tu vida a la actividad científica.

[3]Una prudente modestia me obliga a atribuirlas principalmente a la edad y no necesariamente al talento.

[4]Alias Juanjo; alias *Sargantana Rampante*. Para una justificación este último apelativo, véase J. J. Cerdà, "Polymer depletion-driven colloids and polymer-surface interactions", PhD Thesis, Universitat de les Illes Balears, (2005), pg. X. No dispongo de evidencias experimentales al respecto.

Maxi San Miguel, y en general a todo el personal del IFISC —investigadores titulares, doctorandos, personal administrativo y personal técnico— por prestarme toda la ayuda que he podido necesitar. Evidentemente las circunstancias del trabajo diario propician establecer una más estrecha relación, colaboración o incluso dependencia con ciertas personas. En cuanto a la dependencia, ninguna tan merecedora de reconocimiento como la que todos los doctorandos del IFISC tenemos respecto a los técnicos informáticos, Rubén Tolosa, Edu Herraiz y Mª Antònia Tugores. El trabajo docente hubiera sido mucho más ingrato sin haber contado con la disposición de los profesores del departamento con los que he colaborado —entre otros, Raúl Toral, Romu Romero, María Moreno, Ángel López, Francesc Masdeu, Magdalena Gelabert y Kay Suenaga. Por otra parte, quiero destacar el agradable ambiente de trabajo y el compañerismo que he encontrado entre los auténticos obreros de la ciencia: los doctorandos. Demasiado numerosos para nombrarlos individualmente aquí, son merecedores de toda mi estima y reconocimiento.[5]

Para concluir con los agradecimientos a personas del mundo académico, debo mencionar a Salvador Bal·le como uno de los principales responsables morales de que alguien como yo se decidiera a emprender un viaje tan peculiar e inseguro —a todas las escalas— como es la realización de una tesis doctoral científica[6].

Finalmente, el mérito de esta tesis doctoral no sólo es atribuible a mi esfuerzo personal y al apoyo que he recibido en el ámbito profesional. Una buena parte de ese mérito corresponde a las personas que comparten mi vida y mis esperanzas. A ellas dedico este trabajo, sin más, pues lo que representan para mí es demasiado importante para reducirlo a palabras.

---

[5]En cuanto a mi contribución al buen ambiente entre los doctorandos, sin duda puedo presumir de que ningún habitante de las catacumbas —el conocido y apropiado hábitat natural del *doctorandus precarius*— está en condiciones de acusarme de haber turbado excesivamente la paz y el recogimiento propios de un espacio dedicado al estudio y la reflexión.

[6]En concreto, este individuo es responsable de obnubilar a un alma cándida con promesas de dinero, poder y gloria como resultado garantizado de la actividad científica. A día de hoy, empiezo a albergar alguna ligera sospecha sobre la veracidad de tales promesas.

Contents

1 Physics at the mesoscale

An obliged starting reference in every talk or modern textbook devoted to nanoscience or nanotechnology is the dissertation that Richard Feynman gave at the California Institute of Technology on December 29th 1959, entitled "There is plenty of room at the bottom" [1]. In his talk, Feynman postulated the possibility of a more powerful technology for materials synthesis which could be achieved by a progressive development of techniques and control processes at increasingly smaller scales, down to the observation and manipulation of individual atoms and molecules. The manipulation at the atomic scale would open a wide range of new applications, including the assembly of custom microscopic machines which would work analogously to biosynthetic systems, such as ribosomes, for the synthesis of new materials and compounds. In particular, this technology would allow the development of medicine at the cellular or molecular scale by means of surgical and biosynthetic artificial micromachines.

Feynman's ideas were too advanced for his time and had a very limited diffusion, remaining generally ignored for the next two decades. However, the validity of his foresights began to be confirmed during those years, when the necessary key technologies were developed independently. In 1974, the still prospective processing and manipulation of individual atoms and molecules received for the first time the attractive name of *nanotechnology* [2]. The new technology became a reality and attracted a fast-growing interest after the invention of the scanning tunneling microscope (STM) in 1981 and the subsequent expansion of research on the properties of atomic clusters as a basis for the understanding of collective phenomena in bulk materials. In the early 1990s Feynman's dissertation was rediscovered and he was recognized, probably supported to some extent by his great prestige, as the intellectual forerunner of nanotechnology and its associated theoretical research field, generically called *nanoscience*.

The main Feynman's foresights were the proposed research methodology, which currently is known as the *top-down* approach, and the raise of the main challenge which any approach for studying micrometric and nanometric systems must address: as the scale of interest is reduced, the system properties may exhibit a significant variation as a con-

sequence of a change in the hierarchy of the relevant physical interactions. At submicrometric scales, some of the physical mechanisms which drive the behavior of macroscopic systems are replaced by others which usually are negligible within the macroscopic scope. Therefore, the knowledge of the general and particular leading physical mechanisms and dynamics at submicrometric scales is essential for the accurate modeling of such systems.

A distinctively noteworthy case of submicrometric systems are those with an intermediate, non-microscopic size, known as *mesoscopic systems*. The mesoscopic scale represents the frontier between the domains of Quantum and Classical Mechanics and leads to characteristic physical properties which require specific modeling approaches.

The next sections introduce a brief review on the physical properties observed generally in mesoscopic systems, as well as the basic theoretical concepts and the computer simulation methods used for the study of the mesoscopic morphological transitions presented in subsequent chapters.

1.1 New physics from a distinct hierarchy

The range of length scales characteristic of mesoscopic systems is quite wide: between 10 nm and 1 mm according to the widest definition or between 100 nm and 1 μm for the most restrictive one. The latter definition excludes the smallest systems, which are mainly dominated by quantum effects, and the largest systems, which essentialy show macroscopic properties. The leading physical properties of these systems, in general derived from their small characteristic sizes, can be summarized as follows [3]:

- Mesoscopic systems are usually formed by many atoms or molecules, although not as many as in macroscopic systems. Consequently, most of their properties can be described by Statistical Mechanics, although significant finite size effects may appear frequently in statistical descriptions. Classical Mechanics is also applicable in many mesoscopic systems. However, the statistical fluctuations tend to be more relevant and the frequencies of the mechanical oscillations are higher in mesoscopic systems than the corresponding to the macroscopic scale.

- The ratio between surface and volume is higher for mesoscopic bodies than for macroscopic ones. As a consequence, surface effects such as surface tension in liquids and surface stresses in solids tend to be very relevant in mesoscopic systems. Under equilibrium conditions, there is a significant contribution from the surface

to the system free energy. In non-equilibrium systems the surface usually has an important role in the system dynamics.

- The relevance of surface energy determines the existence of significant surface interactions, such as adsorption and adhesion forces. In some systems, the anisotropy of these sticky interactions leads to the spontaneous arrangement of the system components in defined structures, a process known as *self-assembling*.

- Due to the relatively wider surface area present in mesoscopic systems, the heat transfer is quite faster than in macroscopic systems. Moreover, temperature differences within the system tend to be smaller.

- In fluids, brownian forces driven by thermal fluctuations and viscous friction forces are highly significant. However, in some cases the system symmetries may cancel the friction forces.

- Unlike in the macroscopic case, gravity and inertial effects are essentially negligible in front of the previous effects and interactions in mesoscopic systems.

The distinctive hierarchy of classical interactions found at the mesosocopic scale leads to a very different behavior from what is observed in macroscopic systems. Of course, underlying these classical interactions, there exist the quantum properties of the system, but they are rarely treated explicitely in mesoscopic models: except in the smallest systems, formed by a small quantity of atoms, the quantum description is prohibitively complex either for direct analytical or numerical calculations of the mesoscopic properties.

The top-down approach for the study and control of increasingly smaller systems comes from a Materials Science perspective. Obviously, the mere knowledge of the general leading physical interactions at the mesoscopic scale is not enough for an adequate undestanding of certain mesoscopic features. The properties of the particular constituent materials, including the nature of the species and the type and strength of chemical bonds, might be taken into account somehow depending on the features to be studied. For instance, these properties that determine the structural phase diagram and the transition conditions in the system, which are very relevant characteristics for many technological applications [4]. This suggest an alternative modeling and control strategy, the *bottom-up* approach, in which simple molecular constituents are combined to form more complex structures with specific desirable properties. This process may continue up to the supramolecular level, with the help of eventual self-assembling effects [5]. The

bottom-up approach to supramolecular chemistry of complex nanostructures is suposed to be the best way to the assembling of nanoengineered machines and biochemical catalyzers to the extent allowed by the nanophysics, which is one of the more interesting long-term technological objectives of nanoscience [3].

However, as occurs with the top-down approach, in many cases the mesoscopic properties are very difficult to predict from a purely molecular perspective, namely, from just the atomic or molecular system constituents. This difficulty may stand even when all the microscopic physical mechanisms in the system are well known, since their interplay may be very complex. Therefore, physical or numerical experiments at the actual scale of interest are needed in order to achieve an accurate knowledge of the system properties.

Two of the most interesting system types with relevant mesoscopic properties of technological interest are the solid structures formed by microscopic non-equilibrium growth processes [6] and the systems which include biochemical componentes or some type of *soft matter*, i.e., any solid material which is easily deformed by mechanical stresses or thermal fluctuations at the temperature of interest. In particular, soft matter systems show remarkably interesting mesoscopic behaviors, with complex morphologies frequently formed by self-assembling or self-organization processes, rich dynamics with large ranges of length and time scales and complex phase diagrams [7].

1.2 Structural transitions at the mesoscale: basic theoretical concepts

The different characteristic structures present in mesoscopic systems, the thermodynamic conditions for which there exists a transition between some of these structural phases and the system behavior near to the transition conditions are essential properties with a great theoretical and technological relevance. In particular, the phase transitions found in small non-equilibrium systems [8] and in equilibrium and non-equilibrium soft matter systems [9] are remarkably interesting.

The theoretical modeling of phase behavior is a mature topic within the context of Thermodynamics and Statistical Mechanics. Since the early studies of the 19th century, the number and types of characterized phase transitions have grown considerably. In the late 1960s, a qualitative jump in the modeling of some particularly interesting types of phase transitions was achieved with the discovery of significant relations and properties met by certain system parameters near to the transition point and independently of the

specific details of the system. These ubiquitous features had become well established theories used as a paradigmatic approach for modeling structural equilibrium and non-equilibrium transition in mesoscopic systems. The essential theoretical concepts related to the contents of the remaining chapters are briefly reviewed in the next two sections, in which the equilibrium and non-equilibrium cases have been distinguished.

1.2.1 Equilibrium phase transitions

According to the Statistical Mechanics formalism, the equilibrium configuration of a many-particle system is fully defined by the probability distribution of the different accessible microscopic configurations. If the system is perfectly isolated, it forms a micro-canonical ensemble and all the configurations have the same probability. If the system is coupled with a thermal bath in order to keep its temperature constant, it is considered a canonical ensemble and, assuming that there are no long-range particle interactions in the system, the probability of the distinct accesible configurations follows a Maxwell-Boltzmann distribution [10]. Under these conditions, the system entropy is assumed to be maximized. For systems with significant long range interactions, however, it has been argued that the entropy may show a different behavior [11].

The canonical description fully defines the system equilibrium properties from the set of accessible configurations, $\{C_1, C_2, \ldots\}$, and their corresponding energies, $\{E_1, E_2, \ldots\}$. However, since very different dynamical mechanisms may lead to the same equilibrium conditions, the actual system dynamics is not determined by this modeling approach. This fact allows the determination of the system equilibrium properties from a stochastic simulation without using realistic dynamics, as long as the *detailed balance* condition prevails during the simulation: this condition imposes that the probability for a transition between two given configurations must be the same than the probability of the reversal transition, $P(C_i \rightarrow C_j) = P(C_j \rightarrow C_i)$.

Among the different types of phase transitions found under equilibrium conditions, *continuous phase transitions* are particularly relevant in mesoscopic systems. These transitions have no associated latent heat at the transition point but show instead an associated divergence in some thermodynamic response functions, such as the specific heat, in the macroscopic size limit, i.e., when the system size tends to be infinitely large. However, in a mesoscopic system finite-size effects are likely to be significant. Whenever that is the case, the response functions show just a finite and system-size dependent maximum at the transition point.

Usually, a continuous transition also implies a change in the system morphology, i.e., in the structural arrangement of the constituent particles. In many cases, the two structural phases involved in the transition have a different degree of internal order, hence the transition can be characterized in the first place by defining a representative parameter of the microscopic ordering in the system, which is called *order parameter*, and therefore by studying how it evolves with the change of an adequate *control parameter*, whose variation may lead to the transition. The concept of order parameter was introduced by L. D. Landau in the late 1930s in his theory of continuous order-disorder transitions [10], but its meaning was later generalized to be some physical quantity, not neccessarily unique, which is able to distinguish between the two phases involved in the transition.

The value of the control parameter associated to the transition point, also known as *critical point* in continuous transitions, depends on the thermodynamic conditions and the specific properties of the system. In many cases, including the two systems studied in this work, the transitions are induced by thermal energy variations. Using the previously introduced terms, the system temperature T, is the control parameter of these transitions. Consequently, the term *critical temperature T_c*, will be used in following chapters to refer the critical point of a structural continuous transition led by thermal energy variations.

Since the order parameter in a structural transition is usually related to the system configurational energy, their statistical fluctuations can be taken as an estimation of the associated specific heat. Therefore, the critical temperature of the transition can be identified from a divergence in the statistical fluctuations of the order parameter, or can be calculated from the asymptotic behavior of the finite maxima found in the fluctuations of small, non-macroscopic systems.

Besides the relation between the transition point and the fluctuations of the order parameter, the processes and properties related to the behavior of a system near to a critical point are known in general as *critical phenomena* [12,13]. Among such phenomena, there exist remarkable properties which do not depend on the system details, including power-law divergences and scaling relations. A power-law function, $f(x) = A x^\alpha$, has by definition the property of *scale invariance*: any rescaling of the argument simply introduces a proportional factor in the original function, $f(kx) = A k^\alpha f(x) \propto f(x)$. Therefore, any power-law function is essentially defined by its exponent. Moreover, power-law functions with the same exponent have a mathematical equivalence relation, belonging to the same *equivalence class*.

In equilibrium critical phenomena, the exponents of the power-law relations shown

by different quantities of interest near to the critical point are called *critical exponents*. In fact, strict power-law functions only apply ideally at the critical point, whereas correction terms become significant as the control parameter moves apart from the critical point. Hence, parameters with a critical behavior are represented by a function like

$$f(\epsilon) = A \, \epsilon^x \, (1 + B \, \epsilon^y + \dots), \tag{1.1}$$

where all the exponents are positive and, taking the temperature as the control parameter and $\epsilon = (T - T_c)/T_c$ the relative distance of the control parameter value to its critical value. Just in the limit $T \to T_c$, the function becomes a simple power-law $f(\epsilon \to 0) \sim \epsilon^x$.

Power-law scale invariance is related to different physical properties found at the critical point. For instance, the spatial correlation length of the order parameter tends to the value of the system size, since continuous phase transition occur without phase coexistence. Scale invariance is also associated to spatial structures with a fractal or self-affine geometry. But undoubtedly the most striking property of critical scale invariance is that it only depends on the system dimensionality and symmetries, and not on its microscopic details. This feature leads to the same critical behavior, represented by their critical exponents, in very different and apparently unrelated physical systems, a phenomenon known as *universality*. Moreover, the critical exponents found for different parameters in a system are not independent but satisfy certain mathematical relations and can only take a limited number of distinct values. Thus they define a limited number of distinct equivalence classes, or *universality classes*, found in critical phenomena. The experimental observation of these features inspired L. Kadanoff to introduce the concept of universality in the 1960s. Ever since, the searching for universal behavior is a paradigm of Statistical Mechanics.

1.2.2 Non-equilibrium phase transitions

Any system open to external currents, for instance of energy or matter, does not meet the detailed balance condition and is by definition out of equilibrium, even if it exhibits a stationary state.

Most systems in Nature are subjected to non-equilibrium conditions. However, non-equilibrium thermodynamics is quite more complex than its equilibrium counterpart: for instance, in non-equilibrium systems some relevant thermodynamic quantities, such as the entropy, are difficult to define whereas an extra degree of freedom, the time, is generally relevant [14]. Whenever the system is not too far from the equilibrium

conditions, equilibrium thermodynamics is applied as an approximation. Otherwise, far from equilibrium conditions require alternative approaches which, for many cases, are not yet fully understood or successfully developed, especially in non-stationary regimes.

Far-from-equilibrium phase transitions are a type of non-equilibrium phenomena which remains poorly understood despite the existence of many systems with such behavior, as for example the morphology transitions found in non-equilibrium growing surfaces [15]. The properties of scaling and universality, studied originally in equilibrium critical phenomena, are found also in non-equilibrium phase transitions and are applied as a leading characterization approach. However, non-equilibrium critical phenomena is generally expected to exhibit a higher diversity of universality classes due to the role of time and the symmetries of the evolution dynamics. Besides the non-equilibrium growth of surfaces, most experimental studies on these systems have been limited to phenomenological observations, in contrast with the many and exhaustive experimental studies performed on equilibrium criticality. In practice, controlled empirical observations of non-equilibrium phase transitions are much more difficult to perform. The main difference with respect to the equilibrium case is that the non-equilibrium phases involved in the transition are a result of *distinct dynamical processes*. Sometimes these processes may need an asymptotically infinite time to manifest their true nature, especially in systems with very different time scales in their dynamics. Moreover, in some cases there do not exists physical mechanisms for obtain a direct transition from one phase to the other by simply changing a control parameter. Some paradigmatic theoretical models showing well defined non-equilibrium phase transitions have been developed and extensively studied by analytical approaches and computer simulations [16, 17]. However, experimental realizations of some of these models are still very scarce or even inexistent [17,18].

1.3 Computer simulation methods

Nowadays, computer simulation methods are an essential tool for the study of condensed matter systems in general and particularly of mesoscopic systems. Undoubtedly, no other tool of Science has been experienced a faster and most awesome expansion than computers, considered as generically programmable machines able to perform different intensive calculations, and their application to scientific theoretical modeling. The fact is particularly impressive by noting that the first programmable computers were created less than a century ago, in the 1930s, as a war effort, and only became widely available

for scientific research in the 1950s.

Initially, computers were used by the allied armies during the World War II in crypto-analytical tasks. At the end of the war, the first computer simulations of a physical model of neutron penetration in materials were performed using a stochastic method to support the development of the first nuclear weapons. In the 1950s, the first non-military applications consisted on the simulation of physical properties of liquids [19] and crystals [20]. The current two main types of simulation methods for multi-particle systems, known generically as *Molecular Dynamics* and *Monte Carlo* methods, were developed in those early studies.

Progressively, computer simulations have become one of the three pillars of scientific research, together with mathematical modeling and experimentation. In many cases, computer simulations connect the idealizations and simplifications adopted in mathematical models, for the shake of obtaining closed-form and mathematically elegant solutions, with the instrinsic inaccuracies and the often complex results of experimental observations. Thus, computer simulations support the physical interpretation of the experimental data and the refutation of theoretical models by avoiding some of the simplifications introduced in the mathematical modeling without including all the complexity underlying an experimental system. Moreover, computer simulations are not limited to the fast and efficient performance of intensive numerical calculations, in fact they are intended to be a virtual realization of an actual physical experiment, i.e., they try to reproduce the properties of the physical system within an adequate range of accuracy.

Another characteristic contributing to the expansion of scientific computer simulations is their affordable cost and low consumption of time and resources, especially when compared to the requeriments of many physical experimental approaches. This is favored by the continuously increasing ratio of computing power over costs. For this reason, computer simulations are used for the forecasting of physical properties under experimental conditions difficult to achieve or even for exploring the behavior of not yet synthesized materials.

Computer experiments also favor the study of the fundamental mechanisms involved in new physical phenomena, which may be neither easily derived from the system properties nor accesible to direct experimental observation. These difficulties are especially likely to be found in mesoscopic systems. The development of minimal computational models for the exploration of the essential mechanisms needed to reproduce the studied phenomena has become an invaluable tool for the development and testing of mesoscopic theoretical

models.

A wide variety of simulation techniques have been developed along the years to be applied to systems with very different time and length scales of interest. Figure 1.1 provides a simple perspective of the distinct simulation methods and their scales of application. Within the ranges corresponding to mesoscopic systems, the most widely used simulation techniques are classical coarse-grained varieties of Molecular Dynamics and Monte Carlo methods.

1.3.1 Molecular dynamics for mesoscopic systems

Molecular Dynamics (MD) was developed at the end of the 1950s as a simulation technique for classical multi-particle systems [21–25]. It consists on a simulation during a period of time of the actual dynamics of the system constituents, typically atoms or molecules, when subjected to approximations of known classical physics interactions [26]. MD deals with atomistic positions and velocities by applying Classical Mechanics according to some atomistic two-body or many-body interaction potential. The applied potentials may be defined from quantum approximations and simulations or from experimental measures. Simple molecular interaction models, such as the well known Lennard-Jones
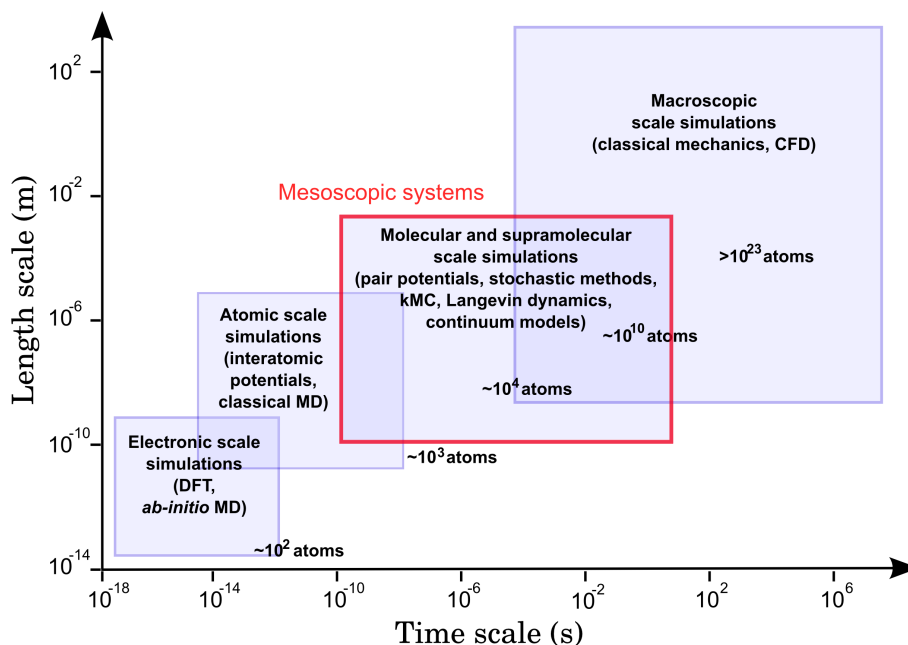

Figure 1.1: Main modeling approaches used at different time and length scales.

potential [27], are widely used in mesoscopic systems and coarse-grained approaches in general.

In many cases MD simulations are performed in the *canonical ensemble*, with fixed values for the number of particles N, the volume V, and the system temperature T [28]. In such cases, since the temperature is defined from the average of the kinetic energies of all system particles, $\langle mv^2/2 \rangle = k_B T/2$, equations of motion must be modified according to a given *thermostat* in order to ensure that the dynamics remains compatible with the fixed system temperature. Different thermostats —such as the Nosé-Hoover, Berendsen and Langevin thermostats [28,29]— are available to approximate the canonical ensemble.

The determination from MD simulations of equilibrium properties led by the statistical behavior of the system, such as energy, heat capacity, etc., requires long simulation times and/or many independent realizations with distinct initial conditions in order to obtain enough statistics for an accurate time and/or realization averaging. In practice, average equilibrium properties are more easily obtained from multiple well equilibrated realizations than from long-run time averages, since the system can exhibit some kind of ergodicity breaking due to very slow dynamics.

Another characteristic which must be taken into account when studying mesoscopic systems is that MD simulations tend to be very demanding in computational power, leading to practical limitations in the accessible time intervals and the quantities of atoms simulated in the system. This limitation is especially important in soft-matter mesoscopic systems which, in many cases, include a solvent —typically water— as a background medium for the constituents of interest.

Non-explicit simulation of a solvent: Langevin dynamics

In order to avoid an explicit simulation of the individual atoms of a background medium with an assumed statistically homogeneous behavior, such as a chemically inert liquid solvent, the Langevin dynamics approximation, based on the Langevin thermostat [29], is widely used. This approximation is based on the stochastic representation of certain dynamical degrees of freedom in the system, specifically the corresponding to the movements of the solvent particles [29,30]. The Langevin equation for the dynamics of a point particle of mass M in a viscous solvent at temperature T is:

$$M\frac{d^2\boldsymbol{r}}{dt^2} = -\nabla U(\boldsymbol{r}) - \gamma M \frac{d\boldsymbol{r}}{dt} + R(t), \qquad (1.2)$$

where $U(\boldsymbol{r})$ is the interaction potential acting over the particle, γ is the viscous coefficient and $R(t)$ is a stochastic factor, a delta-correlated stationary Gaussian process with zero mean $\langle R(t) \rangle = 0$. That expression is deduced from classic theories of Brownian motion, which established that molecular random collisions produce a systematic effect on average, leading to fluctuations at thermal equilibrium. As a consequence, the energy of the system particles is reduced by the viscuous friction with the background fluid and increased by the background thermal fluctuations. The friction and the random forces are related according to the *fluctuation–dissipation theorem* [31]: the covariance of the random force depends on the viscuous coefficient —or collision frequency— as $\langle R(t)R(t') \rangle = 2\gamma k_B TM \, \delta(t - t')$.

Therefore, Langevin dynamics includes viscosity and brownian effects but no other interactions with solvent such as electrostatic effects or hydrophobicity. When needed, such absent interactions may be included as additional terms or taken into account in the potential. For non-point bodies, an analogous additional equation must be introduced to take into account the rotational degrees of freedom.

1.3.2 Monte Carlo methods

The Monte Carlo method (MC) was the first computer simulation technique ever designed for a programmable computer. It was created by J. von Neumann, S. Ulam and N. Metropolis to support, as noted previously, the calculations in the development of nuclear weapons at the end of World War II [32].

MC simulations are based on the iterative random sampling of some probabilistic model which acts as a stochastic representation of the system to be studied. Therefore, MC simulations require at each step the generation of random or pseudo-random numbers, a characteristic which inspired its name to Ulam and Metropolis[1] [33].

The random sampling of a probabilistic model has proven to be a useful generic approach to solve many types of problems, including integration and equation solving, global optimization or queuing theory. It has been applied in disciplines as disparate as Biology, Economics, High-energy Physics or Materials Science.

MC experiments are extensively used in the field of Condensed Matter Physics to calculate equilibrium properties. In such cases, the method works as a global optimizer for the minimization of the system free energy. The minimization is achieved by following a random walk through the system phase space, changing randomly the system config-

---

[1]As a joke, they took the name "Monte Carlo" from the famous casino located in Monaco.

uration. Since the objective of the simulation is to obtain the equilibrium configuration of the system, the phase space trajectories have not necessarily physical meaning. Therefore, equilibrium MC simulations usually do not provide any actual dynamic property of the system unless it has reached the equilibrium.

Since dynamics is a leading factor in non-equilibrium systems, the usual equilibrium MC methods are not adequate for the simulation of such systems. However, there exists a specific Monte Carlo method which can reproduce the actual dynamics of a non-equilibrium system under certain conditions.

Non-equilibrium Monte Carlo: the kinetic Monte Carlo method

The kinetic Monte Carlo (kMC) method is a type of Monte Carlo computer simulation algorithm. Unlike other well known Monte Carlo variants, such as the Metropolis algorithm [19], the kMC method is intended to simulate the actual time evolution of the system. It was independently developed with slight variations by distinct authors from different disciplines in the 1960–1970s [34–37]. The method received many names before its current widely accepted denomination[2]: residence-time algorithm, "n"-fold way, Bortz-Kalos-Liebowitz (BKL) algorithm, dynamic Monte Carlo method or Gillespie algorithm.

The method requires as a starting point a list with the rates of all the relevant dynamic processes which potentially may occur in the initial configuration of the system. The determination of these relevant dynamic processes and their rates is not provided by the kMC method, it must be performed by independent means. At each iteration, one process is randomly selected from the list to be actually carried out, according to a probability distribution over all the processes given by their relative rates. The dynamic time is then increased in a stochastic time step given by the total sum of process rates. Schematically, the algorithm is as follows:

1. Determine the list of the N dynamical events which are relevant to the current system configuration and calculate their rates: $\{R_1, \ldots, R_N\}$.

2. Assign at each event in the list a probability to be selected, $\{P_1, \ldots, P_N\}$, given by its relative rate with respect to the total sum of event rates:

$$P_i = \frac{R_i}{\sum_{i=1}^{N} R_i}. \tag{1.3}$$

---

[2]The name kinetic Monte Carlo has been persistently and widely used among physicists since the 1990s.

Accordingly to that assignation, select randomly one of the events. The probability assignation and the consequent selection can be performed by simply generating a flat random number $r \in (0, 1]$ and taking the event k which satisfies

$$\frac{\sum_{i=1}^{k-1} R_i}{\sum_{i=1}^{N} R_i} < r \leq \frac{\sum_{i=1}^{k} R_i}{\sum_{i=1}^{N} R_i}.$$ (1.4)

3. Increase the dynamic time in an interval given by the total sum of event rates: $\delta t \sim 1/ \sum_{i=1}^{N} R_i$. In order to stress the stochastic nature of the transition, the usual procedure is to calculate another flat random number $r' \in (0, 1]$ and take

$$\delta t = -\frac{\ln r'}{\sum_{i=1}^{N} R_i}.$$ (1.5)

4. Carry out the selected event and determine the new system configuration.

5. Return to the first step.

The main advantage of the kMC method is that it gives the actual time scale and dynamical evolution of the system provided that the dynamical processes are Poisson type, i.e., they are independent and continuous in time. Even it can be used to simulate systems under thermodynamic equilibrium by imposing the detailed balance condition, which implies that each dynamical process has the same probability as its reverse, the kMC method is mainly applied to the simulation of systems out of equilibrium. The method is particularly efficient for simulating the evolution of systems driven by processes with very different time scales [38]. Its main disadvantage is that real systems do not always fit the necessary conditions to apply the method: for instance, in some cases the rates of the dynamical processes are not well-defined or can be difficult to calculate with enough accuracy.

Compared to other Monte Carlo methods, the kMC algorithm guarantees an effective transition at each iteration, but it presents particular implementation issues. For instance, it is essentially a sequential method which gets little or no benefit from parallelization. More importantly, an optimized kMC algorithm can be very hard to implement for systems with a long list of events: in such cases, the process selection at every iteration and the events list update after carrying out the selected process become the main computational bottlenecks. In fact, the calculations associated to these particular steps can be reduced to a problem of computational search. Two methods commonly used to optimize

the search and update of events are the simple binning of the events list by grouping the processes with the same rate [39], assuming that at any time there is a small number of different rate values [38, 40], and the grouping of events in more complex data structures designed for fast searches, such as binary trees [41].

The method has been extensively applied to simulate the characteristic structures arising from non-equilibrium growth processes. In particular, it is the current method of choice for the simulation with minimal atomistic models of the mesoscopic morphologies of thin solid films.

2 Thin solid films

Thin solid films are layers of material with a thickness ranging from fractions of a nanometer to several micrometres, created by individual deposition of atoms, molecules or ions on a substrate. They exhibit unique properties that cannot be observed in bulk materials, such as characteristic morphologies controlled at the nanometric scale and quantum size effects, characterized by the thickness, crystalline orientation and multilayer aspects. The fabrication of thin solid films is currently a well-established materials technology, with more than 50 years of application in industrial fabrication of electronic devices.

From a general perspective, the main current research efforts are focused on the challenging task of incorporating theory and modelling techniques as standard approaches to the study and control of thin film growth. These efforts have driven thin film science to grow into a major research field, requiring knowledge in areas of physics, chemistry, engineering and, in some cases, biology. The study of thin films is by nature highly interdisciplinary and has been one of the unifying themes in the development of the materials science and an essential field in new research areas like surface science and engineering [42].

Thin film processing technologies have gone through a thorough development and innovation during many years, allowing an increasing control over thin film structures and properties.The idea of coating a bulk material with a thin layer of another solid substance in order to improve some of its properties has been used as an empirical technology since the ancient metal ages, when the Egyptians developed for the first time the art of gold beating and gilding [43]. The exceptional malleability of this metal, its chemical resistance to corrosion and its aesthetic attractiveness resulted in the development of physical methods to process it in extremely thin leaves for gilding objects with protective and decorative purposes. Ancient cultures also developed gold coating methods involving not just a physical process but also chemical reactions. For many centuries craftmen explored by experimentation how the processing conditions are related to the optical, mechanical and chemical properties of film coatings.

At the end of the 19th century, scientists became interested in the unexpected deposits

with unusual properties found on the walls of glass discharge tubes [44], developed after the pioneering experiments of William R. Grove [45] and Michael Faraday [46]. This observation was the origin of subsequent new thin film fabrication techniques based on the growth of films by deposition of materials from the vapor phase, with application to fabrication of mirrors and protective coatings. The study of thin films became a formal science field within the context of the Surface Science and Technologies [42] in the 20th century, with the development and increasing availability of the vacuum technology, which provides a highly controlled environment for the growth process, and the high resolution transmission electron microscopy (TEM), which allowed the first direct observations of film structures and its characterization at the nanometric scale [47].

The expansion of the field and its applications have been quite spectacular in the last decades: the techniques of deposition from vapor phases produced by physical means in a vacuum environment, known as physical vapor deposition methods (PVD), experienced a significant developement in the 1940s and the same happened with the techniques of epitaxial growth, the formation of films with the same crystalline structure than the substrate, in the next decade.

In the 1960s appeared the ultrahigh vacuum technique and different surface analytical methods were widely available, such as the low energy electron diffraction (LEED), the scanning electron microscopy (SEM) or the Auger electron spectroscopy (AES). In these years thin film technology began to be applied to the fabrication of high speed switching transistors, leading to the microelectronics revolution, and the first Structure Zone Model from Movchan and Demchishin [48] summarized qualitatively the ubiquitous morphologies found in thin films grown by physical vapor deposition regardless of the material used.

In the 1970s the first well developed vapor deposition techniques involving chemical reactions, called chemical vapor deposition methods (CVD), and the method of fabrication of very perfect monocrystals by deposition at very low rates, known as molecular beam epitaxy (MBE), were introduced. On the theoretical level, Thornton [49,50] generalized the Movchan-Demchishin model to the new morphology zones produced by recent deposition techniques and the first atomistic computer simulation models for thin film growth were developed [51–53].

Since the 1980s, there has been a continuous expansion of industrial applications of thin film technology beyond the revolutionary field of microelectronics and their traditional protective and decorative uses, especially for the fabrication of many types

of devices which benefit from the structural control to the nanometric scale: for instance, optic and optoelectronic devices, magnetic recording systems and antennas, microelectromechanical devices, biomaterials, batteries and solar cells [43, 54–57].

Technological advances have led to the creation of more and better characterization and measurement techniques, with a resolution up to atomic scale, such as the scanning tunneling microscopy (STM) or the atomic force microscopy (AFM). In addition, further refinements to the previous structure zone models have been introduced [58–61] and the non-equilibrium critical behavior shown by their growing surface has attracted an enormous academic interest, with literally thousands of publications about the topic, since this is one of the few known experimental systems that exhibits phase transitions far from equilibrium [6, 62].

The improvements in thin film technology are also leading to the introduction of new thin film materials and applications. For many years, the main technological interest has been focused on the microelectronics industry, which requires the processing of very perfect crystalline thin films of metallic or semiconductor materials. However, in recent years the interest for applications of non-crystalline and/or non-metallic materials has grown quickly. For instance, there is a great interest in the development of amorphous solar cells as a cheaper alternative to the former crystalline designs. Processing of porous polymer thin films is currently being developed for many industrial applications, such as tissue engineering and drug delivery, novel integrated circuit designs or catalysis systems [63]. These novel thin film materials require new processing and measurement techniques, as well as new theoretical models which do not rely on the simpler properties of crystalline metallic films. With this purpose, new X-ray analytical tools for the measurement of thin films porosity, such as the small-angle X-ray scattering method with granzing-incidence geometry (GISAXS), were introduced [64]. In the field of theoretical modeling, however, there has been little progress towards the incorporation of the necessary ingredients required by these new and more complex systems, especially in the case of mesoscopic minimal models. In particular, discrete minimal models are an extensively applied tool for studying the fundamental mechanisms producing the properties of technological interest, such as the distinct surface and inner thin film mesoscopic morphologies. Consequently, a thorough study of these models is an obvious approach to the discovery and understanding of novel leading mechanisms in thin film growth.

The next sections in this Chapter review the current main preparation methods, the physical mechanisms involved, the universal properties and the modeling approaches

applied to thin solid films growth. They are intended to provide a general perspective on the current knowledge on thin films growth, including the main concepts related to the study presented in Chapter 3.

2.1 Preparation methods

Modern thin film deposition processes involve three common basic steps: the production of the appropriate individual atomic, molecular or ionic species from a material source, the transport of these species to the substrate through a medium and its condensation on the substrate, either directly or via a chemical and/or electrochemical reaction, in order to form a solid deposit. The way these steps are implemented distinguises the wide variety of existent deposition processes and technologies.

The most elementary classification of thin film deposition techniques is based on the different methods used to produce the isolated particles from the source material. These methods can be purely physical, like the thermal evaporation of the source material or its irradiation with energetic species or photons in order to obtain the vapor phase, in which case the method is classified as a physical vapor deposition (PVD), or purely chemical, such as the reaction and/or decomposition of volatile precursors on the substrate, which corresponds to chemical vapor deposition methods (CVD). In order to achieve a more accurate control and tailoring of the microstructure and properties of thin films, a considerable effort is currently devoted to the development of novel hybrid experimental methods based on a combination of different pure processes and advanced deposition techniques.

In order to provide a fundamental background on thin film experimental growth processes, the following sections introduce the essential characteristics of the most basic preparation methods, with a focus on physical vapor deposition and a brief review of other methods.

2.1.1 Physical vapor deposition methods

Physical vapor deposition is a technique whereby a physical processes, such as thermal evaporation or sublimation, ionic impingement, arc-based emission or photonic ablation of a target of source material, produces a gas of atoms or molecules which is transferred onto a substrate for its condensation to form a solid film [65]. The vaporization of the source material and its deposition onto the substrate is achieved inside a deposition

chamber with a controlled atmosphere. Usually high or ultra-high vacuum conditions are required. The chamber medium can be also a low pressure inert gas, or a reactive gas when films of compound substances, like oxides or nitrides, are desired.

Another important deposition condition which must be accurately controlled during growth is the film temperature, since it strongly affects the resulting film properties. Experimentally, the film temperature is usually controlled by setting the temperature of the deposition substrate: if the thickness of the film is very much smaller than the substrate dimensions, it can be assumed that the latter acts as a heath bath on the former and both have practically the same temperature at all time.

The two most widely used PVD processes are the thermal evaporation and the high energy ion bombardment of the source material, a technique also known as *sputtering*. These vaporization techniques of the source material provide the basis for many different advanced deposition methods.

Thermal evaporation: molecular beam epitaxy

In evaporation PVD processes, thermal energy is supplied to a source material inside a deposition chamber. The evaporated atoms or molecules travel through the medium of the chamber and condense on the surface of a solid substrate which is typically a few centimeters in size and is thermally stabilized.

An important example of an evaporative method is the film growth technique known as *molecular beam epitaxy* (MBE) [54, 57]. MBE is essentially a two-step process carried out under ultra-high vacuum conditions. In the first step, atoms or molecules are thermally evaporated from solid sources, collimated into beams and directed toward a crystalline substrate. The transport within these beams is a molecular flow without physical or chemical interactions between the traveling particles, which follow straight trajectories to the substrate. This deposition regime is known as *ballistic deposition*. The second step of MBE is the spontaneous migration of the deposited particles, or *adatoms*, over the substrate and the film surface prior to their final incorporation to a stable position within the growing structure[1]. Under a MBE growth regime, deposition rates are kept very low in order to maintain the ballistic deposition regime and led to the *epitaxial growth* of the film. The term epitaxy refers to the imposition of a structural orientation on the particle arrangements in each layer of the growing film by the crystalline structure of the underlying substrate, which acts as a seed crystal. This concept will be further reviewed

---

[1]Adatom mobility mechanisms will be reviewed in detail in Section 2.2.2.

in Section 2.2.4. MBE is conceptually the simplest epitaxial process from an atomistic point of view: in principle, the ballistic deposition process leads to a spatially disordered incorporation of new adatoms onto the film surface, but mobility processes tend to dispose it into layers which are parallel and have the same crystallographic configuration as the substrate surface plane. This method is extensively used by the semiconductor device industry for the fabrication of highly perfect monocrystalline films.

Excluding the fabrication of microelectronic devices, most applications of thin films do not require perfect monocrystalline structures. For instance, porous, polycrystalline or amorphous films are acceptable or even preferable for optical, protective or decorative applications. In general, these types of morphologies are obtained under low or moderate adatom mobility conditions.

Sputtering

Sputter-based deposition processes [56, 65] differ fundamentally from other physical and chemical processes in the kinetics of the particle emission from the source material. In thermal evaporation, for example, energy is supplied to the source material to increase its temperature beyond the melting point under conditions of thermodynamic equilibrium. The sputtering process instead consists on the extraction of atoms or molecules from the surface of the source material by the impact of high energetic particles, usually ions of an inert gas but neutral atoms, molecules or high energy photons are also used. When the bombarding energy exceeds a critical value, known as *sputtering threshold*, which depends on the system conditions, some particles of the target may receive enough energy from the impacts to overcome the surface binding energy and may be emitted, becoming *sputtered particles* which travel to the deposition substrate to condense and form the film. Sputtered particles have also more energy than particles obtained from thermal evaporation or chemical processes. Hence, sputtering deposition is a quenched, or high energy, non-equilibrium process which allows the growth of films under unique deposition conditions. The sputtering process, for instance, achieves the deposition of a variety of species without heating the source materials. Moreover, the high energy of sputtered particles allows the synthesis of exotic materials and reduces the formation temperature of common materials. A typical example is the fabrication of synthetic diamonds at room temperature.

Sputtering deposition has become a common manufacturing process for a wide variety of industries. First and foremost is the electronics industry, which uses sputtering

technology to produce integrated circuits and magneto-optical recording media.

2.1.2 Other methods

Physical methods

The *pulsed laser deposition* (PLD) [66] is a method based on the photonic ablation of the source material. In this technique, a high power laser beam is focused to strike the source material and convert it to plasma. Usually, the plasma reverts to a gas before it reaches the substrate to condense on it. While other source vaporization methods are very well understood, the complex photonic ablation process is not yet completely characterized. Anyway, the great development of the laser technology experimented in the last two decades has made PLD a very competitive method for the fabrication of high quality crystalline films with very complex compositions.

The *cathodic arc deposition* (Arc-PVD) [67] is a kind of ion beam deposition where vaporization of the source material is achieved by means of an electrical arc. The arc literally blasts ions from a small area of the source material, known as cathode spot, providing an extremely high power density on it. The localized temperature at the cathode spot becomes very high and the emission of vaporized material results in a high velocity jet of multiply charged ions, neutral particles, clusters and macro-particles or droplets. The performance of the film deposition is reduced by these droplets since they are in general poorly adhered, hence macro-particle filters are commonly used for the enhancement of film quality. After its emission and filtering, ions are focused to the substrate using electric fields and, in some cases, decelerated on arriving at the substrate in order to select well-defined deposition energies, gradually reaching the regime of ion implantation. Arc-PVD is used for coating of mainly metallic substrates but can be used to coat other materials such as glass or ceramics. Its main application is the fabrication of extremely hard protective coatings.

Chemical vapor deposition methods

In CVD methods [43, 68] the film particles are originated from volatile substances, or *precursors*, which are decomposed into atoms or molecules thermally and/or by chemical reaction with other gases, vapors or liquids. The decomposition of the precursors yields to the deposition of the non volatile reaction products on the substrate. In particular, the steps involved in CVD processes are the transport of reactants to the reaction zone, its chemical reactions to produce new reactive species and by-products, the transport of

the initial reactants and their products to the substrate surface, the chemical and physical adsorption and diffusion of these species on the substrate surface, the heterogeneous reactions catalyzed by the surface leading to film formation, and the desorption and transport of the volatile reaction by-products away from the reaction zone.

Originally, simple CVD processes which do not require vacuum or high levels of electric power were developed and practiced commercially prior to PVD. Nowadays, many variants of CVD processing have been researched and developed, including atmospheric pressure (APCVD), low-pressure (LPCVD), plasma-enhanced (PECVD), and laser-enhanced (LECVD) chemical vapor deposition, giving to CVD the ability to produce a large variety of films and coatings of metals, semiconductors, and inorganic or organic compounds in either a monocrystalline, polycrystalline or vitreous forms, including the creation of films with a widely varying stoichiometry. These techniques have found applications in such diverse technologies as the fabrication of solid-state electronic devices, the manufacture of ball bearings and cutting tools, and the production of rocket engine and nuclear reactor components.

2.2 Mechanisms and kinetics in thin films grown by physical vapor deposition

The structure of thin films formed by different vapor deposition techniques is determined by a wide variety of physical mechanisms which generally can be grouped into two main steps. The first step consists of particle deposition and adsorption on the substrate and the growing film surfaces. The second step involves different mechanisms controlled by adatom transport processes and physical constrains, including nucleation, cluster growth and coalescence, interlayer migrations or lattice selection and frustration. Growth mechanisms strongly depend not just on the nature of the substrate and film materials but also on the deposition conditions, such as substrate temperature, energy of the impinging particles and deposition rates. Moreover, some physical mechanisms are competitive or become relevant for just certain stages of the growth process or under specific conditions. Distinct growth regimes emerge from this complexity, leading to very different characteristic film morphologies. In the next sections, the main physical mechanisms involved in the growth of thin films from physical vapor deposition methods are reviewed.

2.2.1 Adsorption and surface self-shadowing

The deposition process and the corresponding experimental conditions are extremely significant for the properties of thin films grown by physical vapor deposition. In particular, under ballistic depostion and limited adatom mobility conditions, the adsorption mechanisms of the impinging particles and their interplay with the surface structure are the most determining factors for the resultant film morphology.

Adsorption mechanisms

During the deposition process, vapor particles which come into contact with the substrate or the film surface can form chemical bonds with the underlying atoms or be physically adsorbed by the surface close to the contact point[2]. By assuming ideal deposition conditions[3], the film free surface can be considered an abrupt atomic interface between vapor and solid phases, with a surface potential determined by the electronic distribution of the underlying solid atomic structure.

Metallic crystals are also the most simple case of surface potential profiles and one of the most technologically relevant. Since bonding electrons in these materials are delocalized over the atomic lattice, the electronic distribution over the surface has the periodicity of the crystal lattice and leads to a potential with a well at every unoccupied lattice site over the surface, as shown in the example depicted in Figure 2.1. For materials with a highly directional bonding or non-crystalline solid structures the surface potential landscape would be more complex, for instance with a non-periodic distribution of dissimilar wells which eventually may depend on the adatom orientation.

In any case, equilibrium positions over the surface are represented by potential wells on which newcoming particles are eventually adsorbed and remain localized most of the time. Obviously, after adsorption, the local profile of the surface potential will be modified by the presence of the new adatom. This classical picture of the adsorption mechanism of individual atoms or molecules on a surface is a consequence of the quantum effect of decoherence [70]: the quantum state of the newcoming adatom experiments a continuous decoherence due to complex interactions and entanglements with the underlying surface.

---

[2]These processes are called *chemisorption* and *physisorption*, respectively.
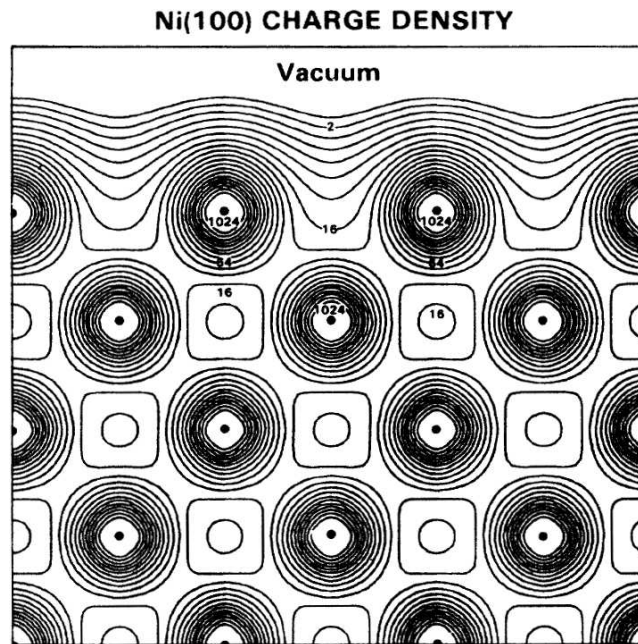[3]Particularly, in the absence of surface impurities.

Figure 2.1: Self-consistent local-orbital calculation of the electronic charge density of a Nickel crystal surface in the (100) plane, after [69].

Deposition trajectories and surface self-shadowing

A key effect in thin films growth related to the deposition and adsorption mechanisms is the *surface self-shadowing effect*. In particular, this is a dominant effect on film morphologies obtained under ballistic deposition and limited adatom mobility conditions, i.e., when the impinging particles reach the growing film by following straight trajectories and are permanently adsorbed without straying far from the first contact point with the surface. Since the first contact points are randomly distributed over the surface, the incorporation of new particles tends to be spatially inhomogeneous and a film with a rough surface is naturally obtained with high probability. The surface self-shadowing effect arises from the interplay between the straight deposition trajectories and the morphology of the growing rough surface: the existence of prominent film structures could block, or *shadow*, certain deposition trajectories to lower surface positions, as illustrated in Figure 2.2, leading to different growth rates for shadowed and non-shadowed regions. In general, when no other mechanisms compensate this effect, the inhomogeneous growth produced by the surface self-shadowing prevents the formation of fully compact and homogeneous film structures, giving rise to the growth of porous morphologies formed by nanometric grains
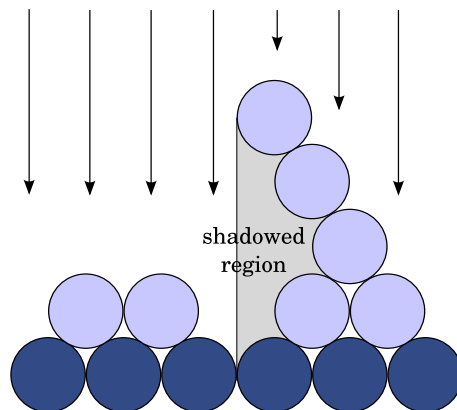
Figure 2.2: Illustration of the surface self-shadowing effect: blocking of lower regions (grey area) by prominent film structures (light disks) for a ballistic deposition process with deposition trajectories (arrows) normal to the substrate (dark disks).

separated by interstitial voids.

The global effect of surface self-shadowing strongly depends on the angle of the deposition trajectories with respect to the surface plane [71]. This is particularly evident in film processing methods where the flux of impinging particles is collimated, such as in MBE. In fact, the accurate control of the deposition angle has allowed the development of a set of processing techniques, such as the *rotating substrate* method or the *glancing angle deposition* [72], for the fabrication of films with very peculiar nanometric grain morphologies, known as *sculptured thin films* [72–74]. The most representative morphologies of sculptured thin films are formed by isolated columns engineered into different shapes, including helices, posts or chevrons [75]. Figure 2.3 shows some experimental examples of these distinctive structures.
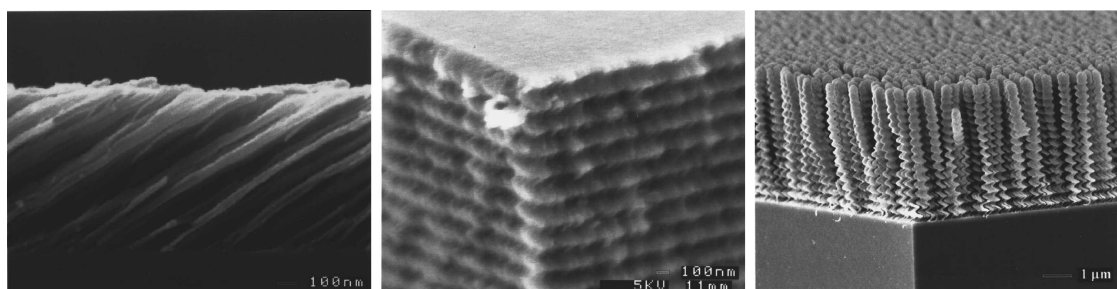
Figure 2.3: SEM micrographs with examples of different nanostructured thin solid films obtained by fixed and variable flux deposition angles. After [72].

2.2.2 Thermally activated processes: surface diffusion

As in any other solid, the atoms or molecules of a thin solid film experience oscillations around their equilibrium positions whose frequency and amplitude increases with the temperature. Added to this effect, in vapor deposition processes the impinging particles tend to have an energy excess with respect to the surface[4] and therefore adatoms would not be initially in thermal equilibrium with it. In any case, if the thermal fluctuations are large enough, a given film particle could eventually overcome the energy barrier of the equilibrium position in which resides and migrate to another unoccupied equilibrium position or even be permanently desorbed [76,77]. Depending on the growth conditions, many different particle migration mechanisms can be observed. However, the rate of these *thermally activated processes* is very much lower than the frequency of the microscopic oscillations and it can be assumed that film particles reside most of the time within an equilibrium energy well. Non-equilibrium metastable positions also can be occupied temporarily.

Whereas the localized adsorption of adatoms is explained by the decoherence of the adatom quantum state, migration processes are a consequence of the opposing quantum effect of recoherence [70]. The eventual recoherence of the adatom state leads to occasional migrations to neighboring energy wells by tunneling through the intermediate energy barriers. After the migration is achieved, decoherence again localizes the adatom destroying all information of the previous state. Provided that the time between migration events is much larger than the typical decoherence time, successive migrations are efectively uncorrelated and can be considered as classical random moves to neighboring unoccupied sites with a given probability rate.

Kinetics of thermally activated processes

In general, thermally activated processes are determinant for the experimental growth regime and the resultant film morphologies. For example, the eventual desorption of adatoms makes necessary the existence of a minimum concentration or vapor pressure of particles at the growing surface to allow a net physical or chemical adsorption and the subsequent effective growth of the film. In turn, the migration of particles between different points of the material is in fact a thermally activated *diffusion process*. It is well known that, according to Fick's Law [78], diffusion mechanisms in solids may produce

---

[4]As noted previously, this energy excess is usually larger for sputtering deposition than for thermal evaporation methods.

the migration of impurities from high to low concentration regions until the whole sample becomes homogeneous. Besides migration of impurities, diffusion processes of the leading material species tend to produce more ordered and compact film structures than the obtained with restricted diffusion conditions, as for example under very low temperatures. Consequently, the relationship between thermally activated processes and film temperature, or equivalently substrate temperature, makes the latter one of the main experimental growth parameters.
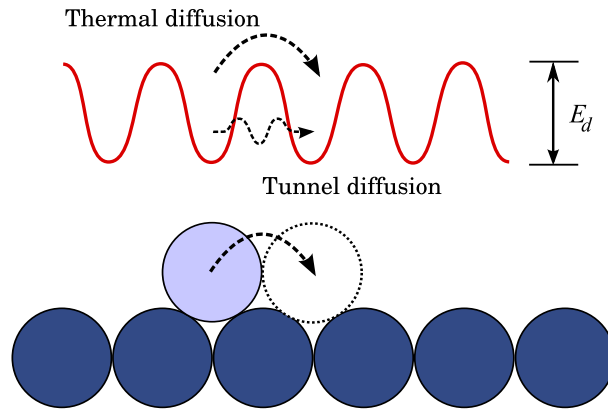
Figure 2.4: Surface energy wells led by the underlying atomic structure and corresponding energy barriers for thermally activated diffusion processes of surface adatoms.

There are very different mechanisms and activation energies associated to the wide variety of possible diffusion processes observed in thin film growth. Since the nature of the thermal fluctuations is essentially stochastic, the activation energy of a particular diffusion process represents its relative probability of actually occur during growth. Therefore, the rate of diffusion processes with a low activation energy is higher than the rate of processes with a high activation energy for any given substrate temperature. The expected rate R_d of a given process with activation energy E_d is related to the temperature by the Arrhenius expression:

$$R_d = \nu\, e^{-E_d/k_B T},\qquad(2.1)$$

where ν is an attempt frequency and $e^{-E_d/k_B T}$ is the Boltzmann thermodynamic factor. The attempt frequency ν must also depend on the temperature. For crystalline materials at low or moderate temperatures, compared to the melting point of the film material, ν is estimated to be the frequency of the microscopic oscillations. For instance, typical values of ν are of the order of 10^{13} Hz at room temperature. The activation energy of a

given diffusion process depends on the bonding strength at the origin and destination positions of the particle. This strength depends, in turn, on the nature of the material and on the *coordination number*, or number or nearest neighbors bonded to the particle at its residence position: a higher coordination number corresponds to a deeper energy well, hence to a higher barrier to overcome and a more stable position. Consequently, the net effect of diffusion processes is to favor the increase of the mean coordination number of the particles, and therefore the global compactment of the material by means of a microscopic ordering of the atomic or molecular arrangements. If the microscopic ordering led by diffusion is high enough, a fully crystalline structure is obtained. The same kinetic principles apply for diffusion in amorphous materials, but in this case the dependence with temperature of the exponential and pre-exponential factors is found to be quite more complex [79]. The activation energies are usually calculated from quantum approximations, such as the Density-Functional Theory [80]. They can also be deduced from experimental observations provided not many different types of activated processes are accesible at the same time in the system.

Surface diffusion

At low and moderate substrate temperatures the most probable diffusion processes are those corresponding to the *surface diffusion* of adatoms: the migration over the film surface is in general more likely than the bulk diffusion because surface adatoms have a lower mean coordination number than bulk particles, hence the energy barriers between equilibrium positions in the surface tend to be smaller than the ones found within the bulk region. Moreover, the eventual excess of thermal energy of the surface adatoms with respect to the bulk particles can additionally contribute to the overcoming of the migration barriers. For both reasons, the lower coordination and the eventual excess of thermal energy, surface particles have a higher mean total energy than those found in bulk.

From a thermodynamic point of view, surface diffusion is the kinetic mechanism which tends to minimize the *surface energy*, considering this quantity as the total energy excess of the surface adatoms with respect to the bulk particles. Since the surface energy is measured as a energy per unit of area, it is often identified as a surface tension which causes mechanical stresses on the solid surface [57].

Among the different mechanisms of surface diffusion, the most simple and probable under limited mobility conditions involves the migration of adatoms by means of successive short-ranged jumps, or *diffusion hops*, typically between nearest neighbor positions.

In this diffusion regime, it is assumed that adatoms follow a random walk over the surface until the temperature drops or its coordination number increases too much to allow more diffusion hops. Acconding to random walk statistics, the root mean square displacement of surface adatoms, or *diffusion length*, is

$$\sqrt{\langle \Delta \delta^2 \rangle} = a \sqrt{R_d \tau} \,, \tag{2.2}$$

where a is the space between nearest neighbor positions and τ is the mean time a given adatom is allowed to diffuse. For a constant substrate temperature, τ essentially depends on the deposition rate.

At relatively high substrate temperatures, more complex surface diffusion mechanisms become accessible. For instance, long range hops or diffusion processes which involve the exchange of positions of two adatoms can be observed [81, 82], as well as different diffusion processes of adatom aggregates or *clusters* [81]. Under these conditions bulk diffusion also becomes significant and, for substrate temperatures well above one half of the material melting point, the regime of transport of individual adatoms and clusters is replaced by the migration of vacancies [83].

Finally, among other less common diffusion mechanisms, there exists a unique type of atomic transport which not relies on thermally activated processes but on the quantum tunneling effect: the tunneling diffusion involves the transport of very light atomic species, such as hidrogen atoms, through small energy barriers in a mechanism almost independent of the temperature [84].

At this point, the most basic processes and mechanisms involved in thin film growth have been introduced. Next sections are devoted to more complex mechanisms derived from them.

2.2.3 Mechanisms at the early stages of thin film growth

The incorporation of new adatoms and its eventual migration over the surface of the substrate and of the first layers of deposited material determines the early stages of thin film growth, giving rise to different mechanisms of increasing range.

Nucleation

Nucleation is the first stage of formation of the film structure and involves the aggregation of individual adatoms in clusters of a size large enough to be thermodynamically stable. At the beginning of the film growth process, the impinging particles are adsorbed by

the substrate surface and, if the thermal energy is high enough, they diffuse over the surface. Eventually, diffusing adatoms can get in contact with other diffusing, impinging or stably adsorbed adatoms and establish a bond, forming a cluster. These small clusters, called *nuclei*, are themodynamically unstable but can also diffuse over the surface. When the deposition parameters are such that nuclei tend to collide with other adatoms before getting disagregated or desorbed, they can incorporate these adatoms and grow in size. If a growing nucleus reaches a certain critical size it becomes thermodynamically stable [85, 86].

A nucleus can grow horizontally and vertically, i.e., in parallel and perpendicular directions with respect to the substrate. The most evident mechanisms for horizontal and vertical growth are the lateral incorporation of adatoms found over the same surface layer on which the nucleus resides and the adsorption of impinging particles deposited over the nucleus surface, respectively. Depending on the materials and the growth conditions, diffusing adatoms also can climb or descend the steps formed by the lateral edges of the nucleus, contributing respectively to its perpendicular and vertical growth.

Critical nuclei can grow in number and size until a saturation nucleation density is reached, at which the mean lateral size of nuclei becomes comparable to the distance between them. The nucleation density and the average nucleus lateral size depend on different parameters such as the energy of the impinging species, the deposition rate, the activation energies of adsorption, desorption and diffusion, and the temperature, local morphology and chemical nature of the substrate. In some cases, these conditions may prevent the nuclei from reaching the necessary density to obtain a complete covering of the substrate, and may even hinder the interactions between nuclei. This growth regime, in which the substrate surface is never completely covered by the deposit, is called *submonolayer deposition*. In general, it requires the adatom surface diffusion rate, R_d, to be lower than the deposition rate, R, as well the adatom diffusion rate for escaping from the nuclei, R_n, to be insignificant in front of the latter ($R_d \geqslant R$, $R \gg R_n$) [87]. The relation between these parameters providing different film morphologies, the dynamical scaling of the nuclei mean sizes at different covering levels and its relation with the nuclei density have been the subject of numerous studies [88, 89].

Isolated stable nuclei are usually called *islands*. When nuclei remain isolated, growing without significant interactions between them, the growth regime is known as *island growth*. Islands can have porous or dense structures, with mainly flat horizontal or non-flat three-dimensional adatom arrangements. Three-dimensional islands, formed by

vertical multilayer stacks of two-dimensional islands, are frequently referred as *mounds*. Examples of film morphologies obtained under island growth regimes are shown in Figure 2.5.
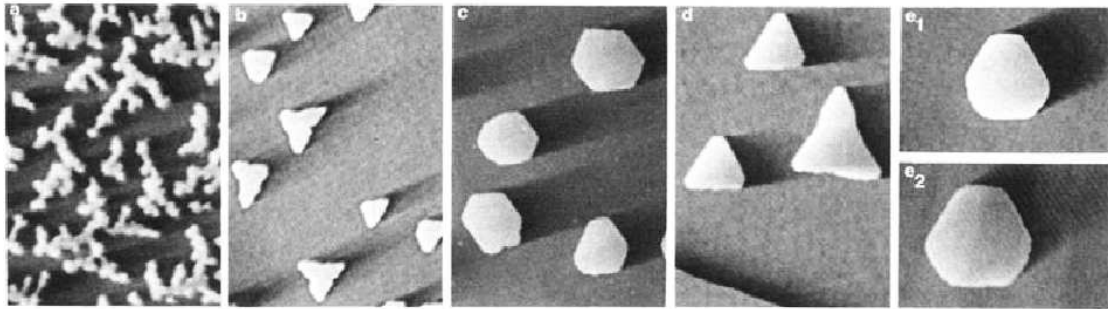

Figure 2.5: Island growth under homoepitaxial deposition of platinum at different substrate temperatures and deposition rates. After [90].

Coalescence and coarsening

If the small islands or mounds come into contact during its growth, they can form larger clusters. This general agglomeration process corresponds to the *coalescence stage* of film growth. Coalescence of nuclei reduces the surface area, hence the surface energy of the deposit, as well as the nuclei density.

Continued deposition and coalescence results in the development of a connected network of film structures with unfilled channels in between which eventually percolates across the entire substrate. With further deposition and proper adatom mobility conditions, the channels can fill in and shrink leaving isolated voids behind. Finally, even the voids can fill in completely to form a continuous film structure.

The previous sequence of growth stages occurs during the early steps of deposition, typically accounting for the first few hundred angstroms of film thickness. However, the growth can continue with a further development of the film structures formed at those early stages. For example, if the film surface is continuous, it tends to *coarse* with the increasing film thickness, reducing the surface energy. Non-continuous morphologies, such as columnar grained structures, can also evolve depending on growth conditions, as will be discussed in Section 2.2.5.

2.2.4 Interlayer barriers and epitaxy

Besides the processes found at the early stages of thin film formation, more advanced growth stages in some systems exhibit other complex mechanisms which may prevent the formation of a perfect crystalline and compact multilayer film even for growth regimes with a high diffusion mobility. These mechanisms include the existence of increased diffusion barriers at the edges of the flat layers forming crystalline film structures and the mismatch between the crystal structure of the substrate and the natural crystal lattice of the film material.

Schwoebel-Ehrlich barriers

Diffusion over flat, layered crystalline surfaces may be limited at interlayer steps by potential barriers of increased depth known as *Schwoebel-Ehrlich* (S-E) *barriers* [91,92]. These barriers can hinder adatom migration to a different layer at the edges of islands, either by passing upward or downward from one layer to another. Figure 2.6 shows a scheme of a simple microscopic interpretation of S-E barriers in a compact lattice of adatoms with non-directional bonds: diffusion over the step of a one-adatom thick layer implies for
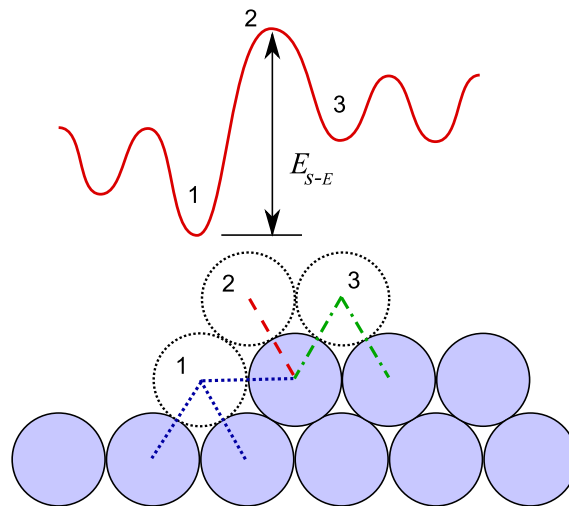
Figure 2.6: Representation of an interlayer step and the associated Schwoebel-Ehrlich barriers for interlayer diffusion processes.

the migrating particle to overpass a position wherein its coordination is minimized and its absolute distance to second nearest neighbors maximized, hence its surface energy is

higher at that transitory position than in any other stable or transitory position at the flat surface of the upper or lower layers. Remarkably, upward migration also leads to a permanent reduction of the adatom coordination with respect to the corresponding to the lower edge position. With this conditions, interlayer diffusion of adatoms at the upper or lower edges of the step is less probable than resting at the same layer by being reflected in the corresponding opposite direction.

Schwoebel-Ehrlich barriers have a strong dependence on the film material and general statements about such processes are difficult to make. In some cases, surface steps are relatively transparent to migrating adatoms, which can pass over the step in either up or down directions without attaching or being reflected at the step edge. For other materials, virtually every encounter of an adatom with the step edge results in attachment or reflection. In other cases, adatoms easily overpass the steps upwards but not downwards (Schwoebel barriers) or, conversely, only downward displacements are easily allowed (Ehrlich barriers). In any case, the presence of a significant Schwoebel-Ehrlich barrier will affect to the effective growth mode and the subsequent film morphology, leading to the appearance of instabilities on the growing surface.

Epitaxy and texture

Epitaxy is the growth of a film with the same crystalline structure than the substrate, which is usually a monocrystal [89,93,94]. There exists two main types of epitaxial growth, depending on the relation between the substrate and the deposited materials. *Homoepitaxy* refers to the growth of a over a crystalline substrate of the same material, a technique used to produce highly pure monocrystals and films with precise variations of desired impurities, such as dopants in semiconductor films. On the other hand, *heteroepitaxy* is the epitaxial growth of a film over a substrate of a different material. Heteroepitaxy is used when no monocrystalline substrates of the same material of the film can be obtained as well as when a film with alternate layers of different materials is desired. However, film structures grown with heteroepitaxial methods can produce structures with mechanical strains, speciallly when the mismatch between the substrate and the film natural lattices is high. Mechanical strains tend to relax by creating crystallographic defects or dislocations [57]. Usually these effects are highly undesired for practical applications. In order to minimize strains and defects, substrate materials with the minimum possible lattice mismatch with respect to the film material are used.

Another relevant aspect related to the crystallographic structure of thin films is the
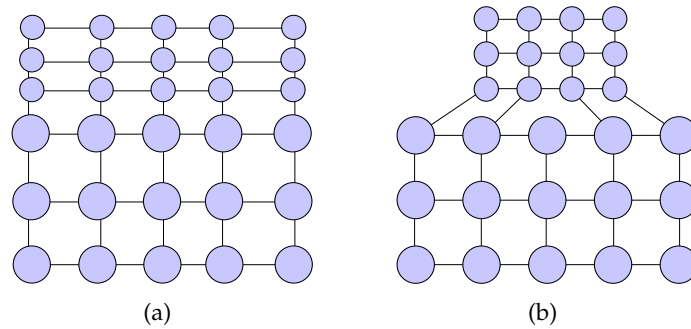
Figure 2.7: Main types of heteroepitaxy. (a) Heteroepitaxy with a strained lattice structure. (b) Heteroepitaxy with a defect relaxed structure.

formation of polycrystals and the mechanisms of *texture selection* during growth [43]. In general, the distribution of crystallographic orientations of the monocrystalline grains, or crystallites, forming a polycrystalline material is called *texture*. Except for epitaxial growth under low deposition rates and high diffusion regimes, thin films exhibit a polycrystalline or amorphous structure. The polycrystalline case involves the formation of islands at the early stages of thin film growth with different crystallographic orientations. During coalescence, these crystallographic facets and orientations are frequently preserved in the growing islands and at the interfaces between initially disoriented, coalesced particles. Finally, islands become the crystallites forming the film, often with a columnar shape. Crytallites may have a preferred orientation, forming an anisotropic texture, or have an uniform distribution of orientations corresponding to an isotropic texture. Deposition conditions are determinant for the resultant film texture, selecting different levels of anisotropy. In some cases, different growth mechanisms, including epitaxy and activated processes, lead to a competing selection of textures which may also depend on the stage of the growth process. In general, grain growth processes in thin films are quite more complex than in bulk materials.

2.2.5 Growth modes

In a previous section the most relevant physical mechanisms involved in thin film growth have been reviewed. Under the influence of such mechanisms, different growth regimes can be observed to produce diverse microscopic and mesoscopic film morphologies.

A very common categorization of microscopic growth modes for the early stages of film formation is based on general considerations on surface energy [95]. In particular,
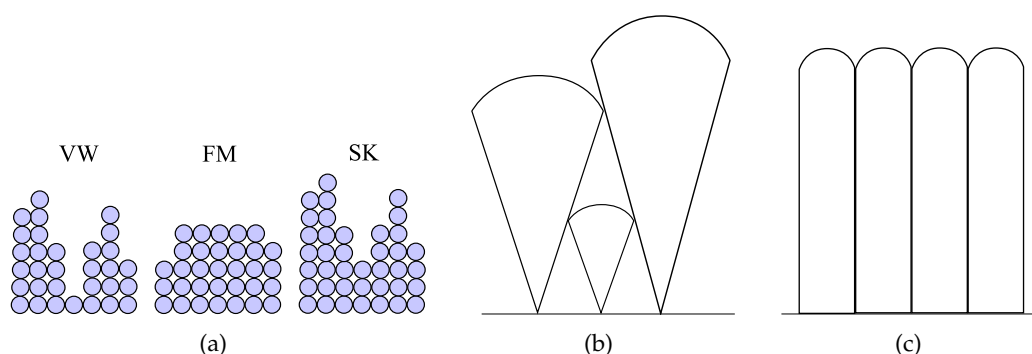
Figure 2.8: Early growth regimes of vapor-deposited thin solid films and mesoscopic structures developed at advanced growth stages. (a) The three growth regimes at the early stages of thin film formation: Volmer-Weber (VW), Frank-Van der Merwe (FM) and Stranski-Krastanov (SK). (b) Competitive columns developed under low and very low diffusion regimes. (c) Non-competitive columns obtained under high surface diffusion regimes.

it compares the propensity of deposited particles to bond to the substrate or to other surface film adatoms when a complete covering of the substrate has not been reached. Obviuously, the preference for the substrate or surface of the deposit depends on the mean surface energy of the particle at each position. When the surface energy of adatoms is lower at the substrate surface, the film grows under a flat layer-by-layer regime, called the Frank–van der Merwe (FM) growth mode, which is the desired regime when an epitaxial monocrystalline film is expected. Conversely, when the most energetically favorable bonding is made with other film surface adatoms, three-dimensional well defined islands grow until coalescence. This type of growth is commonly called the Volmer–Weber (VW) growth mode. A combination of both FM and VW modes, called Stranski–Krastanov (SK) mode, is also possible. In this case, the film material follows initially the layer-by-layer growth regime. However, after a few crystalline flat monolayers of film material are formed, subsequent deposited adatoms tend to gather into well-separated clusters instead of keeping a planar growth. The occurrence of this mode is most likely observed when the first few layers of film material are strongly strained by heteroepitaxial effects from the substrate. This regime transition and its experimental control has attracted great interest as a fabrication method of nanostructures [96]. The three early growth modes are schematized in Figure 2.8(a).

For long enough deposition processes, the growth regimes of the early stages and their governing mechanisms give way to the development of structures with characteristic morphologies at mesoscopic length scales. The selection of mesoscopic growth modes in

physical vapor deposition is mainly controlled by means of the most influential experimental deposition parameters: the substrate temperature, the deposition rate and the deposition trajectories [97]. In particular, the substrate temperature is the main experimental parameter influencing the mobility conditions of the deposited particles. At very low substrate temperatures the mesoscopic morphology is formed by amorphous competing grains with a nanometric conical shape and a rough growing surface. Figure 2.8(b) shows a schemematic representation of this type of "growth-death" structures. At moderate substrate temperatures instead, a structure of non-competing columnar grains is obtained, as shown in Figure 2.8(c). For higher substrate temperatures films are formed by more compact structures, with equiaxed crystallites or even with a fully compact structure with a smooth surface. Remarkably, each growth mode produces a characteristic morphology of the film surface. In the context of surface science, it is frequent to distinguish between *stable growth* regimes, where the shape of the surface remains essentially unchanged during growth, and *unstable growth* regimes, for which the surface experiences a significant evolution. According to this criterion, growth regimes with low and moderate diffusion lengths correspond to the unstable growth of rough or columnar surfaces [98], the latter being strongly affected by the existence and nature of Schwoebel-Ehrlich barriers. On the other hand, the high diffusion regimes which give way to smooth surfaces correspond to a stable growth.

Probably the most surprising characteristic of thin film mesoscopic morphologies grown by vapor deposition is the universality of their structural properties. Next section provides a more detailed review of the typical mesoscopic morphologies and a brief insight into their universal properties.

2.3 Universal properties: mesoscopic morphologies and surface scaling

The basic properties of thin films, such as composition, crystal phase and orientation, film thickness and, in general, film morphologies at different length scales, are determined by the deposited materials and the conditions of deposition. Consequently, the same occurs with derived characteristics of high technological interest like the optical, electrical or mechanical properties of the film. In particular, there is an enormous variety of mesoscopic morphologies of films formed by deposition from vapors. The final structures can be highly perfect monocrystals with a flat surface, polycrystalline films with equiaxed or

columnar grains or largely amorphous films with an increasingly rough surface.

The early studies of the 1960s on mesoscopic structures of thin films grown from vapor deposition showed that the same characteristic morphologies appear in most experimental cases with a main dependence on reduced deposition parameters rather than on the particularities of the film materials. The universality of these morphologies has proven to be quite robust: for instance, the columnar morphology obtained under limited diffusion conditions is persistent over six orders of magnitude in film thickness [99]. This observation inspired the development of a qualitative classification of film morphologies in what is known as a *Structure Zone model* (SZM).

A specific aspect of thin films structure, the morphology of their surface, has been intensively studied within the context of interface growth processes, using the dynamic scaling framework to characterize the kinetic roughening of the surface and a non-equilibrium phase transition between rough and columnar interfaces. In this context, the universality of the dynamical behavior of the growing film surfaces has been for many years a permanent central topic, in spite of which it still lack a fully satisfactory explanation.

2.3.1 Universal mesoscopic morphologies: Structure Zone Models

In 1969, Movchan and Demchishin combined the previous partial studies on thin film morphologies and gave rise to the first qualitative Structure Zone model [48]. The model identifies different characteristic film morphologies as a function of the substrate temperature, T, expressed as a fraction of the melting temperature of the film material, T_m. This reduced temperature, T/T_m, has a weak dependence on the nature of the film material. The model distinguished three structure zones, corresponding to the growth of films with a rough surface (Zone I), with a columnar structure (Zone II) and with a smooth surface (Zone III). In the 1970s, Thornton introduced another structure zone between Zones I and II, called transition zone or *Zone T*, which is observed in sputtering processes [49, 50, 100]. A graphical scheme of the extended SZM from Thornton is shown in Figure 2.9. In the following years, more structure zones were added to the orginal model to take into account diverse deposition parameters, and their relationships to the underlying growth mechanisms were studied: for instance, Messier identified an additional transition zone, the *Zone M*, in sputtering processes with low-energy bombardement and studied the morphology and growth mechanisms of the competing columns of Zone I [58, 101]. Other authors studied the effects of parameters such as the presence of impurities [59], the ion irradiation during deposition [102] or the biaxial deposition [61]. The current knowl-
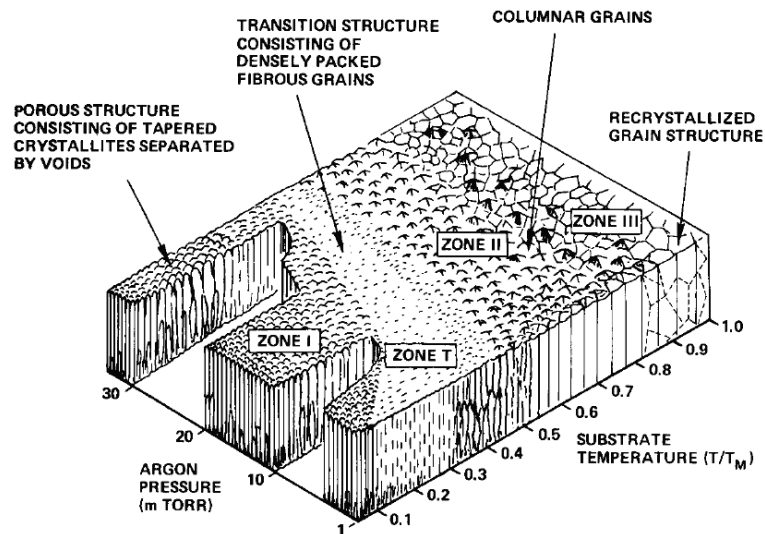
POROUS STRUCTURE
CONSISTING OF TAPERED
CRYSTALLITES SEPARATED
BY VOIDS

TRANSITION STRUCTURE
CONSISTING OF
DENSELY PACKED
FIBROUS GRAINS

COLUMNAR GRAINS

RECRYSTALLIZED
GRAIN STRUCTURE

ZONE III

ZONE II

ZONE I

ZONE T

1.0

0.9

0.8

0.7

0.6

0.5 SUBSTRATE
TEMPERATURE (T/T$_M$)

0.4

0.3

0.2

0.1

30

20

ARGON
PRESSURE
(m TORR)

10

1

Figure 2.9: Thornton's Structure Zone Model of thin solid films growth. After [100].

edge of the three main structure zones, defined in the original and simplest model from Movchan and Demchishin, can be summarized as follows:

- *Zone I:* for low substrate temperatures (typically $T/T_m < 0.2$–0.3), the diffusion length is lower than the natural lattice spacing, hence practically has insignificant effects. Under these conditions the growth is dominated by the deposition mechanisms. As a result, a porous and often amorphous film structure of competing cone-shaped grains with 10–20 nm in diameter and fractal properties is obtained. The surface is rough, with a "cauliflower-like" aspect. The surface roughness increases with the film thickness, leading to a self-simmilarity observed for up to three orders of magnitude in magnification [99, 101]. Surface roughness is a consequence of the disordered growth lead by the experimental fluctuations in deposition rates and distribution of trajectories, in the absence of the opposite ordering effect of diffusion.

- *Zone II:* at moderate substrate temperatures (0.2–$0.3 < T/T_m < 0.4$–0.5) surface diffusion is significant and leads to the formation of compact clusters or islands at the early stages of growth. The characteristic size of the clusters is of the same order of the diffusion length. Two-dimensional islands grow on top of other islands to form vertical columnar grains, usually crystalline, separated by tight boundaries. The characteristic diameter of these columns increases with the reduced temperature as

a result of the competing interplay between the random deposition and the surface diffusion. The top of crystalline columns may be faceted.

- *Zone III:* at high substrate temperatures ($T/T_m > 0.5$) the bulk diffusion becomes significant and leads to the formation of equiaxed crystallites with a size of the same order of the film thickness. The surface is smooth except for the grain insterstitial grooves. Depending on the deposition conditions, epitaxial effects and texture selection may be significant.

The specified temperature limits may increase with the deposition rate, R, and may be lower when the surface diffusion is favored by sputtering or other kinetic enhancement methods.

The technological relevance of SZM is evident, since every specific application for thin films will have a particular optimum morphology. For instance, the Zone I structures are appropiate for applications which benefit from film porosity, such as gas detectors, catalytic or light absorbing systems. On the other hand, they are inappropiate whenever a high electrical resistance, optical scatterings or electrical leakages are undesired.

As many of the modeling approaches developed for the characterization of thin films growth, the different SZM and their essentially universal nature have been mostly established from studies of metallic and metallic compound films. However, recent experimental studies suggest that this universal behavior can be found also in thin films grown from non metallic materials [103, 104], enhancing the interest of SZM as an ubiquitous description tool.

Unfortunately, the accurate application of the different SZM to experimental processes is limited by some practical difficulties. In particular, the actual zones are sometimes hard to identify experimentally because most observations are limited to the surface morphology and, from a theoretical point of view, there is not yet a defined structural parameter unambiguously used among authors to characterize the non-equilibrium transitions between zones, which tend to be quite smooth, when the properties of the whole film structure —and not just the surface— are considered. However, SZM are tools frequently referenced in theoretical and experimental studies and the universal properties they describe are relevant for most modeling approaches, particularly as a way to link models and universal experimental properties.

2.3.2 Surface roughening and dynamic scaling

The preferred approach to study the increasing roughness experienced by thin film surfaces during their growth by vapor deposition under low diffusion regimes is, since its introduction in 1985 by Family and Vicsek [105], the dynamic scaling framework. This approach assumes the existence of simple scaling relations between certain characteristic parameters of the surface that exhibit a limited set of distinct power law dependences with the system size. As pointed in Section 1.2.1, the value of a power law exponent defines a universality class to which all the power law functions with such exponent belong. In this case, the power law behavior is suposed to be determined by the dynamical mechanisms of growth. Hence, different growth processes governed by the same dynamical mechanisms are expected to show the same power law dependence with system size, belonging to a unique universality class of growth. Conversely, similar growth systems with different underlying dynamical mechanisms are expected to show strong differences in their scaling behavior. Moreover, when the approach was introduced, the number of distinct universality classes found in nature was expected to be small.

The most usual parameter for the scaling analysis of the dynamical evolution of thin film surfaces is some measure of the *interface thickness*, also called *surface width* or *surface roughness*. By definition, such parameter would characterize the distance between the highest and the lowest point in the surface and, eventually, the heights distribution. In general, surface heights are measured with respect to a plane perpendicular to the direction of growth —usually the substrate plane. Often, the interface roughness parameter, $W(L, t)$, is taken as the root mean squared deviation of the surface heights with respect to their mean value:

$$W(L, t) = \left[\frac{1}{L} \sum_i [\, h(\mathbf{r}_i,\, t) - \langle h(\mathbf{r}_i,\, t) \rangle \,]^2 \right]^{1/2}, \qquad (2.3)$$

where $h(\mathbf{r}_i,\, t)$ is the height of the surface at the point $\mathbf{r}_i$ of the reference plane in a given time t and L is the characteristic film width, i.e., the characteristic lateral size of the film. During the initial stages of film growth, $W(L, t)$ shows a power law dependence with time:

$$W(L, t) \sim t^\beta \qquad (t \ll t_x), \qquad (2.4)$$

where β is the *growth exponent*, which characterizes the time evolution of the surface roughness, and t_x is the *crossover time* or *saturation time*. After t_x, $W(L, t)$ reaches a

saturation value, $W(L)$, which depends on the system size as

$$W(L, t) \sim W(L) \sim L^\alpha \qquad (t \gg t_x),$$
(2.5)

where α is the *roughness exponent*. It characterizes the spatial correlations of the surface profile before saturation. The saturation time shows a dependence with the film width too:

$$t_x \sim L^z$$
(2.6)

where z is the *dynamic exponent*. This dependence relations with the sistem size identify the saturation of the interface thickness as a finite size effect.

According to the Family–Vicsek hypothesis, the exponents α, β and z are not independent. Since the following scaling relation is assumed

$$W(L, t) \sim L^\alpha f\left(\frac{t}{L^z}\right),$$
(2.7)

the exponents are related according to

$$z = \frac{\alpha}{\beta}.$$
(2.8)

This scaling relation allows the collapse of the $W(L, t)$ curves obtained for different system sizes when rescaled with their respective saturation values. Such collapse evidences the essential equivalence of the curves.

The finite size saturation of the surface thickness is a consequence of the existence of correlations of surface heights at different points. In particular, under low surface diffusion regimes, the height of a given adatom of the film surface tends to be similar to the heights of their close neighbors in the surface. Estimations of the lateral correlation length —parallel to the reference plane— for surface height pairs, $\xi_\parallel$, obtained from height-height correlation functions provide a measure of such similarity. This parameter shows a defined time evolution analogous to the surface thickness: before the saturation time is reached, $\xi_\parallel$ grows as

$$\xi_\parallel \sim t^{1/z} \qquad (t \ll t_x).$$
(2.9)

Therefore, the dynamic exponent characterizes the coarsening process of the rough surface morphology before saturation. The saturation time corresponds to the instant at which $\xi_\parallel$ reaches the system size and, consequently, can not grow further:

$$\xi_\parallel \sim L \qquad (t \gg t_x).$$
(2.10)

The scaling exponents α, β and z can also be obtained from height-height correlation functions [6, 15].

The scaling analysis and the identification of a limited set of different universality classes has been successfully applied to many non-equilibrium theoretical models of growth [16, 106–108]. Its application has included the characterization as non-equilibrium phase transitions of the different growth regimes and film morphologies obtained by varying the adatom mobility conditions [109–111]. However, there are some serious issues in the application of this approach to experimental systems. First, accurate experimtal measures of the surface profile are hard to obtain since most observation techniques only provide a single-valued profile of the exposed interface, ignoring surface regions shadowed by overhangs [43]. On the other hand, in many experimental systems various transient regimes can be observed, with associated crossovers between different scaling behaviors. As a consequence, it can be difficult to identify the actual growth regime at a given instant. In addition, some technological applications may require film thicknesses below those needed to reach the final transient or saturation regimes predicted by theoretical models, whereas realistic numerical simulations of growth up to actual experimental film dimensions are in most cases computationally very expensive. This type of *finite time* issues are ubiquitous in studies of non-equilibrium systems. Finally, there is a growing opinion among authors which suggests that the assumptions implied by the current scaling analysis framework, including the existence of a reduced number of universality classes, are too simplistic and further insights into the leading mechanisms for the interface behavior are required in order to develop a more accurate framework [112, 113].

2.4 Simulation methods and models

In general, growth modeling is a challenging topic present in many science fields [6, 15]. Whenever possible, growth problems are reduced to studying the stable patterns and the dynamical evolution of the interface which defines the boundaries of each growing entity. This abstraction simplifies the modeling task, allowing the use of approaches and tools from surface science to problems as diverse as the fire-front propagation in a forest, the growth of a cancer tumour or the growth of a thin solid film. However, the understanding of the wide variety of mechanisms and scales involved in thin film growth processes, from the microscopic mechanisms and the early stages of growth to the formation of defined mesoscopic structures, requires many different modeling approaches.

The first studies on growth of crystalline thin films adopted different approaches for the modeling of systems with stable [114] and unstable [115] surfaces. Using strong simplifications for the underlying physical mechanisms, stable growth was initially studied using very simple discrete or atomistic simulation models. On the other hand, the limited knowledge of the physical mechanisms which lead to the instabilities of rough film surfaces forced the adoption of analytical models of unstable interface growth. The increasing understanding of the physical mechanisms involved, led by the progress in experimental methods and the subsequent refinements of the theoretical models, has provided in recent years an accurate picture of both stable and unstable thin film growth modes, bridging the initial gap between the atomistic and the analitycal modeling approaches.

In next sections some key models for thin film growth by physical vapor deposition will be briefly reviewed, with a special attention to those more closely related to the approach used in the study presented in Chapter 3.

2.4.1 Atomistic simulation approaches

Atomistic simulations are often associated to the application of realistic molecular dynamics to atomic and molecular systems. However, coarse-grained atomistic models based on simple dynamics or stochastic approximations are also useful or even required in many cases to overcome the limitations imposed by the computational costs of realistic dynamics, as occurs for the study of thin films growth at mesoscopic scales.

Simulations based on first principles or realistic classical dynamics within studies on thin films growth are restricted to the calculation of pseudo-empirical potentials or the determination of the relevant microscopic mechanisms involved in the growth process and their statistical rates, which can be incorporated to coarse-grained models [116, 117].

Common ingredients of stochastic atomistic models

Most coarse-grained atomistic models assume very crude approximations to the dynamics and growth mechanisms. For instance, molecular dynamics has been applied to coarse-grained growth models based on simple interaction potentials and, frequently, low dimensional systems [118–121]. But probably the most common approaches to study the advanced stages of growth and their corresponding mesoscopic morphologies are based on the stochastic treatment of growth dynamics, originally via equilibrium Monte Carlo techniques or through non-equilibrium Kinetic Monte Carlo methods in recent years. Often, stochastic models also include other crude approximations, such as the simulation

of film growth in (1+1) dimensions[5], i.e., a low dimensional representation of the film structure, or the space discretization in simple fixed lattices as a simple representation of the crystalline structure of deposited materials. On top of these geometry simplifications, more or less simple growth *rules* can be defined, including the selection of the succesive locations for the discrete growth process led by adsorption of new adatoms —or for the converse process of adatom desorption— and the rules for the thermally activated adatom diffusion processes. Remarkably, the term "rule" indicates the discrete nature of the stochastic representation of growth dynamics. Indeed, in many cases only a limited set of the suposedly most significant dynamic processes are represented in the model. In some models for unstable growth, a further simplification is adopted by replacing any explicit representation of adatom diffusion processes after adsorption by different relaxation rules during the adsorption process itself.

Some key models

The origin of the basic ideas applied in stochastic simulation models for thin films growth is found in the lattice gas model [122] —a extremely simple atomistic representation of density fluctuations and nucleation for gas-solid phase transitions— and their subsequent development can be placed within the context of elementary paradigmatic growth models from Surface Science, such as the Eden model —originally, a two-dimensional model for the growth of bacterial colonies [123]— or the Diffusion Limited Aggregation (DLA) model —a representation of growth from aggregation of particles which follow random walk trajectories [124].

Among the simplest models for growth from processes of particle deposition over a substrate without diffusion there is the Random Deposition (RD) model —an independent growth of vertical columns which leads to a fully uncorrelated surface [15, 114]— and its variations, including models with modified geometries [15, 125] and the broad family of solid-on-solid (SOS) models, which introduce surface correlations in the RD scheme by imposing adsorption restrictions and may include relaxation mechanisms [15, 108, 126, 127]. The main interest of these models resides on the scaling behavior of the surface, which in some cases can be exactly determined through analytical calculations.

---

[5]Within the context of thin films studies, the dimensionality of the system is usually indicated by specifying separately the lateral dimensions —typically, the dimensionality of the substrate— and the vertical dimension, which essentially represents the direction of growth. Therefore, a two-dimensional film structure has a one-dimensional substrate and is noted as a (1+1)-dimensional system, whereas a three-dimensional film structure grows on top of a two-dimensinal substrate and is referred as a (2+1)-dimensional system.

Ballistic Deposition (BD) is a slightly more complex atomistic model of growth and one of the most widely used in thin film modelling. It was originally introduced in 1959 for the study of porous structures formed by colloidal aggregates [128, 129]. The model consists on the deposition of particles onto the surface of the aggregate by following straight trajectories from distant random positions. Once the particle reaches the surface, it adsorbs into the contact point or, if the space has been discretized, into a close unoccupied lattice site. Consequently, the model is able to simulate porous structures and surface self-shadowing effects, displaying characteristic surface scaling properties.

In the 1970s, the interesting surface behavior displayed by BD—arguably associated to a mechanism also present in thin films growth: the surface self-shadowing— attracted the interest for its application to the study of such experimental systems. The pioneering off-lattice hard-sphere model of Henderson and co-workers, presented in 1974 for the modelling of amorphous thin films [52], led to the extensive application of BD simulations in thin film growth studies.

Soon after Henderson's work, simple BD models without adatom diffusion mechanisms began to be widely used for the modeling of the kinetic roughening and fractal-like structures shown by the surfaces of the Zone I thin film morphlgies, corresponding to the growth from PVD processes under low adatom mobility conditions [101, 105, 130, 131], as well as for the study of the effects led by the incidence angle of the deposition trajectories [53, 71, 132].

More interestingly, BD can be combined with surface diffusion models in order to study the interplay between the random deposition, the surface self-shadowing and the adatom mobility mechanisms, which determines the emergence of Zone II growth regimes and the characteristics of their corresponding morphologies.

In general, elementary surface diffusion mechanisms can be introduced in simpler growth schemes, such as in SOS models [114], for the simulation of layer-by-layer growth of crystalline films. However, BD models allow both elementary and more refined approaches to diffusion mechanisms if needed. In 1983, Outlaw and Heinbockel introduced the realistic approach of rescaling the diffusion barriers according to the local microscopic configuration [133]. Most current simple approximations for surface diffusion in BD models include Arrhenius-like diffusion rates, such as Equation (2.1), with energy barriers depending on the coordination number of the migrating particle. In 1985 Müller refined the Outlaw–Heinbockel scheme by incorporating an empirical estimation for the diffusion rates of a specific material which implicitely takes into account not only the local

microstructure but the enhancement of diffusion mechanisms with the increasing substrate temperature. This scheme successfully represented the evolution from Zone I to Zone II morphologies led by temperature, in very good agreement with the experimental observations which led to the first SZM.

Amorphous films are usually simulated through the ballistic deposition of hard discs or spheres without any bonding symmetry in a fully off-lattice scheme, whereas monocrystalline films are easily represented by simple lattice schemes. The simulation of polycrystalline films, texture competition and complex epitaxial effects requires instead more sophisticated techniques and so far there exists very few approaches to this issue. Gilmer, Huang and co-workers developed a BD multilattice scheme which seems the most successful technique to date [134,135]. Another model based on a local definition of bonding symmetries with variable orientation has been applied, due to its complexity, just to a SOS scheme [136].

Altogether, current development of atomistic simple models based on stochastic dynamics can be considered rather successful in the theoretical study of surface scaling behavior [15,16], the mechanisms at the early stages of growth [137,138] and the characterization of the mesoscopic morphologies formed under extreme growth regimes [122,139], either for the relatively high diffusion rates which lead to the growth of monocrystalline films as well as for rough approximations to amorpous films formed under very low adatom mobility conditions. In fact, extreme conditions facilitate an adequate tradeoff between accuracy and simplifications of the different ingredients needed in this type of simulation models.

On the other hand, the incorporation of some aspects of film growth, including those needed for the adequate representation of intermediate growth conditions and more complex bonding symmetries associated to novel film materials, have been so far disregarded due to presumably difficulties in its efficient implementation or by the limited availability of related experimental studies led by their novelty as interesting topics with potential technologial applications.

2.4.2 Scaling behavior and analytical approaches

Parallel to the development of atomistic simulation models, great efforts have been devoted to obtain analytical models for the characterization of the surface behavior during growth and its connection to atomistic simulation models and experimental observations. In particular the dynamic scaling hypothesis, with their assumedly limited number

of distinct universality classes, represented a great stimulus to establish a representative analytical model for each known universality class determined from experiments and/or atomistic simulation models.

Most analytical models of surface growth are based on stochastic differential equations, or Langevin equations, for the single-valued surface heights, $h(\mathbf{r}, t)$. For instance, the surface behavior of the RD model can be easily described by a simple Langevin equation: $\partial h(\mathbf{r}, t)/\partial t = R + \eta$. Their only two terms correspond to the constant mean deposition rate, R, and to a noise term, η, which represents the random distribution of deposition trajectories.

Another more complex, but still linear equation is the Edwards–Wilkinson (EW) model [140], which reproduces the surface scaling behavior of the RD with a steepest descent relaxation of the newcoming particles. The EW equation replaces the constant mean deposition rate with a relaxation term, $\nu \nabla^2 h$, acting as the effect of a surface tension, ν, which tends to smooth the surface profile.

But probably the most widely applied and studied analytical model in the context of thin solid films is the Kardar–Parisi–Zhang (KPZ) equation [141]. The KPZ is obtained from the EW equation by adding a non-linear term, $(\lambda/2)(\nabla h)^2$, which represents the lateral growth of the interface. Consequently, the KPZ equation reads:

$$\frac{\partial h(\mathbf{r}, t)}{\partial t} = \nu \nabla^2 h + \frac{\lambda}{2}(\nabla h)^2 + \eta(\mathbf{r}, t). \tag{2.11}$$

The main success of the KPZ equation is to reproduce the scaling behavior of the BD model, including different SOS deposition models [130, 142, 143]. Atomistic simulations in (1+1)-dimensions with such model provided accurate values for the scaling exponents: $\alpha = 0.47 \pm 0.02$ and $\beta = 0.33 \pm 0.01$ [130, 131]. An elaborated scaling analysis for the KPZ equation leads to $\alpha = 1/2$, $\beta = 1/3$ [15], evidencing the correspondence between both types of models.

The effects of surface diffusion can also be modeled by the derivation of Langevin equations from a master equation for the dynamics [6, 144, 145].

However, as already pointed in Section 2.3.2, the increasingly available experimental evidences on thin films surface behavior have proven to be more complex than the predictions of the atomistic and analytic models, showing the existence of many different "anomalous" scalings which do not fit to the theoretical models. For this reason, there is an increasing adoption of phenomenological approaches based on refined fittings of the equations to the experimental parameters, dropping the search for universal properties

to a latter step [113].

3 Mesoscopic morpholgy transitions in thin solid films: effects of microstructure coordination

After several decades of intensive experimental and theoretical research on thin solid films growth and its applications, there exists a deep understanding on many of the leading mechanisms and related properties of such systems. But the picture is far from being complete: each improvement on experimental processing methods or measurement techniques opens new perpectives and theoretical challenges.

For many years the main research efforts have been focused on the accurate modeling and processing of highly crystalline metal and semiconductor films due to the enormous expansion and economic weight of the microelectronics industry. The microstructural properties inherent to metallic crystals allowed the use of modeling approaches with strong simplifications and assumptions which are unlikely for other systems, even under coarse-grained qualitative approaches. The increasing interest in new and very different technological applications based on thin films made from metallic oxides, rare-earths or organic compounds is pushing theoretical modeling towards a revision of past assumptions in order to adapt the current modeling tools to such new systems. Moreover, the tremendous increase in available computing power experienced since the early theoretical studies on thin film growth brings an opportunity to incorporate new necessary and eventually more complex ingredients into the old simpler simulation models.

In particular, the traditional approaches used in minimal atomistic simulation models for the study of film morphologies at mesoscopic scales include non-directional bonds and in-lattice or randomly disordered particle arrangements for crystalline and amorphous film structures, respectively, which are approximately correct assumptions for materials with microstructures mainly formed by metalic or ionic bonds. These simplifications allow the use of simple lattices or fully off-lattice schemes in the computer implementations of such models. However, covalent or intermolecular bonding based materials are expected to exhibit distinct structural behaviors due to the directionality and eventually

limited maximum coordination of these bonding types.

Having the main research efforts focused on metalic crystals, there has been also a certain disregard for the study of thin film bulk properties[1]. The theoretical studies on film morphologies have been performed mainly from the perspective of the surface structure and its dynamical evolution during growth. However, important film properties such as the mechanical resistance and the thermal or the electrical conductivities are determined not only by the film surface but also by the underlying structure. Therefore, different theoretical studies on film bulk properties, including those based on minimal simulation models, are becoming more frequent in recent years [146–148].

This chapter presents a theoretical study intended to address some basic questions on the minimal modeling of non-metallic amorphous and polycrystalline thin films grown by physical vapor deposition under simple experimental conditions. The study has been performed from a modeling approach that establishes a tradeoff between a perspective as much generic as possible and the capability to reproduce the essential experimental properties summarized by the simplest Structure Zone model. Specifically, two main points have been addressed in the study:

i) The first point concerns how to efficiently incorporate more complex bonding symmetries and coordination constrains into a mesoscopic simulation model, as a first step towards the adequate simulation of the surface and bulk properties of crystalline and non-crystalline films formed by diverse metallic and non-metallic materials with mesoscopic dimensions, which is the case of many thin films processed for different technological applications.

ii) The second point addresses how these new type of modeling constrains would affect to the different mesoscopic morphologies led by distinct adatom mobility conditions, as described by the simplest Structure Zone Model, from the novel perspective of their bulk properties.

The presentation of the study begins in the next Section with the introduction of the chosen mesoscopic growth model, the new generic approach for definition of arbitrary bonding symmetries and the details of the corresponding computational implementation,

---

[1]In the context of thin solid films, the term "bulk" should be understood as the region below the growing surface. Under limited adatom mobility growth regimes, this region is usually considered as a "frozen" structure. Since the structures of thin films grown by physical vapor deposition are the result of particular non-equilibrium growth processes, the bulk properties of a thin film have not necessarily to be the same than the corresponding to the true macroscopic bulk material.

specially developed for this study. Section 3.2 introduces the specific conditions used in the simulations and presents the results obtained for (1+1)-dimensional systems, whereas the results corresponding to the (2+1)-dimensional cases are described in Section 3.3. Finally, Section 3.4 is devoted to summarize the main conclusions of the study.

3.1 A generic mesoscopic model of thin solid films grown by physical vapor deposition

The simulation model developed in this study includes many of the common characteristics of previous atomistic minimal models for the growth of thin films from physical vapor deposition under limited adatom mobility conditions: it includes explicit ballistic deposition trajectories and surface self-shadowing, off-lattice particle locations and thermally activated surface diffusion of adatoms. However, it includes a novel scheme for the definition of the bonding symmetries which provides, at the cost of an increased complexity of its computational implementation, the combined features of previous simpler models without losing the ability to simulate mesoscopic scale structures in reasonable computing times. The main advantage of the scheme consists of its flexibility, either to easily simulate different (1+1) and (2+1)-dimensional bonding symmetries within the same framework and to reproduce related complex effects, such as texture competition and epitaxy. Even (1+1)-dimensional microstructures have an evident computational advantage over the more costly (2+1)-dimensional ones, the simulation of both types of microstuctures is justified by the abstract perspective of the study: a growth model with such characteristics is not only interesting for being applied to thin films growth but has also an intrinsic interest as a generic non-equilibrium growth model for which its dependence with the dimensionality should be understood. A detailed description of the model is provided in the following sections.

3.1.1 Particle deposition and microstructure definition

In the model the growth units or adatoms are represented as hard disks of radius a whose centers may be located at any position in the continuous space. These units are ballistically deposited on a substrate with lateral periodic boundary conditions at a mean rate R. The ballistic trajectories are taken to be normal to the substrate, which is initially configured as a flat monolayer of fixed adatoms with given arrangement. Bonds between adatoms are restricted to nearest neighbors. On making the first contact, either with the adatoms on

the film surface or directly with the substrate, the incoming particles are instantaneously relocated to the closest available site defined in the microstructure considered.

In order to define different bonding symmetries a set of relative positions, the so-called *active positions*, is defined locally around each particle of the film as the possible locations at which other film particles can bond, instead of locating the adatoms on a fixed lattice or completely off-lattice, with no local microstructure restrictions, as is usual in previous models. In other words, bonding sites for first nearest neighbors are not fixed with respect to the substrate frame but are localized around the exposed adatoms. This local definition of the microstructure provides a simple representation of some non-crystalline structural features which can not be reproduced in simple lattice schemes, such as substrate lattice mismatches and dislocations. Moreover, it is possible to define complex microstructures formed by a superposition of diverse and even mutually exclusive simple symmetries. For instance, it is possible to define combined microstructures composed by different rotations of the same simple symmetry. This composition can be understood as an extremely simplified discrete representation of the orientational degree of freedom of adatoms with a significant bonding directionality. Such type of combined microstructures constitute also an alternative approach, arguably more realistic, to the multilattice scheme introduced by Huang and Gilmer for the simulation of texture competition during thin film growth [134, 135, 149, 150]. Less realistic combinations of distinct simple symmetries with different maximum coordination numbers can also be defined in order to study from an abstract perspective the behavior of such microstructural parameter.

Figures 3.1 and 3.2 show respectively the different (1+1) and (2+1)-dimensional microstructures used in this study. For the (1+1)-dimensional case four different microstructure combinations have been used: the purely square (*sq*) and the purely hexagonal (*hex*) lattices, with respectively a maximum coordination number of 4 and 6, the hexagonal-square (*hex-sq*) microstructure –formed by the superposition of the previous ones as a two-dimensional projection of the three-dimensional face-centered cubic lattice– and the square-square (*sq-sq*) microstructure obtained by the superposition of two purely square lattices, one horizontal as the substrate and the other one tilted 45°. As shown in Figure 3.1, both composite microstructures, *hex-sq* and *sq-sq*, have mutually exclusive active positions that lead to a maximum coordination number of 6 and 4, respectively, and can produce nonregular arrangements of particles with interesting features such as shadowing of active positions by close off-site adatoms and lattice frustration. For the (2+1)-dimensional case, two microstructures were considered: a close-packed hexagonal lattice (*3d-hex*),

having a maximum coordination number of 12, and a superposition of three pure simple cubic lattices (*3d-cs*), one following the x-y-z axis plus another two rotated 45° around the x axis and y axis, respectively. The latter combined microstructure has also mutually exclusive positions and a maximum coordination number of 6.

In both the (1+1) and (2+1)-dimensional cases, the available sites to accomodate the incoming particles from their first contact position with the film surface are the active positions of the surrounding surface adatoms which are unoccupied and non-shadowed —neither by neighbors bonded to the owner of the active position nor by close non-bonded particles. After a new surface adatom is accommodated, bonds with their nearest neighbours are established according to the defined microstructure and the corresponding new unoccupied active positions are created around it.

3.1.2 Surface diffusion

In order to simulate the thermally activated diffusion of the surface adatoms during the film growth the kinetic Monte Carlo method (kMC), introduced in Section 1.3.2, has been applied. This method evaluates the transition probabilities between states of a system governed by a set of stochastic events with a given mean rate. In the case of thin film growth, at each kMC step the events are composed of the deposition of a new particle with a constant mean rate R, and all the possible diffusive hops of the surface
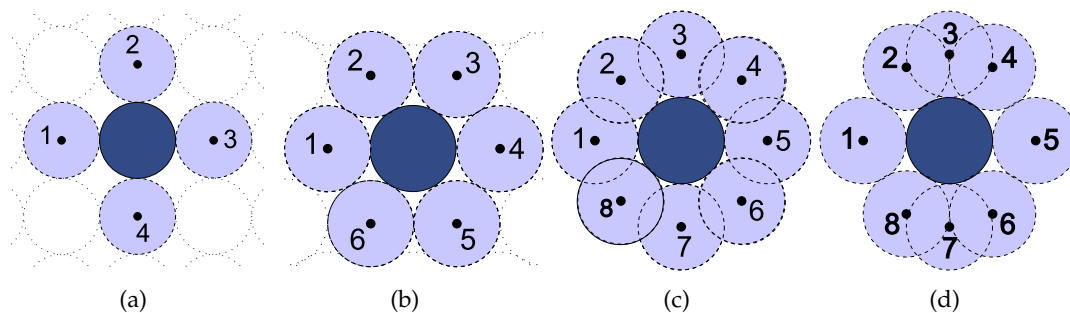
Figure 3.1: The four (1+1)-dimensional microstructures used in this study, with their active positions labeled. (a) Simple square lattice (*sq*); the adatom is buried when active position 2 is occupied. (b) Simple hexagonal lattice (*hex*); the particle is buried when positions 2 and/or 3 are occupied. (c) Double square lattice (*sq-sq*), with mutually exclusive active positions; the particle is buried when positions 2, 3 and/or 4 are occupied. (d) Combination of the square and hexagonal lattices (*hex-sq*) —a two-dimensional projection of a three-dimensional *fcc* lattice— also with mutually exclusive active positions; a particle is buried when positions 2, 3 and/or 4 are occupied.
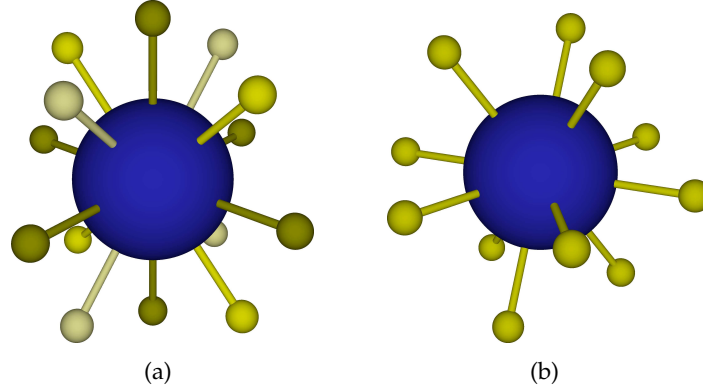
Figure 3.2: The two (2+1)-dimensional chosen microstructures, with their active positions drawn as small conected spheres. (a) Superposition of three cubic simple lattices with different orientations; its maximum coordination number is 6. (b) A close packed hexagonal lattice, with a maximum coordination number 12.

particles, whose mean rates themselves obey an Arrhenius-type generic relation given by Eq. (2.1). In particular, the activation energy E_d for a diffusion hop between two given positions labeled as i and j would depend on the local surface configuration. A very rough estimation of E_d consists on simply taking the coordination number of the adatom at its origin position, n_i, multiplied by the single bond potential, ϕ:

$$R_{i \to j} = \nu \, e^{-n_i \phi / k_B T}. \tag{3.1}$$

Moreover, the coarsest estimations take the frequency of the thermal fluctuations, ν, as a constant independent from the temperature. When applied to the simple diffusion rules commonly used in mesoscopic simulation models, however, these estimations are known to be incorrect, especially for relatively high temperatures, i.e., for temperatures approaching to one half of the material melting point, T_m. As already pointed in Section 2.2.2, accesible diffusion mechanisms become more numerous and complex as the temperature increases. In particular, an estimation such as Eq. (3.1) for the rates of simple diffusion mechanisms tends to produce unrealistically smooth transitions between the Zone I and Zone II mesoscopic morphologies. On the other hand, a direct atomistic representation of the many diffusion mechanisms activated at high temperatures would make any computational model impractical for mesoscopic simulations. An affordable solution to these issues consists on keeping the simple diffusion rules whereas empirical estimations of the dependence with temperature of the activation energies and the ther-

mal fluctuations are applied. Obviously, this empirical approach applies at the cost of losing almost any generality in the model parameters, i.e., it forces to select very specific system conditions in order to obtain accurate results.

According to the previous considerations, a model with a known accurate empirical estimation of the surface diffusion rates has been selected as a comparative reference for this study: the estimates of K.-H. Müller for Nickel vapor deposited thin films [151, 152]. Müller's model was found to reproduce particularly well the experimental transition point between Zone I and Zone II morphologies [151] and has been used since its introduction by different authors [109, 153–156].

Müller's model assumes temperature-dependent thermal fluctuations with frequency

$$\nu = 2\,k_B T/h, \tag{3.2}$$

where h is the Planck's constant. Therefore, the characteristic mean rate for each possible hop between two given surface positions i and j is:

$$R_{i \rightarrow j} = \nu\, e^{-E_{i \rightarrow j}/k_B T}, \tag{3.3}$$

where $E_{i \rightarrow j}$ is the activation energy barrier for that particular hop. Müller estimated these barriers heights in terms of the number of bonded neighbours at the origin and destination positions (respectively N_i and N_j) as

$$E_{i \rightarrow j} = \begin{cases} Q, & N_i \leq N_j \\ Q + (N_j - N_i)\phi, & N_i > N_j \end{cases} \tag{3.4}$$

where ϕ is the bonding potential and Q is the surface diffusion activation energy, which is given as a function of the substrate temperature, T, and the melting point of the material, T_m, by the empirical expression of Neumann and Hirchswald [157]:

$$Q = \left(5 + \frac{20}{3}\frac{T}{T_m}\right)k_B T_m, \ \ (T < 0.5\,T_m). \tag{3.5}$$

At each simulation step the list of the rates for the M possible dynamical events of the system —the mean rates of the $M - 1$ possible diffusion hops given by Eq. (3.3) and the mean deposition rate R— is composed. The diffusion events are restricted to the displacement of surface adatoms to neither occupied nor shadowed active positions found within a given distance range from the current position of the migrating adatom. For all the chosen microstructures, except the *sq*, that single-event diffusion range has been limited to a

distance of one adatom diameter, i.e., to first nearest neighbors positions. Despite this limitation, the density of active positions in the *hex*, *sq-sq* and *hex-sq* microstructures provides enough diffusion trajectories to allow the formation at high temperatures of crystalline structures from a random deposition process. However, in the case of the *sq* microstructure the hop range must be increased to second nearest neighbors positions in order to obtain the same behavior. Adatoms are considered to belong to the surface when they are not "buried" by the presence of bonded neighbors in their top active positions, as indicated in Figure 3.1 for the (1+1)-dimensional microstructures. In this general scheme for a very simplified representation of surface diffusion no explicit Schwoebel-Ehrlich barriers have been considered.

Once the list with all the event rates is composed the kMC algorithm, represented by Equations (1.3) to (1.5), is applied using some appropiate optimization techniques.

3.1.3 Algorithm optimizations

The kMC algorithm can be considered a very efficient stochastic method since it does not requires unsuccessful attempts in any step. It is also an essentially *sequential* algorithm which hardly obtains any significant benefit from computing parallelization, despite the diverse efforts made with that purpose [158–160]. In most pratical cases, kMC optimizations are focused instead on the searching through the collection of event rates and its update after every featured event.

Due to the complexity introduced by the local definition of bonding symmetries and the simulation of ballistic trajectories in the model developed for this study, optimizations for searching and updating of event rates must be combined with an efficient spatial searching of adatoms which may be close to any given trajectory or active position, in order to determine shadowing effects. The chosen optimization method is based on a fast indexing of spatial locations in the simulation cell through a multi-level spatial partitioning. This strategy, frequently used in kMC simulations [41], can be efficiently implemented using advanced data structures such as n-trees. In particular, a quad-tree structure [161], whose (1+1)-dimensional scheme is shown in Figure 3.3, was chosen for the present model.

The lowest partition level is used directly for the fast spatial location of adatoms and active positions, whereas in combination with the upper partition levels it is also used for the fast searching of diffusion events. It is formed by boxes with edges of around four adatom diameters in length. Every box indexes the positions of the adatoms located
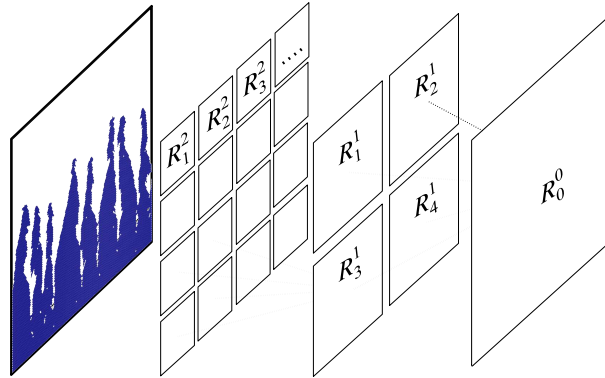
Figure 3.3: Fast search scheme for spatial location and selection of adatoms and activated processes based on a quad-tree structure. Only the three higher levels of the quad-tree are shown. At every level, each partition stores the sum of the rates corresponding to all the possible activated processes that can be experienced by the adatoms located therein. Partitions at the lowest level store also the positions of the adatoms.

within their limits, whereas adatoms themselves carry all the information of their active positions and the diffusion events which are accessible for them accordingly to their current neighborhoods. Boxes from the lowest level also store the rates sums of all the diffusion events of their adatoms.

In the first upper level the diffusion rates stored in lowest boxes are summed up in groups of 2x2 boxes for the (1+1)-dimensional case and 2x2x2 in the (2+1)-dimensional one. This grouping process continues through upper levels until obtaining a single box with the sum of all the diffusion events rates of the system. The searching for the specific diffusion event which accomplishes the criterium given by Eq. (1.4) in every kMC step is quickly performed by descending levels through every specific box which matches the criterium. As the worst case, in every level it will be necessary to check all the boxes grouped together in the box selected in the upper level.

Altogether, the implementation requirements led by the chosen scheme are probably more complex than the corresponding to any previous similar simulation model, especially for the needed data structures. In order to deal efficiently with this complexity, the model was implemented from scratch with the C++ programming language, using object-oriented techniques and dynamic data structures from its standard library [162].

3.2 Simulations in (1 + 1) dimensions

For the sake of comparison with the Müller's original simpler model, the computer experiments from which the following results have been obtained were performed using the corresponding physical parameters of Nickel:

$$T_m = 1720 \text{ K}, \ \phi = -0.74 \text{ eV}, \ a = 0.352 \text{ nm}. \tag{3.6}$$

Deposition rates, R, will be measured in units of monolayers per second (ML/s), i.e., in terms of the minimum possible vertical speed of growth, obtained just when a fully compact structure develops. Substrate widths, L, as well as any other measure of length, will be espressed in adatom radius units, a.

3.2.1 Mesoscopic morphologies and epitaxy

As the substrate temperature is changed, the development of different characteristic mesoscopic film morphologies is observed. Figure 3.4 shows the some examples of film morphologies that emerged for each microscopic symmetry combination considered at the same sequence of different substrate temperatures and obtained after depositing 15000 particles onto a horizontal flat substrate of 160 adatoms wide with a close-packed arrangement. That amount of deposited particles guarantees a physical vertical thickness of more than 20 nm for the represented films, i.e., a mesoscopic thickness. In the next section it will be proved that for such film thicknesses the growth process has reached practically a stationary regime.

In each case, the obtained mesoscopic structures show that there exists a substrate temperature below which low-density morphologies formed by competing dendritic structures are always observed. These structures are characterized by the self-affine surface geometry typically observed in purely ballistic deposition models without surface diffusion. As the substrate temperature increases, surface diffusion becomes significant and dendritic morphologies give way to more compact fibrous structures growing along a preferential axis parallel to the deposition trajectories. With even greater surface diffusion, the former fibrous structures become compact giving rise to densely packed grains that grow vertically as non-competing columns whose thickness increases with the diffusion. This behavior is qualitatively independent of the underlying microstructure and characterizes the transition from the typical morphologies of the Zone I, which are porous and fractal-like, to those of the Zone II, where pronounced faceting develops until the ap-

pearance of structures limited by smooth surfaces described in the context of the SZM.
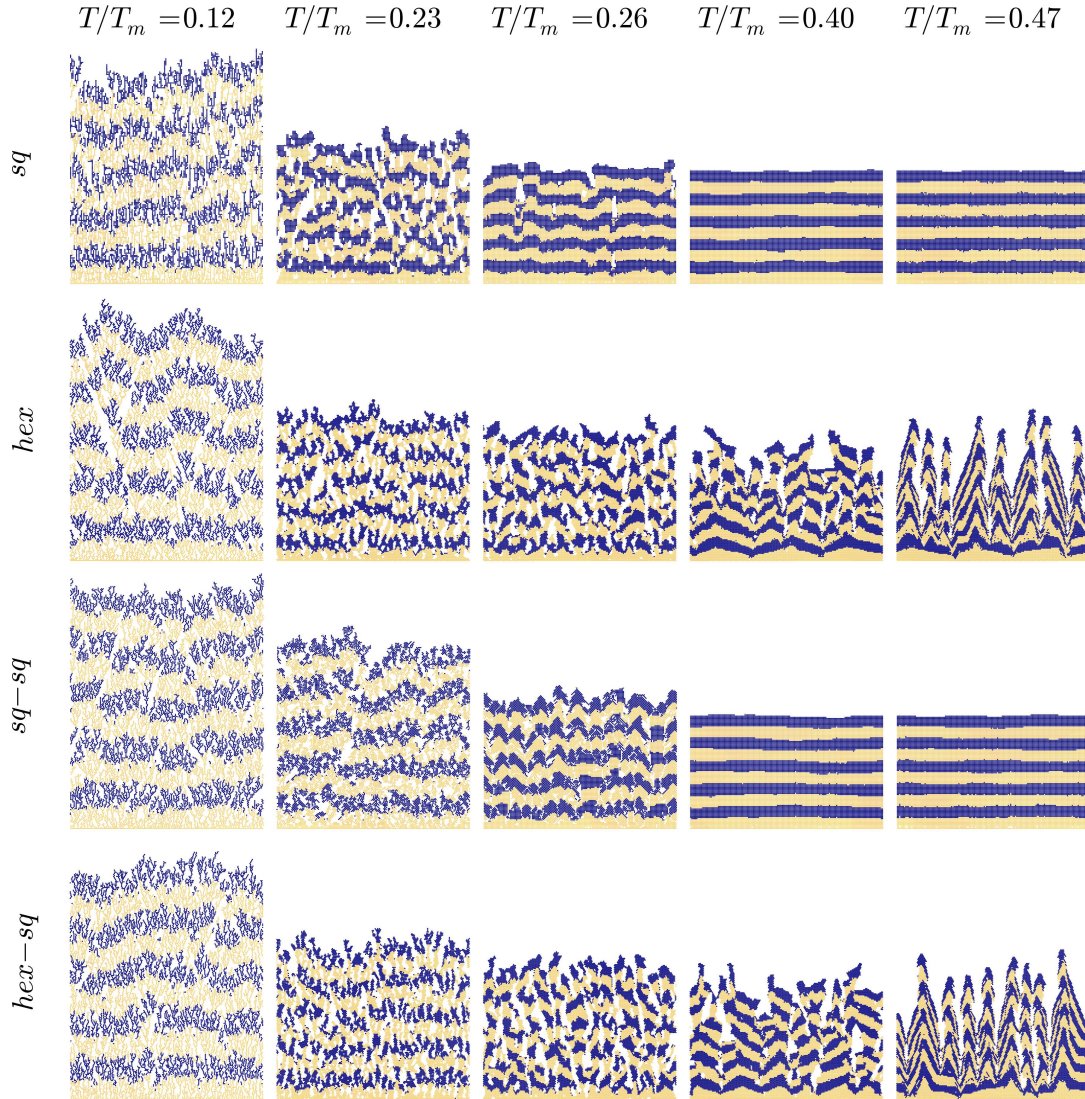
Figure 3.4: Film structures obtained for each given microstructure at different substrate temperatures. Every sample corresponds to the deposition of 15000 particles at a fixed rate of 1 monolayer per second (ML/s) onto a horizontal flat substrate formed by 160 adatoms disposed in a close packed arrangement. To aid the eye, the color of particles is changed every 10 deposited monolayers.

However, although the qualitatively universal character of the Zone I and Zone II morphologies is reproduced, the sequence of emergent mesoscopic structures as the substrate temperature is varied seems to be significantly influenced by the underlying microstruc-

ture. In particular, the width of the non-competing compact columns in the microstructures with a maximum coordination number of 4 —the *sq* and the *sq-sq* microstructures— increases considerably more with the substrate temperature than the corresponding to the microstructures with a maximum coordination number of 6 —the *hex* and *hex-sq* ones. This behavior can be better illustrated by a quantitative calculation of the mean horizontal width of the compact columns for each microstructure, l_c. Figure 3.5 shows the result of calculating such parameter by sampling the horizontal lengths of compact regions, identified by having a local packing density above 0.75 of the maximum value allowed by the microstructure[2], at the central regions of the films introduced in Figure 3.4. It is remarkable the difference between the hexagonal and square composite microstructures: at high temperatures, the characteristic widths for *hex* and *hex-sq* microstructures are very similar and obviously lower than those observed for the *sq* and *sq-sq* ones.
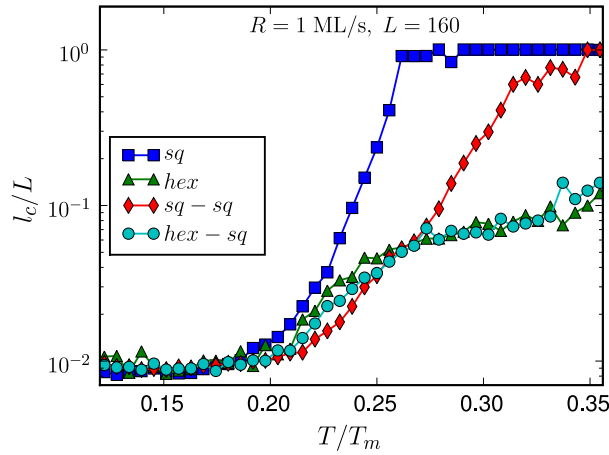
Figure 3.5: Mean horizontal width of the compact columns, l_c, defined as having a packing density above 0.75 of the maximum possible value, divided by the total substrate width, L, as a function of the reduced substrate temperature for every (1+1)-dimensional microstructure.

The compact columns of the *hex* and *hex-sq* microstructures not only increase more their horizontal width with temperature but have also wider interstitial voids at high temperatures, for which an epitexial growth regime is assumed. The emergence of such morphological instabilities during epitaxial growth is generally associated to the existence of Schwoebel-Ehrlich barriers hindering the interlayer migration of surface particles, as

---

[2]This is $\pi/2\sqrt{3}$ for a (1+1)-dimensional hexagonal lattice and $\pi/4$ for the square lattice with the same dimensions.

noted in Section 2.2.5. However, since there are no explicit S-E barriers in this model, one should conclude that distinct implicit interlayer barriers are emerging directly from the dynamic interplay between microstructure symmetries and epitaxy. Specifically, the key factor leading to this behavior is waht are the particular locations of the active positions found in the upper corners for every microstructure and their compatibility with the substrate arrangement during epitaxial growth. Under this growth regime, only the lattices from the microstructure which match the substrate arrangement are selected. In the *sq* and *sq-sq* microstructures, the upper corners have active positions incompatible with the horizontal close-packed substrate arrangement (*sq-sq*) or do not have any active position at all (*sq*). Conversely, the hexagonal lattices in the *hex* and *hex-sq* microstructures have active positions in the upper corners which match perfectly with the substrate. This means that the upper corner positions of the hexagonal lattices are *stable* positions during epitaxial growth: if one of such active positions from an adatom placed in the edge of a layer is ocuppied, it will difficult the interlayer migrations between the upper layer and the former. The unstability under epitaxial growth of the upper corner positions in the *sq-sq* microstructure makes unlikely for an adatom to remain enough time in such positions for leading to an effective hindering of interlayer migrations. Since no upper corner positions exists and direct migrations to second-nearest neighbors have been allowed in the *sq* microstructure, no implicit S-E barriers are possible in such case.

An experimental evidence of similar implicit interlayer barriers emerging from purely dynamical effects has been published almost simultaneously to these results by R. Ganapathy an co-workers [163]. In their experimental system, intended to study the epitaxial growth of colloidal crystal films, adatoms are replaced by spherical colloids with just a depletion interaction, i.e., a short-range attractive interaction, and deposited on a substrate with a hexagonal lattice arrangement which leads to a film crystalline phase consisting on a hexagonal close-packed structure. Their results show the existence of step-edge and corner barriers that are responsible for a columnar film morphology and have necessarily a diffusive origin, in full agreement with the present simulations.

The previous finding and its interpretation can hardly be understood without taking into account the net effect of surface diffusion and epitaxy. Surface diffusion tends to increase as much as possible the coordination of adatoms in the film structure, whereas epitaxy determines the particular crystalline lattice selected for the film and hence the maximum coordination number allowed. This behavior can be illustrated by studying epitaxy and, particularly, the texture competition effects which should emerge in the
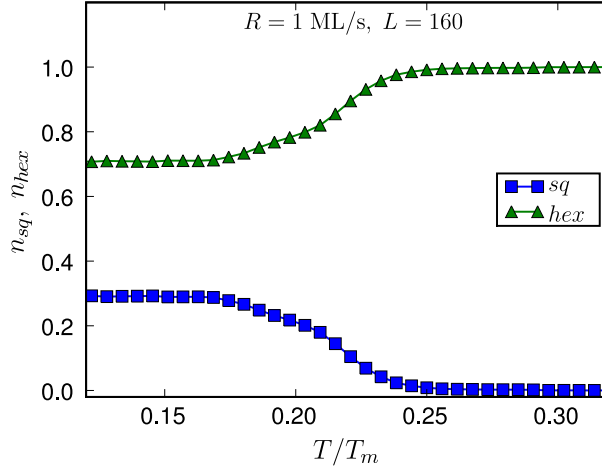
Figure 3.6: Competition between the two bonding symmetries with different maximum coordination numbers coexisting in the *hex-sq* microstructure: ratio of the square and the hexagonal bonding positions, n_{sq} and n_{hex}, as a function of the substrate temperature. Results for 15000 deposited particles and a substrate size of 160 adatoms, averaged over 10 realizations.

combined microstructures, *sq-sq* and *hex-sq*. Such effects are analized by computing the mean number of bonds corresponding to each bonding symmetry present in the microstructure at different substrate temperatures and substrate arrangements.

Coexistent symmetries with different maximum coordination number: the *hex-sq* microstructure

When coexistent lattice symmetries have a different maximum coordination number, as is the case for the composite *hex-sq* microstructure, the deposited particles in the film growing under high substrate temperatures tend to accommodate according to the lattice symmetry with the higher maximum coordination number, in this case, the hexagonal lattice, since the positions with a higher coordination are found to be more stable energetically when visited by the diffusing particles.

This behavior is illustrated in Figure 3.6, where the fraction of bonds in the square and hexagonal lattice symmetries as a function of the substrate temperature is plotted. At low temperatures, when surface diffusion is negligible and growth is purely determined by ballistic deposition, the fraction of bonds belonging to the hexagonal lattice is higher than the one corresponding to the square lattice due to the wider effective adsorption window with respect to the vertical deposition trajectories of the upper hexagonal active
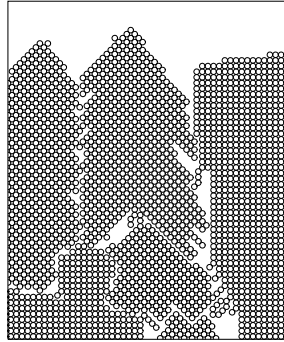
Figure 3.7: Detail of the clusters of horizontal and diagonal square lattice domains formed by texture competition at intermediate temperatures in the *sq-sq* microstructure ($T/T_m =$ 0.29 K, horizontal substrate symmetry).

positions. As expected, the fraction of hexagonal lattice bonds tends to increase with the susbtrate temperature, until becoming the only type of bonds allowed by the epitaxial growth regime at high temperatures.

Coexistent symmetries with the same maximum coordination number: the *sq-sq* microstructure
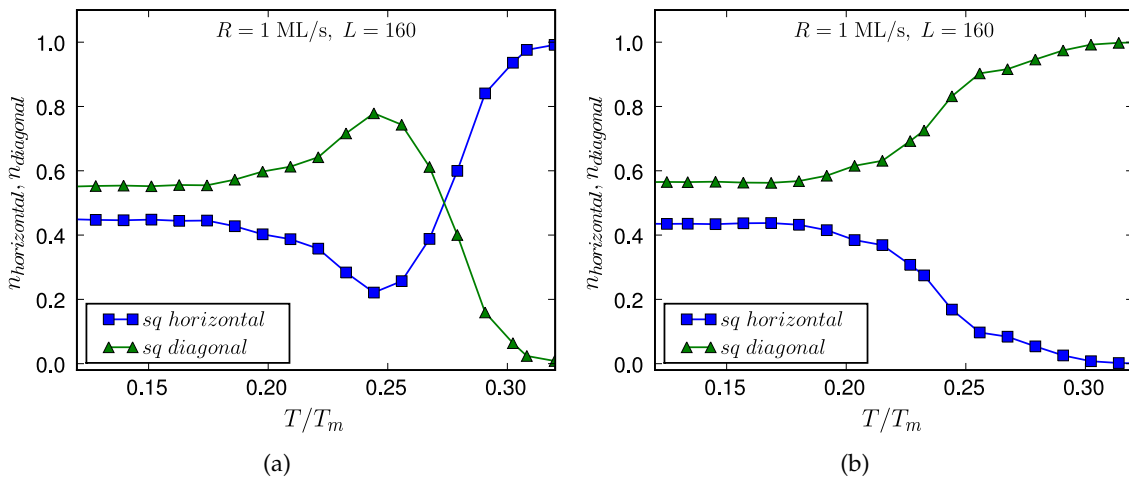
Figure 3.8: (a) Mean ratio of bonds for the horizontal and the diagonal square bonding symmetry orientations as a function of the substrate temperature with a horizontal substrate; (b) same results with a diagonal square substrate. The sampling of the bond type fractions is the same than the corresponding to Figure 3.6.

In the *sq-sq* microstructure, there is no energetically selective mechanism to discriminate between the two compact configurations allowed by the underlying composite bonding symmetries at moderate temperatures. As a result, a polycrystalline film may develop as is illustrated in Figure 3.7. However, as the surface diffusion strengthens with the increasing substrate temperature and epitaxial effects become significant, competing homogeneous growth takes place with the final extinction of the symmetry incompatible with the substrate arrangement. Figures 3.8(a) and 3.8(b) show the bond fractions of each lattice obtained with a horizontal and a diagonal square substrate arragements, respectively. Again, at low temperatures there is a slight preference for one of the lattices, in this case the diagonal square, led by the same type of geometrical property of the adsorption process pointed for the *hex-sq* microstructure. As the substrate temperature increases, the fraction of the initially preferred lattice also increases due to the ordering effect of the surface diffusion, until a temperature of approximately $T/T_m \sim 0.24$ K is reached. Above such temperature, epitaxy becomes significant and the lattice compatible with the substrate tends to be selected independently from which lattice is preferred at lower temperatures.

3.2.2 Surface properties

In spite of the fact that the central topic in this work is the study of the bulk properties of thin films grown up to a mesoscopic thickness and their eventual dependence with the microstructure coordination, it is interesting to test the expected surface roughening under low adatom mobility conditions. The highlighted bands of the low-temperature morphologies drawn in Figure 3.4, which for $T/T_m \lesssim 0.12$ represent the effective time evolution of the surface due to the negligible migration of deposited adatoms in such conditions, show qualitatively how the surface is relatively smooth during the deposition of the first layers and becomes more rough soon after.

A more detailed analysis of the surface roughening at low temperatures has been performed, using the scaling formalism introduced in Section 2.3.2, as a test for the validity of the simulation model. Figure 3.9(a) shows the time evolution of the surface width parameter, $W(L,t)$, defined in Equation (2.3), for the *hex-sq* microstructure and three different substrate sizes (L=80, 160, 320) measured in adatom radius units. $W(L,t)$ grows initially by following a power law, as predicted by Equation (2.4), with a growth exponent β. At a given crossover time, t_x, the interface width reaches a steady saturation value, $W(L)$. According to Equations (2.5) and (2.6), these latter parameters also have a
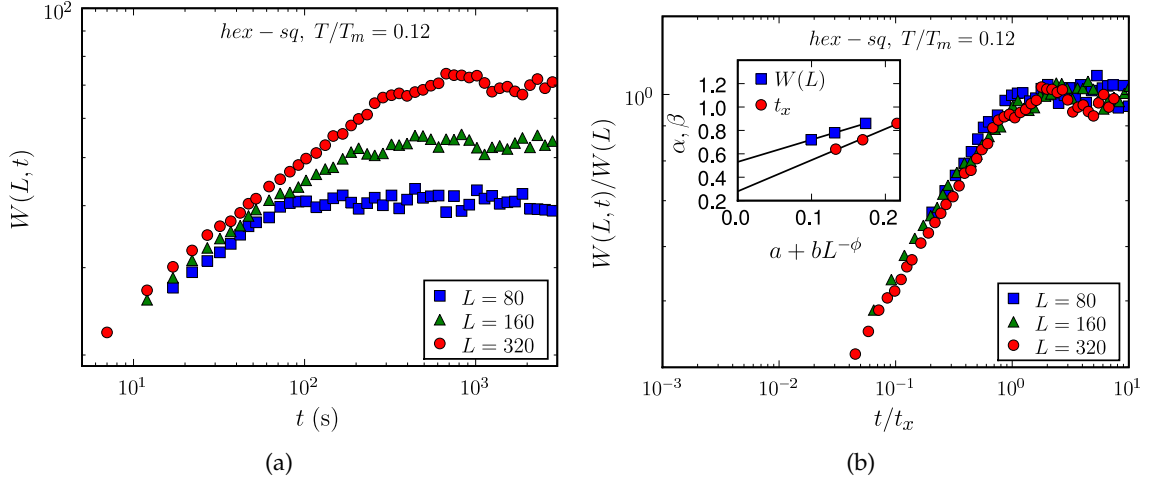
Figure 3.9: (a) Time evolution of the root mean squared deviation of the surface height, $W(L,t)$, averaged over 100 realizations for the *hex-sq* microstructure, a reduced substrate temperature $T/T_m = 0.12$ and three different substrate sizes. (b) Rescaling of the different $W(L,t)$ curves with their corresponding crossover times, $t_x(L)$, and saturation values, $W(L)$. The inset shows the calculation of the roughness exponents, α and β, in the limit of an infinite substrate size, $L \to \infty$.

power law dependence with the substrate size determined respectively by the roughness exponent, α, and the dynamic exponent, z. The dependence of the $W(L,t)$ curves with the substrate size allows their collapse when rescaled with their corresponding parameters $t_x(L)$ and $W(L)$, as shown in Figure 3.9(b). The inset corresponds to the estimation of the associated scaling exponents α and β in the limit of an infinite substrate width. This calculation of the asymptotic values of the scaling exponents is required since the values obtained directly from the relations (2.5) and (2.6) show a dependence with L:

$$\alpha(L) = \frac{\log(W(L))}{\log(L)}, \quad z(L) = \frac{\log(t_x(L))}{\log(L)}, \quad \beta(L) = \frac{\alpha(L)}{z(L)}. \tag{3.7}$$

However, this dependence tends to defined asymptotic values as L increases. Therefore, the asymptotic exponents can be obtained by fitting a dependence model to the values calculated from simulation data and extrapolating the fitting to the limit $L \to \infty$. Here a three parameters dependence model given by $f(L) = a + bL^{-\phi}$, as in other previous studies [130], has been assumed. The results of this calculation for the case of the *hex-sq* are $\alpha = 0.53 \pm 0.06$ and $\beta = 0.30 \pm 0.08$. Simulations with the other microstructures provide similar results. Thus, according to the known values for the scaling exponents reviewed in Section 2.4.2, this result confirms that the simulation model reproduces consistently

the asymptotic behavior of the ballistic deposition universality class for every studied microstructure. Moreover, besides serving as a test for the simulation model, this result indicates that the different bonding symmetries have little impact on the asymptotic scaling behavior of the surface morphology during growth under low adatom mobility conditions.

3.2.3 Steady growth bulk properties

Besides its main purpose —checking the potential effects of microstructure on the surface dynamic scaling— the previous result illustrates a well known property of thin film growth under low adatom mobility conditions: after an initial transient regime in which the surface properties vary significantly in time, a persistent steady evolution regime is reached. In order to study consistently the mesoscopic bulk properties of films grown under a wide range of adatom mobility conditions and distinct bonding symmetries, one may be interested in determining if something similar occurs for the evolution of the bulk properties within the corresponding range of substrate temperatures and, if so, under which conditions one can compare different morphologies by assuming that they are obtained under a steady growth regime. The advantage of studying the bulk properties at different temperatures by comparing the results from steady regimes instead of from transients is evident in terms of simplicity. Moreover, this point is particularly relevant when simulating the growth of film structures with a mesoscopic thickness, which requires a careful choice of the system dimensions: the simulation of an excessively large system may lead to impractical time consuming computations, especially at high temperatures, i.e., when many surface diffusion processes are accessible while the film grows up to a mesoscopic thickness. Therefore, before starting any intensive simulation study, it is very convenient to determine what is the minimal mesoscopic system size which represents, at any temperature of interest, the same growth regime —preferably steady— in all cases.

The determination of the minimal conditions for a steady bulk growth regime at any given substrate temperature can be achieved through a preliminary observation of an adequate structural parameter for the bulk, such as some estimation of the film bulk density or of its complement, the porosity. Here the following rough estimation of the bulk density, similar to other definitions of bulk density or porosity proposed in recent

studies [147, 148], is used to characterize the time evolution of the bulk structures:

$$\rho(L,t) = \frac{N(t)}{L\, h_{max}(t)},\qquad(3.8)$$

where L is once again the size of the substrate, $N(t)$ is the number of deposited particles and $h_{max}(t)$ the film thickness, i.e., the maximum height of the structure with respect to the substrate, at time t. Figure 3.10 shows the time evolution of this parameter during the initial phase of growth for different substrate sizes, substrate temperatures and every given microstructure for a fixed mean deposition rate of R=1 ML/s. From this results one can conclude that after approximately 100 seconds the growth process is very close to a steady regime for every microstructure, substrate width and temperature. Figure 3.10(a) also shows that a susbtrate width of $L/a = 160$, i.e., with 80 adatoms in a flat compact arrangement, leads to structures with a density very similar to the corresponding to wider substrates. Other more sophisticated bulk density estimations, such as the accurate calculation of the occupied volume fraction under the single-valued film surface, yields to an equivalent asymptotic behavior. Consequently, results shown in Section 3.2.1, corresponding to the deposition of 15000 adatoms on a substrate with a size of L/a=320 during approximately 94 seconds, can be considered as representative of a steady growth regime as previously announced. Moreover, the comparison between the different transients and steady values of density led by every microstructure observed in Figure 3.10 also provides an illustration alternative to the Figure 3.5 of the distinctive effects of the bonding symmetries on the bulk structure at different temperatures.

Once determined the minimal conditions for reaching a steady growth process in all the cases of interest, the practical conditions for the intensive simulation of mesoscopic bulk morphologies with (1+1)-dimensional microstructures can be selected: in general, the rest of results presented in this section have been obtained with conditions slightly above the minimal required for the steady regime. For instance, for a substrate of L/a=320 and a deposition rate of R=1 ML/s, structures with up to 20000 adatoms have been simulated.

The rough estimation of the bulk density provided by Eq. (3.8) is enough for identifying transients and steady growth regimes. More interestingly, the evolution of such type of simple structural parameter with the susbtrate temperature has proven to roughly exhibit a sigmoidal shape in previous studies [148, 151, 154], presumably related to the bulk transition between Zone I and Zone II morphologies. However, no accurate characterization of such evolution has been performed to date. On the other hand, Figures 3.6 and
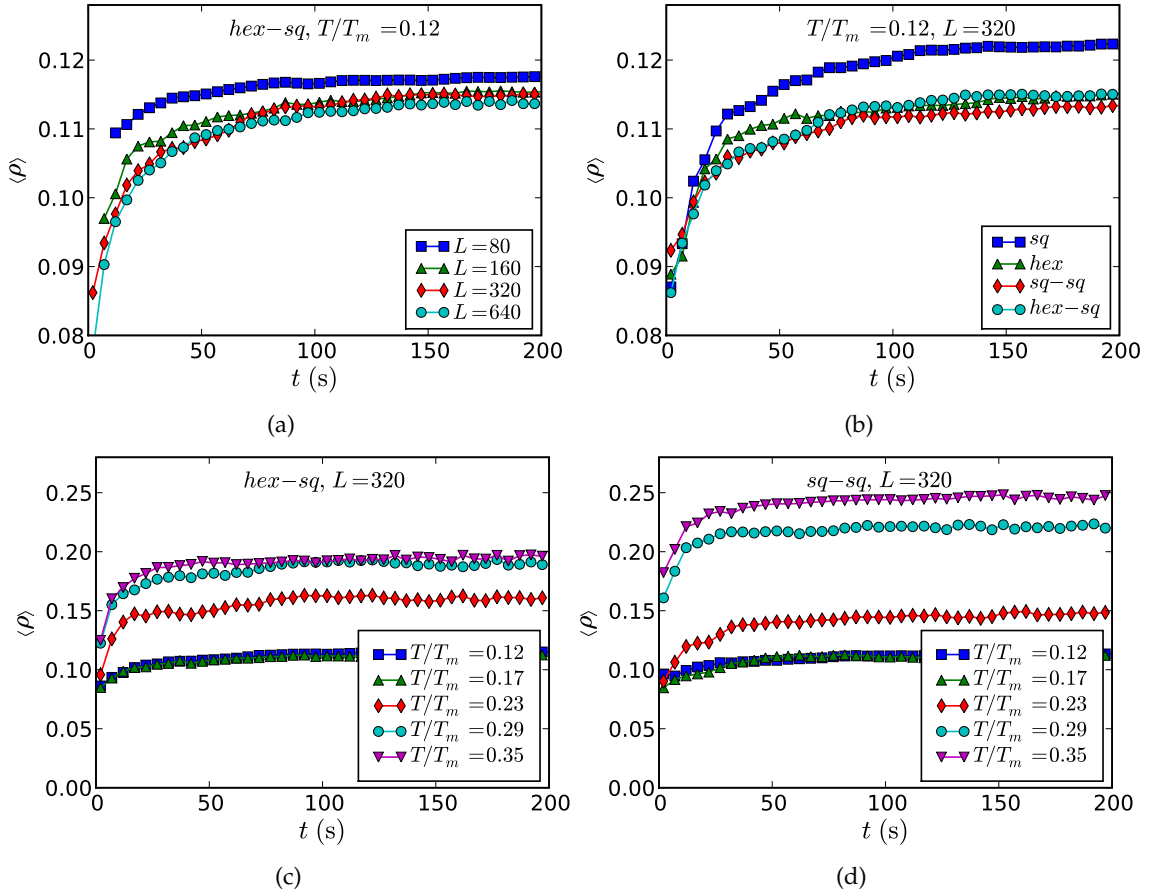
Figure 3.10: Mean values of the bulk density $\langle \rho \rangle$ at the early stages of the growth process, for a fixed deposition rate of R=1 ML/s, as a function of time: (a) For the *hex-sq* microstructure, a reduced substrate temperature $T/T_m = 0.12$ and different substrate sizes. (b) For every type of microstructure with $T/T_m = 0.12$ and a reduced substrate size $L/a = 320$. (c) For the *hex-sq* microstructure with $L/a = 320$ and different substrate temperatures. (d) The same for the *sq-sq* microstructure.

3.8 also show an interesting behavior of the bond fractions with the substrate temperature which points to this type of parameters as good candidates for the characterization of the bulk structural transition. According to these observations, two bulk structural paramaters have been chosen in this study to characterize, by means of refined measures and statistics, the bulk transition between Zone I and Zone II mesoscopic morphologies as different substrate temperatures are selected: the *mean packing density* and the *mean coordination number*.

Mean packing density

The most recent computational studies on bulk properties of thin films and their connection with the surface properties are based on rough estimations of the bulk densities or porosities as the main characterization parameters [146–148,154]. As pointed previously, the value of these rough parameters in simple atomistic simulations tends to increase with the surface diffusion by following a sigmoidal law. Moreover, this sigmoidal behavior can be used to determine the limits between the Zone I and Zone II morphologies, in good agreement with the leading experimental results [48,151]. For this reason, a more refined estimation of the density is expected to be a good statistical parameter for studying the novel and presumably subtle effects introduced by the different bonding symmetries with respect to Müller's well proven and structurally simpler minimal model.

The refined calculation of the morphology densities of films grown at different substrate temperatures and deposition rates has been obtained from a local sampling of the bulk structures. This parameter is called here *packing density* and noted as P in order to clearly distinguish it from the pointed more common and simple estimations of film density as a global volume fraction obtained from some approximation to the geometry of the film free surface. The sampling has been performed by calculating the local volume fraction within a circle of radius $r/a=5$ centered at a randomly selected adatom of the bulk region, i.e., from a central area of the film structure that excludes the lower and upper regions in heights of 0.15 of the total film thickness. In order to perform a detailed statistical examination its behavior, 500 samples of the packing density obtained with this procedure were taken from 10 film structures simulated for every given temperature and deposition rate.

The main Figure 3.11(a) shows the variation in the mean packing density with the deposition parameters, the substrate temperature and the deposition rate, in the (1+1)-dimensional system for three different microstructures and at two different representative deposition rates, $R=1$ and $R=100$ ML/s, whereas the inset shows the corresponding statistical fluctuations of the parameter. The *sq* microstructure has been excluded just for the sake of clarity. As expected, the packing density has in all the cases a minimum value for low substrate temperatures which identifies the dendritic, purely ballistic structures of films grown under very low adatom mobility regimes corresponding to the Zone I. As the selected temperature is increased, the packing density experiences a marked growth until it reaches the saturation value of a locally compact structure, as corresponds either to the

morphologies of compact columns of the Zone II or to a fully monocrystalline structure[3]. By increasing the deposition rate, the sigmoid-shaped curve moves consistently towards higher temperatures. More remarkably, in all the cases there exists a maximum in the statistical fluctuations of the mean packing density within the transition region between the Zone I and Zone II morphologies. This behavior is notably analogous to the observed for the order parameter in a continuous equilibrium phase transition. According to this analogy, one can use the fluctuations maxima to identify the transition points or characteristic temperatures, T_c, which in this system represent the limits between the morphologies of Zones I and II. This criterium for identifying the limit between two structure zones from simulation data is more consistent than the proposed in previous studies [151, 154].
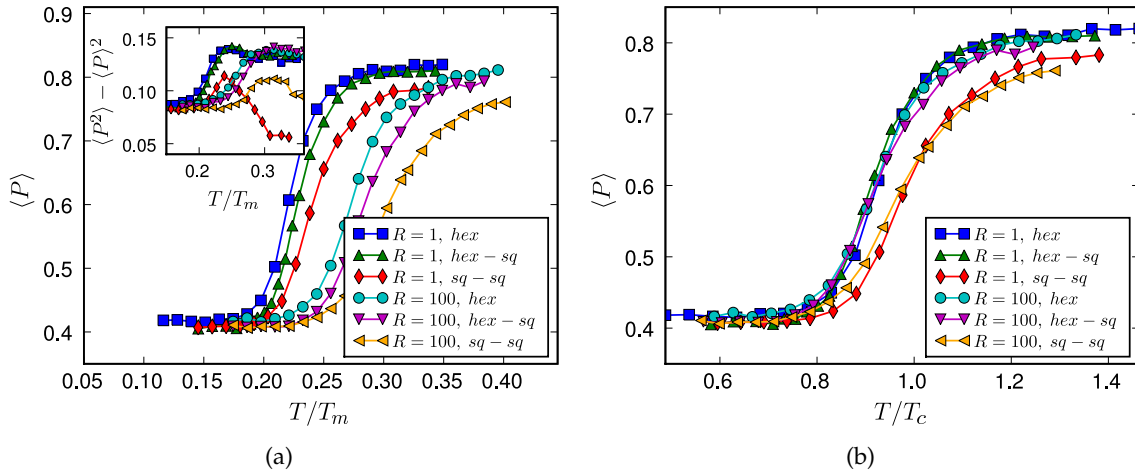
Figure 3.11: (a) Plot of the bulk mean packing density $\langle P \rangle$ versus the substrate temperature T, obtained for different microstructures and at deposition rates, R=1 and R=100 ML/s. The maxima of their statistical fluctuations (inset figure) determine the charecteristic transition temperature of each curve. (b) Collapse of the mean packing density curves onto a master curve when rescaled according to the characteristic transition temperature T_c.

Despite the described parametrization neither corresponds physically to a true equilibrium phase transition nor is an adequate characterization of a non-equilibrium phase transition, the analogy between the behavior of the steady mesoscopic morphologies and a continuous equilibrium phase transition is clearly useful and will be assumed as the approach to analyze the remaining results to be presented in this section. For instance,

---

[3]To understand this point it must be noted that the calculation of the packing density based on a local sampling centered in occupied adatom positions tends to ignore the instertitial voids between compact structures in the film.

the previous treatment of the mean packing density as a true order parameter can be extended even further and provide additional insights: the transition curves of the mean packing density can be rescaled with their corresponding transition temperatures, T_c, in order to obtain their collapse. However, such collapse leads to two different master curves depending on the maximum coordination number of the underlying bonding symmetries, as shown in Figure 3.11(b). This result confirms a distinctive evolution of the film morphologies in the vicinity of the limits between structure zones depending on the maximum coordination number, as anticipated by the qualitative observation of the film samples shown in Figure 3.4. This is the first clear indication of a significant effect from the material microstructure on the evolution with the main deposition parameters of the mesoscopic bulk morphologies of thin films.

These numerical experiments allow the construction of an approximate phase diagram for the deposition parameters corresponding to Zone I and Zone II (1+1)-dimensional morphologies from the characteristic transition temperatures. This diagram is shown in figure 3.12. One can observe that the limits between Zone I and Zone II are very similar for every given microstructure, except for the case of the purely square one, the sq. This result can be attributed to the effect of the transparent hops to second-nearest neighbor positions allowed just for this case, resulting in a drastic reduction in the transition temperature.

In summary, the effect of the maximum coordination number of the different bonding symmetries is shown to be significant when one considers how the film morphology
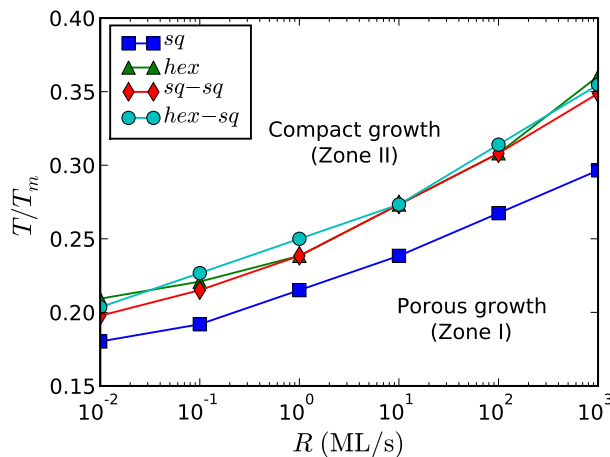
Figure 3.12: Phase diagram for the structure zone I and structure zone II growth regimes obtained for each given microstructure.

changes with the deposition parameters close to the limit between structure zones, but not for determining the position of such limit in the space of the deposition parameters.

Mean coordination number

The other quantity used in this study to characterize the evolution of the film morphologies with the deposition parameters is the mean coordination number, c_n. This parameter can be easily obtained from computer experiments by simply averaging the number of bonds, i.e., the number of occupied active positions, of each adatom from 10 different film samples simulated for every given temperature and deposition rate. The numerical data also allow to compute separately such statistics for the bulk and the surface adatoms, which are identified respectively with the "buried" and "non-buried" adatoms as defined by the criterium introduced in Section 3.1.1.

Figure 3.13 shows the results of these measurements as a function of the substrate temperature for a deposition rate of R=1 ML/s. In the figure the mean coordination number obtained for just the bulk adatoms (bulk) has been distinguished from the one obtained for all the adatoms in the sample (total). For the sake of clarity, the results for the microstructuctures with a maximum coordination number 4 and the corresponding to a maximum coordination number 6 have been plotted separately. Qualitatively, these parameters exhibit a behavior very similar to the mean packing density: both the total and
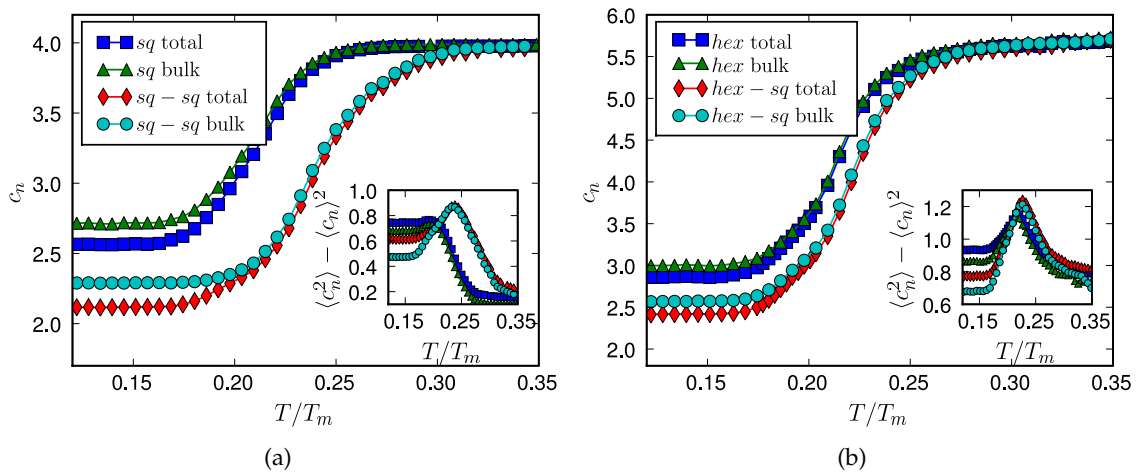
Figure 3.13: Total and bulk mean coordination number as a function of the substrate temperature for a deposition rate R= 1 monolayer/s, and their statistical fluctuations (inset): (a) *sq* and *sq–sq* microstructures; (b) *hex* and *hex–sq* microstructures.

the bulk mean coordination numbers change from relatively small values at low substrate temperatures to the maximum value allowed by each underlying microstructure at high temperatures. More precisely, for the *sq* and *sq-sq* microstructures, for which the film eventually forms a fully compact monocrystal at high temperatures, the mean coordination number reaches its maximum value of 4 (Fig. 3.13(a)), whereas for the *hex* and *hex-sq* microstructures the maximum value achieved is slightly below its maximum theoretical value of 6 (Fig. 3.13(b)) since this parameter detects the reduced coordination led by the interstitial voids present in the columnar morphologies. The resultant evolution curves have a rather more complex shape and are more sensitive to the different microstructures than the analogous curves obtained for the mean packing density. The existence of a small range of temperatures below the characteristic transitional temperature where the mean coordination number seems to increase linearly is particularly remarkable. The location of the maximum of the corresponding statistical fluctuations (shown in the insets) is similar for the bulk and total values. The characteristic temperatures corresponding to the fluctuations maxima for the different microstructures considered are slightly lower than the characteristic temperatures derived from the analysis of the mean packing densities: whereas the characteristic temperatures obtained from the mean coordination number are found within a range from $T/T_m = 0.19$ to 0.24, the corresponding to the mean packing density were found between $T/T_m = 0.23$ and 0.25. As one might expect, the bulk values of the mean coordination number are higher than the total values for every substrate temperature, but it is noticeable that the differences are considerably larger at low temperatures where the surface diffusion is weak or negligible.

The complex behavior observed in the mean coordination number can be better understood by further analysis of this parameter restricted to only the surface adatoms. The results for a deposition rate of R=1 ML/ s are plotted in Figure 3.14. One can observe that the mean coordination number of a surface adatom grows with the substrate temperature in a rather different way in comparison to what happens in the bulk and with the total mean coordination numbers: in this case the parameter exhibits a stronger dependence on the microstructure and a more complex behavior of its fluctuations. In particular, there are two maxima in the fluctuations associated to the two combined microstructures, i.e., the *sq-sq* and the *hex-sq* microstructures. These double peaks are found at $T/T_m = 0.19$ and $T/T_m = 0.28$ for the *sq-sq* case and at $T/T_m = 0.19$ and $T/T_m = 0.22$ for the *hex-sq*, whereas there is no clear maximum for the *sq* microstructure and a single peak at $T/T_m = 0.20$ is observed for the *hex* one. The location of the characteristic temperatures
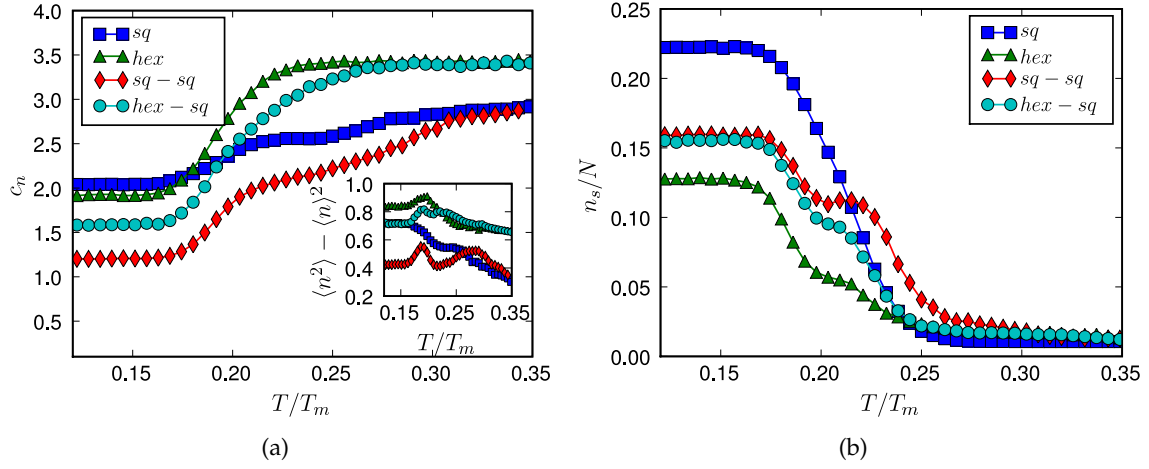
Figure 3.14: Statistics for the surface adatoms: (a) mean coordination number and its statistical fluctuations (inset) versus the substrate temperature at a deposition rate $R= 1$ monolayer/s for the different microstructures; (b) total number of surface adatoms, n_s, divided by the total number of adatoms, N, under the same conditions.

given by these maxima, considering the first peak when double peaks are present, is in every case slightly below the characteristic temperatures associated to bulk and total values. Therefore, the coordination transition from low to high values takes place at lower temperatures in the surface than in the bulk region. This behavior can be understood by noting that surface adatoms cannot, by definition, reach the maximum coordination number allowed for the bulk adatoms for any given microstructure. Consequently, surface adatoms reach their maximum coordination at lower temperatures.

In addition to this intrinsically complex behavior, the statistical contribution of the surface adatoms to the averaged total coordination number is not constant along the transition curves since, as is shown in Figure 3.14(b) , the number of surface adatoms decreases with substrate temperature. This is an evident consequence of the film compactation with the temperature and the "non-buried" criterium for the definition of surface adatoms and finally explains the differences between the bulk and total curves observed in Figures 3.13(a) and 3.13(b) at low temperatures.

3.3 Simulations in (2 + 1) dimensions

The simulations and analysis approach performed for the (2+1)-dimensional microstructures are analogous to the already presented for results in (1+1) dimensions. Despite the

abstract perspecive assumed in this study and the increased computatinal cost implied by these simulations, it is worth checking if the interesting and subtle effects caused by the different microstructures on the bulk mesoscopic morphologies are also observed in higher system dimensions.

Mesoscopic morphologies

Figure 3.15 shows two sequences of mesoscopic film morphologies obtained at different substrate temperatures and corresponding to the two (2+1)-dimensional bonding symmetries defined in Figure 3.2, the *3d-hex* and the *3d-cs* microstructures. The samples have been obtained from the deposition of 50000 particles at a fixed mean rate of $R=1$ ML/s onto a flat square substrate, formed by 40x40 adatoms disposed in a close packed hexagonal —for the *3d-hex* microstructure— or square lattice —for the *3d-cs* one. According to an analysis analogous to the presented in Section 3.2.3, these system parameters have been found to be in the lower limit of bulk steady growth regimes.

As previously observed in the (1+1)-dimensional case, low-density dendritic structures are found at substrate temperatures at which surface diffusion is negligible. As the substrate temperature increases, diffusion becomes significant and the film tends to be formed of more compact structures. From a careful qualitative observation of such samples, one can conclude that the microstructure with a smaller value of the maximum coordination number —the *3d-cs* symmetry, with a maximum value of 6— shows more compact structures at the same substrate temperature than the microstructure with a higher maximum coordination number —the *3d-hex* microstructure, with a maximum value of 12. Another characteristic that can be observed in a direct inspection of the film morphologies is once again the development of columnar structures with small interstitial voids at high temperatures.

Structural parameters

As the inspection of the film samples suggests, a statistical behavior similar to the observed for the cases in (1+1) dimensions has been found in general for the structural parameters of the (2+1)-dimensional morphologies. The results for the evolution with the substrate temperature of the mean packing density for two deposition rates, $R=1$ ML/s and $R=10$ ML/s, are shown in Figure 3.16. The sigmoidal shape for such evolution is reproduced for each microstructure, but it displays a more pronounced disparity between the microstructures due to the increased difference in the maximum density allowed in
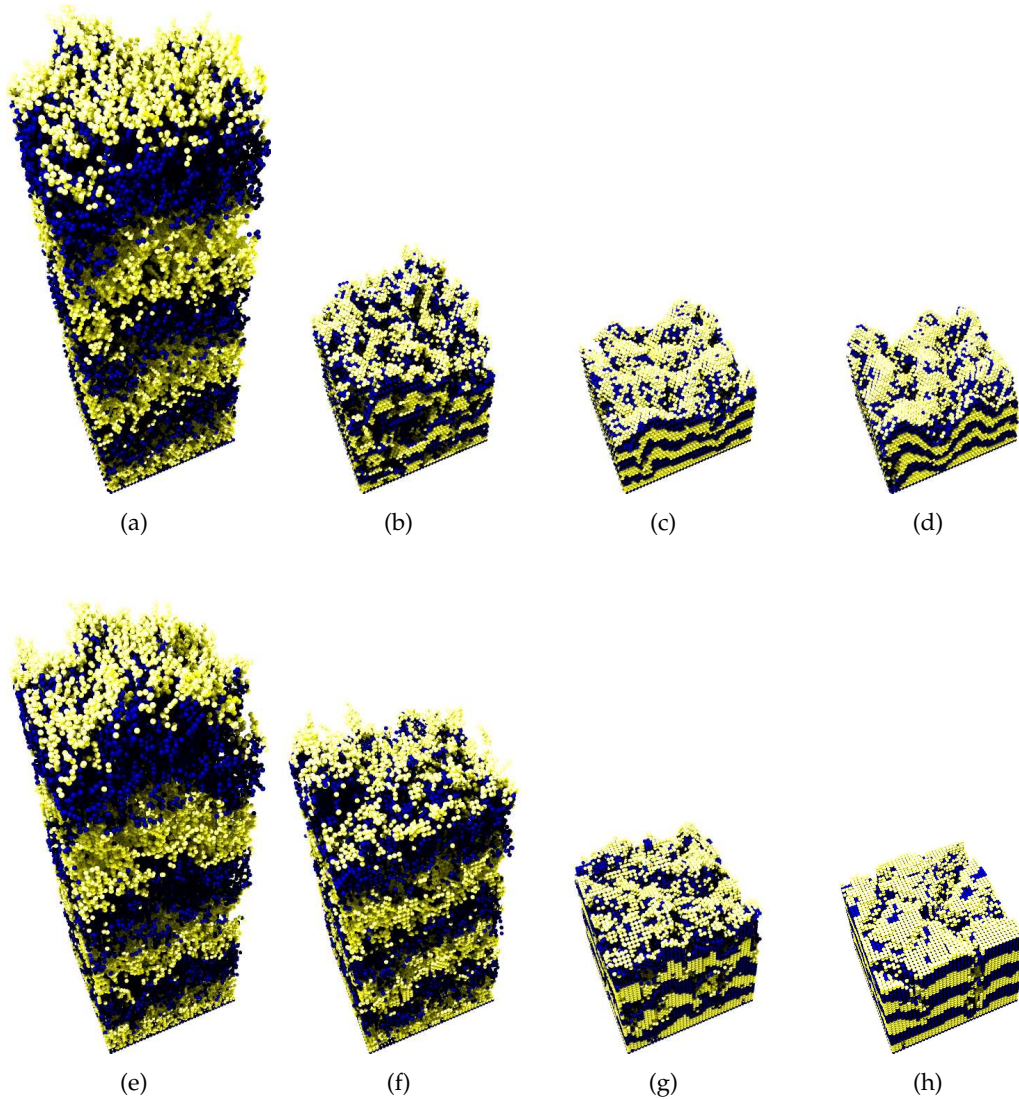
Figure 3.15: Examples of mesoscopic film morphologies obtained for the *3d-hex* (upper row) and *3d-cs* (lower row) (2+1)-dimensional microstructures from the deposition of 50000 adatoms onto a flat substrate at a fixed mean deposition rate of R= 1 ML/s and different substrate temperatures: (a) and (e) T/T_m=0.17; (b) and (f) T/T_m=0.23; (c) and (g) T/T_m=0.26; (d) and (h) T/T_m=0.30.

each case, as one can observe in Figure 3.16(a). The characteristic temperatures defining the limits between Zone I and Zone II morphologies, T_c, determined by the maxima in the fluctuations, confirm the previous qualitative observation that the transition for the *3d-cs* microstructure takes place at lower temperatures. Again, the rescaling of the curves

with their corresponding values of T_c leads to their collapse onto a master curve for each type of microstructure.
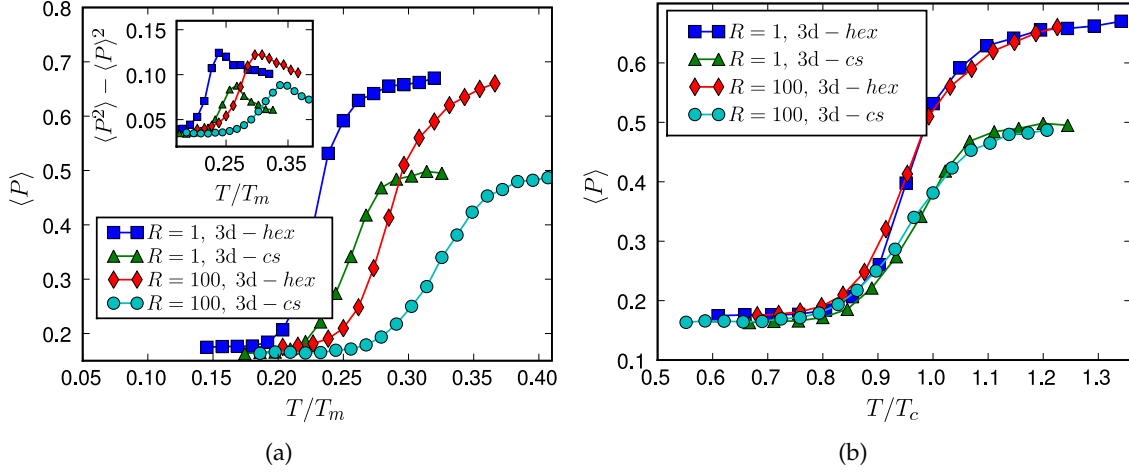
Figure 3.16: (a) Mean packing density and its fluctuations (inset figure) as a function of the substrate temperature for the (2+1)-dimensional microstructures and deposition rates of $R = 1$ and $R = 100$ ML/s. (b) Collapse of the same curves when rescaled with the characteristic temperatures, T_c.

Finally, the behavior of the mean coordination number in (2+1) dimensions has been found to be qualitatively the same than the observed for the low dimensional cases: an slight anticipation of the morphology transition in the surface adatoms as the substrate temperature increases is obtained again.

In conclusion, the effects of the different coordination numbers of microstructures found in (1+1) dimensions persistently manifest in (2+1) dimensions.

3.4 Discussion and concluding remarks

The study presented in this Chapter has addressed the question of how the maximum coordination number allowed by the bonding symmetries of the deposited materials affects the mesoscopic morphologies of thin solid films grown by a simple physical vapor deposition process. This is an early effort towards the accurate mesoscopic modeling of non metallic and/or non crystalline materials, eventually with a strong bond directionality. With this purpose, a computational simulation model has been developed and intensive numerical experiments have been performed.

The study has assumed an abstract perspective that is not intended to predict quantitatively the experimental properties of any particular thin film system. Instead, the goal was to obtain a qualitative description of the mentioned effects on the evolution of the morphologies of thin films with the relevant deposition parameters as described by the simplest Structure Zone Model. In particular, the study has been focused on the bulk properties of the film mesoscopic structures. In order to achieve this objective, a careful tradeoff between the incorporation of specific and generic modeling approaches for the principal mechanisms of the system has been necessary in the development of the simulation model. On the one hand, a specific accurate empirical model for the mesoscopic simulation of surface diffusion of a given material, chosen to be Nickel, has been necessary in order to reproduce the experimental limits between Zone I and Zone II morphologies, which are well known for that particular case, because of the strong dependence of the simulation results on the accuracy of the diffusion model. On the other hand, a generic novel approach for the definition of arbitrary bonding symmetries has been introduced in the simulation model, which has been used to study the effects of different (1+1) and (2+1)-dimensional abstract bonding symmetry definitions.

In order to study consistently the mesoscopic bulk properties of the growing films, the conditions for reaching a steady growth regime have been determined for every case. This determination has allowed the optimization of the computing costs associated to the simulated system size for obtaining an adequate characterization of the steady bulk properties. The smooth evolution between dendritic, low density structures obtained at low substrate temperatures, commonly identified as Zone I morphologies, and the densely-packed non-competing columnar structures associated to high substrate temperatures and Zone II morphologies are reproduced by the model. Despite that the diffusion model does not include any explicit interlayer energy barrier, the microstuctures with allowed bonding positions in the corner of an interlayer step present remarkably pronounced columns in a wide range of substrate temperatures. This anticipates the possibility of formation of columnar morphologies in a non-equilibrium growth system of physical deposition and surface diffusion, due to purely dynamical effects. This finding has been confirmed by very recent independent experiments.

The novel approach for the definition of bonding symmetries has proven to reproduce epitaxy and crystalline texture competition effects, so far only reproduced in multilattice schemes which hardly can represent local lattice frustrations.

The characterization of the evolution of the bulk structures with the deposition param-

eters has been performed from a careful statistical estimation of two refined structural parameters: an accurate local estimation of the fraction volume occupied by adatoms, the mean packing density, and the mean coordination number of all the adatoms in the sample structure. The behavior of these structural parameters calculated for steady growth regimes has shown a strong analogy with the corresponding to the order parameter of an equilibrium continuous phase transition. Of course, the evolution with the fixed deposition parameters of the film structures grown from the different associated non-equilibrium processes does not represent a true equilibrium continuous phase transition. Neither the structural parameters could be considered adequate order parameters, since they are intensive parameters with bounded fluctuations which, for steady growth cconditions, do not exhibit any dependence with the system size as required by a true critical behavior. However, the mere analogy is shown to be useful in its own right, simplifying the analysis and providing subtle insights to the effects of the different maximum coordination numbers associated to distinct bonding symmetries.

The analysis of the behavior of the structural parameters as a function of the deposition parameters shows the existence of significant quantitative effects of the distinct bonding symmetries in the vicinity of the boundaries between structure zones I and II. The microstructures with a lower maximum coordination number, both in (1+1) and (2+1) dimensions, tend to be relatively more compact under the same deposition conditions than the corresponding to a higher maximum coordination number. In all cases, the mean packing density presents a maximum in its fluctuations which can be identified as the limit between the Zone I and Zone II characteristic bulk morphologies, providing a consistent and accurate criterium compared to the previous inconsistent criteria used by different authors. The position of these boundaries in the deposition parameters space is rather similar for all the microstructures and consistent with previous theoretical and experimental results, except for a case in which the dynamical rules for surface diffusion are significantly different. The mean coordination number shows even a stronger influence of the different microstructures, displaying in general a less smooth behavior. It also evidences that the surface adatoms tend to reach their maximum coordination number at lower temperatures than their bulk counterparts.

In general, the results obtained in these simulations confirm the robustness of the simplest Structure Zone Model, showing that the boundaries between different structure zones depend mainly on the diffusion mechanisms, whereas remaining rather independent from the bonding symmetries. However, the latter may determine the quantitative

behavior of the structural evolution near to the zone boundaries.

4 Magnetic filaments

In 1963 Salvatore Bellini, from the Istituto di Microbiologia of the University of Pavia, made the first observation of the existence of some anaerobic bacteria found in bog sediments with an unique ability to remain aligned with the Earth's magnetic field [164, 165]. In their internal technical reports, he proposed the name *magnetosensitive bacteria* for such organisms. However, his finding was a result of an accidental observation and remained unpublished until further observations were carried out and published by the microbiologist Richard Blakemore in 1975 [166]. Blakemore coined the generic and currently accepted terms of *magnetotactic bacteria* to name such magnetosensitive unicellular organism. After Blakemore's observations, magnetotactic bacteria have become a subject of increasing research interest, especially from a biophysical perspective.

The ability of magnetotactic bacteria to align with an external magentic field is based on the presence of a number of intracellular mineral bodies, or mineral organelles in their cytoplasm. These organelles are formed by solid crystals of different materials, such as magnetite (Fe_3O_4) or greitite (Fe_3S_4), with a permanent magnetic moment at room temperature. Figure 4.1(a) shows a micrograph of a magnetotactic cell, with its magnetic organelles as dark spots. Such magnetic organelles, called *magnetosomes*, are sinthetized by bacteria in many different nanometer-sized shapes [167], as illustrated by Figure 4.1(b). However, in most cases they are found to form straight chains with all the magnetic moments aligned and adding together into a net moment high enough to allow the passive rotation of the cell as a result of its interaction with the geomagnetic field. Such straight chains of aligned permanent magnets are not stable structures [168] and require a surrounding network of cytoskeletal filaments to keep them as an essentially one-dimensional system [169].

For many years the study of magnetotactic bacteria has been an interesting subject in the context of different biophysical transversal pieces of research, such as those on biomineralization including applications to the study of evolution and the origin of life [172, 173]. Magnetosomes have been also suggested as cellular biomarkers [174]. Most remarkably, the magnetic structures found within magnetotactic bacteria have inspired
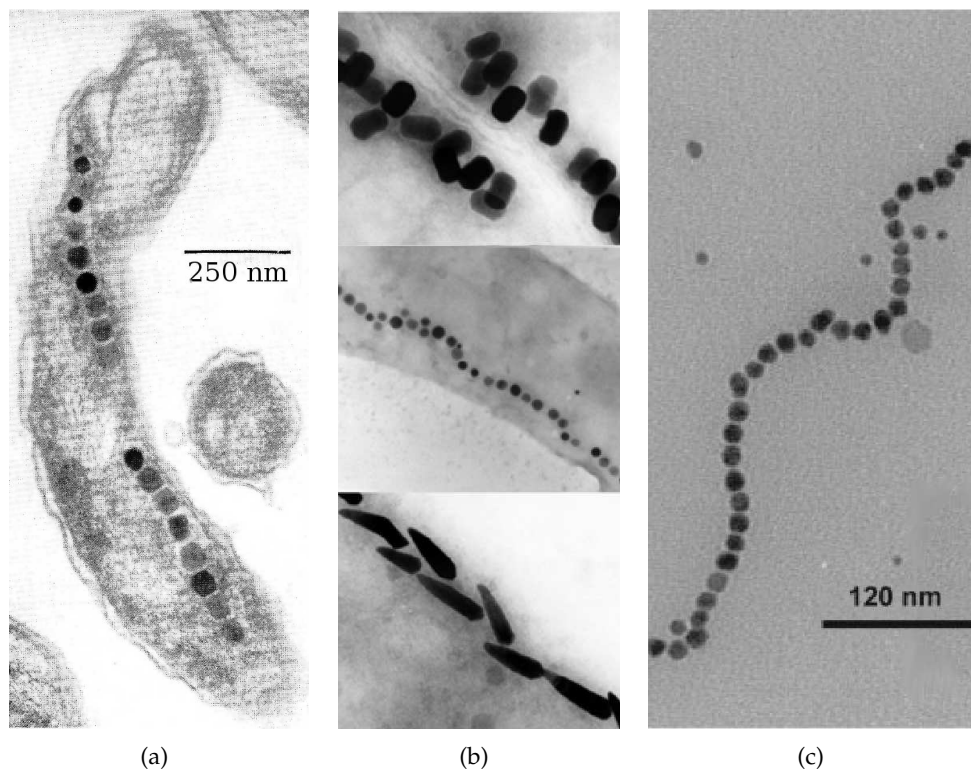
Figure 4.1: (a) Early electron micrograph of a magnetotactic bacteria, *Magentospirillum Magneto-tacticum Strain* (MS-1), with aligned magnetosomes as dark spots. After [170]. (b) Different examples of magnetosome morphologies within magnetotactic bacteria. From top to bottom: prismatic, cubo-octahedral and bullet-shaped crystals. After [167]. (c) Synthetic magnetic filament prepared from the self-assembly of polymer-coated cobalt ferromagnetic particles with a diameter of approximately 20 nm. After [171].

new concepts with a great potential for novel technological applications outside the field of biophysics.

In general, the study of magnetic systems is an important research topic in nanoscience and nanotechnology. For instance, molecular and polymeric magnetic systems have attracted increasing interest in recent years [175–177]. Nevertheless, the small scale of molecular magnetic systems imposes limitations to their magnetic properties. In particular, it is extremely difficult to observe significant magnetic properties in molecules at room temperature [176]. Instead, submicrometric ferromagnetic crystals exhibit remarkable magnetic moments under these conditions. For this reason, the idea of having a supramolecular mesoscopic system formed by a chain of submicrometric permanent magnets linked by polymers or other molecules to form a flexible or semiflexible fila-

ment, is particularly attractive. This idea has led to the recent appearance of shyntesis and modeling methods for such type of mesoscopic magnetic structures, called generically *magnetic filaments*. Figure 4.1(c) is an example of an artificial magnetic filament synthesized from cobalt nanometric spherules coated with polymers.

The key aspect for the technological application of magnetic filaments is the fact that their behavior can be accurately controlled by appropriate external magnetic fields without affecting the surrounding system constituents, at least for most materials and substances found in biological and technological systems. Due to to this unique advantage, magnetic filaments can be used in multiple and diverse technological applications including biomedical uses, data storage, chemical and micromechanical nanosensors, patterned nanometric watermarks or actuators in microfluidics applications.

Many of the potential applications of magnetic filaments involve the interaction of the magnetic chain with different surfaces. Therefore, the understanding of the behavior of such magnetic chains in the neighborhood of a surface is crucial for the development of new applications. To address this problem one can take advantage of the previous extensive studies on the interaction of long flexible or semiflexible chains with surfaces performed in the past within the field of polymer physics. Despite the differences in the size scale and the presence of long-ranged anisotropic magnetic interactions even in absence of external fields, one might expect that many modeling tools from polymer physics would be useful in the study of magnetic filaments near attractive surfaces. From this perspective, the next chapter presents a computational study of the effects of the intrinsic magnetic interactions on the adsorption transition of a magnetic filament, considered as a mesoscopic polymer-like structure, into an attractive flat surface.

The next sections within this chapter provide further insight on the unique properties of nanometric permanent magnets and magnetic filaments, their synthesis methods and the most prominent modeling advances in the field, as well as the basic theoretical concepts related to the study of transitions in polymer-like structures near attractive surfaces.

4.1 Ferromagnetic nanocrystals: a matter of size

Nanoparticles with ferromagnetic or ferrimagnetic properties, i.e., with a permanent magnetic moment even in absence of external fields, are the basic building blocks of magnetic filaments, playing a role similar to the monomers in a polymer. The synthesis of ferromagnetic nanoparticles, either from biomineralization in magnetotactic bacteria

[178] or by more conventional chemical methods [179–182], is subjected to the strong dependence on the system size exhibited by the magnetic properties of materials at submicrometric scales [183].

In general, bulk magnetic materials are composed of different regions with an uniform magnetization. These *magnetic domains* have typical sizes in the range of tens to few hundred nanometers. The global magnetic properties of a bulk magnetic material depends on the relative orientations of their constituent domains. For instance, in absence of any external field, ferromagnetic and ferrimagnetic materials have their magnetic domains mostly aligned in a particular direction, leading to a net magnetic moment. In paramagnetic materials instead the domains are highly disordered and the net magnetic moment is zero, except when an ordering external field is applied.

Figure 4.2 is a qualitative scheme of how the magnetic behavior of a ferromagnetic material varies with its characteristic size. By decreasing the size, the total amount of magnetic domains in the material also decreases. As a side effect, its *coercivity* —the resistance of the material to become permanently demagnetized by a strong enough external field— increases. This tendency persists until the diameter of the particles reaches the typical domain size D_S of the material. At such critical size the material becomes a single-domain particle and its coercivity is maximal. For even smaller sizes, the coercivity of the
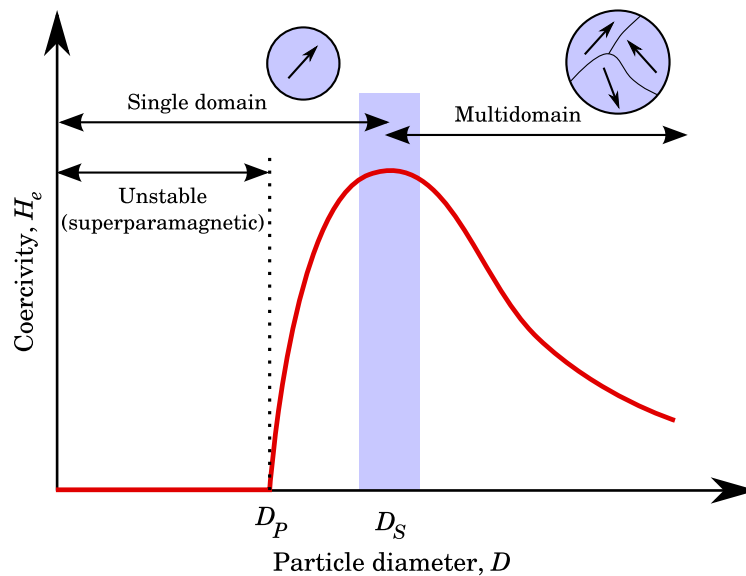
Figure 4.2: Qualitative scheme of the magnetic behavior of a ferromagnetic material as a function of its characteristic size.

single-domain particle decreases due to the increasing relative relevance of the effects of thermal fluctuations. At a critical diameter, D_P, the coercivity vanishes and remains zero for even smaller particles. At these sizes the particles become superparamagnetic which means that the magnetization is reversed spontaneously as a thermally activated process with a given mean rate, which leads to zero net magnetization on average.

Obviously, the optimal condition for a ferromagnetic nanoparticle intended for technological applications involving either unstructured powders or defined structures such as magnetic filaments, is to constitute a single magnetic domain with a maximum coercivity. In other words, such particles should have the same diameter as the typical domain size.

4.2 Synthetic magnetic filaments

The synthesis of magnetic filaments by linking submicrometric magnetic particles with macromolecules is a recent experimental achievement of supramolecular chemistry. In essence, the fabrication methods are bottom-up processes in which the magnetic beads are coated with appropiate bridging molecules responsible of the chemical assembling in a one-dimensional chain. The successive improvements of such methods have led to the synthesis of filaments with increasing lengths. However, the fabrication and manipulation of magnetic beads for their assembly in magnetic filaments has followed also a top-down approach, starting with micrometric beads and progressively reducing their sizes and enhancing their magnetic properties.

In the first seminal works, from the lates 1990s, micrometric latex beads filled with paramagnetic materials were linked with polystyrene [184, 185]. The use of DNA as bridging molecules was also achieved for the first time using micrometric paramagnetic beads in 2005 [186]. The first magnetic filaments created with submicrometric beads (0.5–0.8 μm) were reported in 2003 [187]. In 2005 were announced magnetic filaments with mesoscopic lengths up to 50 μm, whereas arrays of filaments with lenghts up to 200 μm and ratios of chain length to bead diameter as large as 125 were obtained in 2007 [188, 189]. Filaments with bead diameters below 50 nm were achieved in next years by using materials with strong ferromagnetic properties such as magnetite and cobalt [171, 190–196]. In 2010, the one-dimensional assembling of ferromagnetic particles of cobalt with a size as small as 23.5 nm has been obtained [197]. These examples illustrate the recent origin and the impressive experimental expansion of the subject.

The synthesis of mesoscopic low-dimensional structures and in particular, the assembly of chain-like mesoscopic systems is a very active research subject beyond the scope of magnetic filaments. The development of novel assembly methods for non-magnetic materials susceptible of being applied to the synthesis of magnetic filaments is an alternative source of improvements. For instance, a new method for a very selective end-to-end assembling of anisotropic gold-coated nanometric particles reported very recently [198] could be a promising approach for the fabrication magnetic filaments.

4.3 Modeling approaches and basic concepts from Polymer Physics

Besides the improvements in their synthesis methods, the characterization of the properties of magnetic filaments has been so far mainly limited to the study of few specific aspects such as the behaviour of single magnetoresponsive filaments far from any surface as a function of the external magnetic field [199–204], the application of magnetic filaments as magnetic micro-swimmers in the presence of non steady external fields [205–207] and the study of the equilibrium shapes of twisted magnetic filaments [208]. These studies were based on equilibrium Monte Carlo simulations with in-lattice classical spin chain models, on dynamical simulations with simple analytical models based on Kirchhoff elastic rods [209, 210] —a frequently used mechanical approach for the modeling of elastic filaments— and on experimental measurements of the elastic properties of different types of magnetic filaments.

On the other hand, there exists a more mature research field in which the behavior of chains formed by discrete structural units linked with deformable bonds has been studied for many years: Polymer Science. Of course, polymers are large molecules composed by small, usually repeating, molecules linked by covalent bonds, not supramolecular systems. However, they are complex enough to require in many cases statistical approaches and coarse-grained models to study their physical properties. Thus, it is reasonable to expect that at least the most abstract modeling approaches from polymer physics would be useful to the study of magnetic filaments. Moreover, in spite of the difference in scale, one would expect that both systems share some physical properties that can be present at different scales. In particular, the central question addressed by the work presented in the next chapter —the characterization of the adsorption process of a semiflexible chain by an attractive surface— has been extensively studied in polymer systems and, therefore, the current knowledge on polymer physics under analogous conditions has been used as

a the starting point for the modeling approaches applied to the present study.

The simplest way to describe polymer chains is the *ideal chain* or *freely jointed chain* model [211]. In such a model the monomers are represented as connected immaterial one-dimensional rigid rods with a fixed length and random orientations. No interactions between monomers or with the background medium —usually a solvent— are considered. Therefore, the structure has no other geometric constrains than the monomer sequence connectivity and the chain behaves statistically as a *random walk*, including the possibility of overlaping monomer positions. In polymer physics, this type of structure is also known as *random coil*.

Diverse variations of the ideal chain model include geometric constrains in the monomer orientations in order to represent the experimental bonding angles and, eventually, the flexibility of the bonds. Alternatively, the polymer can be represented by means of a continuous flexible or semiflexible filament. In general such simple models disregard any long range interaction to facilitate their analysis which, in many cases, lead to known analytical solutions.

Despite its simplicity, ideal models are able to reproduce some universal properties exhibited by real polymers under certain conditions. However, in most cases it is necessary to consider non ideal effects to model the actual behavior observed in real polymers.

4.3.1 Non-ideal mechanisms affecting real polymers

In general, non-ideal chain properties arise from diverse types of long range effects, such as effective interactions between non bonded monomers —which may be distant in the chain sequence but close in space— or between monomers and the surrounding solvent particles. The most relevant of such non-ideal effects, namely, the effects of excluded volume and monomer-monomer and monomer solvent interactions, are described below.

Excluded volume effects

One of the main effects on real polymers disregarded by ideal models is the fact that monomers are not zero or one-dimensional entities, but have a dimension and, therefore, actually occupy some volume. Steric effects due to the electrostatic repulsion between the electronic clouds found around the molecules forbid the spatial overlap of different monomers in the chain. In other words, a monomer can not occupy the volume occupied by other monomers. Therefore, this *excluded volume* effect reduces the total number of configurations available to a real polymer, forcing it to adopt, on average, structures more

expanded than the ones corresponding to an ideal chain. Statistically, the configurations of a real polymer subject to excluded volume effects differ from a pure random walk, tending instead to resemble random trajectories which avoid self overlaps. This trajectories are known as *self avoiding random walks* (SAW) [211, 212].

Van der Waals interactions and solvent effects

In real polymers, besides the covalent bonds that keep the chain connectivity and the excluded volume effects, there may also exist weak attrative forces of Van der Waals type between monomers that are relatively close in space. Monomers have also interactions with the solvent that can be either attractive or repulsive. In fact, the nature of such interactions depends on the system's temperature and on the chemical composition of the polymer and the solvent altogether. These effects strongly influence the global structure of the polymer.

When the system composition and temperature lead to an effective attraction between monomers and solvent, the system is considered to be under *good solvent* conditions and the resultant polymer tends to adopt a coil structure that maximizes the contact between monomers and solvent. Therefore, the contour volume of the polymer tends to be higher than the corresponding to an ideal chain.

On the other hand, *poor solvent* conditions correspond to an effective general attraction between monomers. When poor solvent conditions are imposed, the polymer tends to adopt a compact, globule-like structure which minimizes the contact between monomers and solvent.

In some systems it is possible to observe a transition between the expanded coil structures typical of a good solvent and the globule structures led by a poor solvent by varying the system temperature [213, 214]. This coil-globule transition has been the subject of extensive studies in Polymer Physics. One of their most interesting properties is that at some point of the transition the system shows a mutual cancellation between the excluded volume effects and the effective attraction between monomers, which to an ideal behavior of the chain. Under such specific conditions, known as *theta conditions* or *theta point*, the polymer is exclusively dominated by entropic effects and the experimental measurement of local properties becomes easier [215].

4.3.2 Structural parameters

From the previous discussion, one can deduce that polymers present many different time-varying conformations depending on their nature and conditions. Consequently, the structural characterization of polymers, usually carried out by means time and/or ensemble averages, is an essential point in the study of their behavior. For this purpose, different structural parameters are commonly used to describe the polymers structures and universal properties. The study presented in the following chapter makes reference to some of the most common structural parameters used polymer physics which are defined next.

Gyration tensor and derived parameters

The gyration tensor, $G_{\alpha,\beta}$, describes the variance, or second moments, of the positions of a set of immaterial points. It is equivalent to the inertia tensor obtained with a constant value of mass for every point. Different structure descriptors can be deduced from the gyration tensor to characterize molecular structures and, particularly, to describe macromolecules and polymers. In the latter case, the tensor is constructed for the positions of the chain monomers.

The terms of the gyration tensor for a polymer chain of N monomers are defined as:

$$G_{\alpha,\beta} = \frac{1}{N} \sum_{i=1}^{N} S_i^{\alpha} S_i^{\beta},$$

(4.1)

where $\alpha, \beta = x, y, z$ are the cartesian axes and $\mathbf{S}_i = \mathbf{r}_i - \langle \mathbf{r} \rangle$ is the displacement vector from the average position of the set of monomers, $\langle \mathbf{r} \rangle = \frac{1}{N} \sum_{j=1}^{N} \mathbf{r}_j$, to the position of the i-th monomer, $\mathbf{r}_i$.

The gyration tensor is a symmetric and therefore diagonalizable matrix. Their ordered eigenvalues are called principal moments of the tensor:

$$\lambda_x^2 \leq \lambda_y^2 \leq \lambda_z^2.$$

(4.2)

These principal moments can be combined to obtain the diverse structural parameters mentioned above, such as the asphericity, the acylindricity or the relative shape anisotropy. However, the most simple and widely used —in polymer physics— of the structural parameters that can be obtained from the gyration tensor is the *radius of gyration* of the chain. The quadratic radius of gyration is simply defined as the sum of the

principal moments of the gyration tensor obtained for the monomer positions:

$$R_g^2 = \lambda_x^2 + \lambda_y^2 + \lambda_z^2 = R_{xx}^2 + R_{yy}^2 + R_{zz}^2. \tag{4.3}$$

The radius of gyration is a simple structure descriptor that roughly measures the dimensions of the chain. More interestingly, it can be determined experimentally for real polymers by radiation scattering methods [212]. When the spatial distribution of the chain monomers is isotropic, the quadratic radius of gyration can be calculated without the need of explicitly computing the gyration tensor and their eigenvalues [211]:

$$R_g^2 = \frac{1}{2N^2} \sum_{i,j} (\mathbf{r}_i - \mathbf{r}_j)^2 = \frac{1}{N} \sum_{k=1}^{N} (\mathbf{r}_k - \langle \mathbf{r}_k \rangle)^2. \tag{4.4}$$

In general, the mean size of a chain shows a power law dependence on the number of monomers [215]. This is the case for the radius of gyration, $\langle R_g \rangle \propto N^\nu$. The exponent ν is, in fact, the inverse of the fractal dimension of the chain, $d_F = 1/\nu$. For ideal chains, i.e., for a polymer under theta conditions, $\nu = 1/2$, whereas $\nu = 3/(d+2)$ for good solvent and $\nu = 1/d$ for poor solvent conditions, where d is the system dimensionality [215,216]. For the case of good solvent conditions, the expression $\nu = 3/(d+2)$ is obtained by minimizing the free energy of the system assuming that it has only two main contributions: an entropic term corresponding to a gaussian random distribution of the chain bond orientations which is proportional to R_g^2/N, and a repulsion term that takes into account the excluded volume effects and is proportional to N^2/R_g^d [215].

End-to-end distance

Another simple parameter for the structure characterization of polymers is the displacement vector, or end-to-end vector, that joins both extremes in a polymer chain. Hence, for a chain with N monomers, the quadratic norm of the end-to-end vector, or quadratic *end-to-end distance*, is defined as:

$$R_{ee}^2 = (\mathbf{r}_1 - \mathbf{r}_N)^2. \tag{4.5}$$

The maximum possible value of the end-to-end distance corresponds to a fully stretched chain and is also called the *contour length* of the chain, while smaller values would indicate more complex geometries. In the absence of correlations between the positions of the monomers, the mean quadratic end-to-end distance and the radius of gyration

satisfy, in the thermodynamic limit, the relation $\langle R_{ee}^2 \rangle \propto \langle R_g^2 \rangle$ [217], which implies that both quantities follow the same asymptotic scaling.

In general, the presence of an attractive surface near a polymer introduces a structural anisotropy which affects the values and the asymptotic behavior of the structural parameters R_g and R_{ee} of the chain. In particular, the parallel and perpendicular components of such parameters with respect to the attractive surface are no longer equivalent and the configurational entropy of the chain tends to decrease as the adsorption process takes place.

Persistence length

The persistence length, l_p, is formally defined as the correlation length of the bond-angle correlation function. It is directly related with the stiffness of a polymer since it basically measures the length scale up to which the chain behaves as a rod. The refered correlation function is defined as the average $\langle \hat{\tau}_i \cdot \hat{\tau}_{i+x} \rangle$, where $\hat{\tau}_i$ is the unitary vector tangent to the chain backbone at the position of the i-th monomer. Therefore, the bond-angle correlation function is expected to behave as $\langle \hat{\tau}_i \cdot \hat{\tau}_{i+x} \rangle = \exp(-x/l_p)$.

Structural motifs during adsorption on surfaces: loops, trains and tails

The adsorption of a polymer by an attractive surface is a continuous phase transition [218]. This means that it does not occurs abruptly, by adsorbing all the monomers in the chain at the same time, but in a continuous process dominated by fluctuations during which the mean number of adsorbed monomers varies and tends to increase as the adsorption takes place. Therefore, the chain can be represented as a composition of diverse segments, or structural motifs, with different characteristic morphologies defined with respect to the adsorption surface. The most widely used classification of such adsorption structures distinguishes three types of motifs, known as *loops*, *trains* and *tails*.

The definitions of loops, trains and tails that will be used in the next chapter are schematized in Figure 4.3: a *train* is defined as a consecutive sequence of adsorbed monomers, a *loop* is a chain sequence in which all the monomers are not adsorbed but have adsorbed neighbors at both extremes of the segment, whereas a *tail* is a sequence of non adsorbed monomers in which one of their extremes is an end of the chain.

The statistics of loops, trains and tails are commonly used to characterize adsorption processes and to study of diverse aspects of the behavior of grafted polymers [219–221].

4.3.3 Critical behavior of polymers near attractive surfaces

There are numerous studies of the adsorption process of non-magnetic chains. For instance, the transition from a desorbed to an adsorbed state in good solvents has been investigated in detail [222–238] and poor [235,239–251]. For the case of semi-flexible ideal chains, Khokhlov *et al* [252] obtained an analytical solution to the adsorption problem showing that it is a continuous phase transition in the limit of an infinite chain length. The influence of the chain stiffness on adsorption has also been studied through numerical simulations with coarse-grained models [229, 253–255]. Computer simulations have been also carried out to determine the phase diagrams of systems with competing forces [241–250, 256–258]. For neutral polymers the conformational adsorption phases have been studied using multicanonical computer simulations [259]. In addition to the main phases of adsorbed and desorbed conformations, several other phase transitions, such as the freezing transitions between globular entropy-dominated conformations and energy-dominated crystalline low-temperature structures [260], have been observed. The case of the adsorption of charged polymers onto surfaces has also received considerable attention [261]. Very recently, the coil-globule transition near an attractive surface [262] and the adsorption of random copolymers from a melt onto a solid surface [263] have been analyzed.

For the conditions that will be considered in the next chapter to describe the adsorption of a magnetic filament controlled by the system temperature, we need to take into account excluded volume and good solvent effects. For this reason, the relevant details of the current knowledge on the critical behavior of non-ideal polymers near attractive surfaces
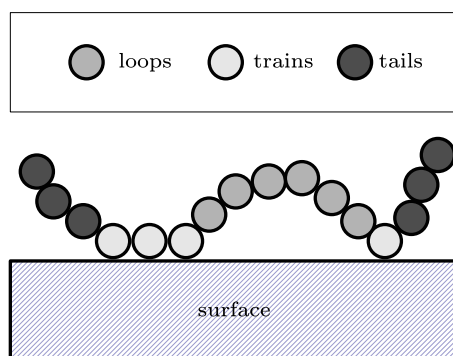
Figure 4.3: Schematic representation of the different types of structures developed by a partially adsorbed polymer-like chain.

in a good solvent are summarized next.

Scaling relations for non-ideal chains in a good solvent

The universal properties and scaling relations for the temperature-controlled adsorption process of a single non-ideal polymer chain under good solvent conditions were established by Eisenriegler and coworkers [225]. This study was based on the pioneering works by de Gennes, Diehl and others, and was carried out by means of Monte Carlo simulations and a theoretical approach based on the mapping of the polymer adsorption process to the problem of correlation functions in the n-vector model of magnetism in the $n \to \infty$ limit. The model included a short-ranged attractive interaction with the surface and represented the polymer as a self-avoiding random walk on a regular lattice with at least one of their monomers in permanent contact with the surface.

The main finding of Esenriegler and coworkers regarding the adsorption energy of the chain, U_{ads}, was its dependence on the chain length, N. For finite chains they have shown that

$$\frac{U_{ads}}{N} \propto \begin{cases} N^{-1}, & T > T_c(N) \\ N^{\phi-1}, & T = T_c(N) \\ \text{const.}, & T < T_c(N) \end{cases} \tag{4.6}$$

where $T_c(N)$ is the transition temperature for a chain of N monomers. Therefore, the adsorption energy scales as a power law of the chain size at the transition point, $U_{ads} \propto N^\phi$. Due to finite size effects, a wide crossover region is expected and the predicted behavior for $T > T_c(N)$ and $T < T_c(N)$ would be obtained only for temperatures far enough from the transition point, $T_c(N)$. The exponent ϕ was deduced by fitting the results for different chain lengths. They obtained $\phi = 0.58 \pm 0.03$. For the finite size scaling analysis of the adsorption energy, the relation

$$U_{ads}/N^\phi = h\left(\tau N^\phi\right) \tag{4.7}$$

was established. In such relation, as usual, $\tau = (T - T_c(N \to \infty))/T_c(N \to \infty)$ represents the relative distance to the critical temperature, $T_c(N \to \infty)$, which can be obtained by extrapolation of the finite size transition temperatures, whereas $h(x)$ is the following scaling function:

$$h(x) \propto \begin{cases} x^{-1}, & x \to \infty \\ \text{const.}, & x \to 0 \\ |x|^{(1-\phi)/\phi}, & x \to -\infty \end{cases} \tag{4.8}$$

Hence, the adsorption energy has the following asymptotic behavior:

$$U_{ads}/N \propto \begin{cases} 0, & T \geq T_c(N \to \infty) \\ |\tau|^{(1-\phi)/\phi}, & T < T_c(N \to \infty) \end{cases} \tag{4.9}$$

5 Transitions of semiflexible magnetic filaments near an attratctive surface

The present work is focused on the study of the influence of the magnetic interactions on the adsorption process of a semiflexible magnetic filament by an attractive flat surface. Magnetic filaments and their behavior near attractive surfaces have an unquestionable interest because of their potential for novel technological applications. This study is also a preliminary theoretical approach to these novel systems which intends to determine what are the most adequate modeling strategies for this case.

The behaviour of the adsorption of non-magnetic polymers on attractive surfaces is well known. In general, the adsorption process is favored by the chain length and the stiffness, letting it to take place at higher temperatures. The addition of a permanent magnetic moment to the particles forming a polymer-like supramolecular chain is expected to produce significant effects on this behavior. Unlike magnetic filaments, ferrofluids have been already studied to a certain extent and can provide some prospects of what can one expect from the magnetic interactions effects. On the one hand, it is known that in ferrofluids the magnetic particles tend to form chain-like structures with a head-to-tail arrangement of the dipoles [197, 264]. Therefore, it is reasonable to suppose that the magnetic interactions would contribute to increase the chain stiffness and, consequently, would favor the adsorption process as the stiffness does. On the other hand, it is also known that ferrofluid particles tend to form annular structures [264] that are found to be the ground state of the system in quasi-two dimensional geometries [265]. Hence, the magnetic interactions would have an influence on the chain morphology that could be very different from the one own to the stiffness as the system energy decreases. However, it is not trivial to anticipate what the effect of the dipolar interactions will be on semiflexible magnetic filaments near an attractive surface.

In order to determine the nature of such influence, extensive Langevin Dynamics (LD) simulations using a novel coarse bead-spring chain model for the filaments have been carried out, and the effects of the temperature, the strength of the magnetic interactions,

the stiffness and the length of the chain have been thoroughly studied.

This Chapter is organized as follows: in Section 5.1 the numerical model and the details of the performed simulations are presented, Section 5.2 is devoted to introduce the obtained results and finally a summary and a discusion of the conclusions is presented in Section 5.3.

5.1 A coarse-grained model for semiflexible magnetic filaments

The coarse-grained simulation model developed for this study represents magnetic filaments as bead-spring semiflexible chains composed of N identical spherical particles of diameter σ with a point magnetic dipole of permanent magnetic moment μ located at their centers. Since pair potentials with abrupt discontinuities are difficult to manage in dynamic simulations, continuous expressions have been used in general for the model interactions. However, except for the magnetic interactions that are effectively long-ranged, the rest of the model interactions are considered as short-ranged; onsequently adequate cutoff distances have been specified for each of their components in order to avoid negligible potential evaluations.

5.1.1 The filament model

The model intrachain interactions are displayed schematically in Figure 5.1, Excluded volume effects are explicitly considered by imposing a mutual steric repulsion to the chain beads. This repulsion is described by a truncated-shifted Lennard-Jones pair potential (tsLJ) also known as Weeks-Chandler-Andersen potential [266]:

$$U_{tsLJ}(r) = \begin{cases} U_{LJ}(r) - U_{LJ}(r_{cut}), & r < r_{\text{cut}} \\ 0, & r \geq r_{\text{cut}} \end{cases} \tag{5.1}$$

where r is the distance between the centers of the interacting monomers and $U_{LJ}(r)$ is the standard Lennard-Jones expression [27]:

$$U_{LJ}(r) = 4\epsilon_e \left[\left(\frac{\sigma}{r} \right)^{12} - \left(\frac{\sigma}{r} \right)^6 \right]. \tag{5.2}$$

For the sake of simplicity, reduced units have been used for the model definitions, so that the values $\sigma = 1$ and $\epsilon_e = 1$ have been taken for the previous expression. The cutoff radius for the tsLJ potential has been set to $r_{\text{cut}} = 2^{1/6}\sigma$, what means a soft-core repulsion between monomers. The one-dimensional connectivity of the chain is kept by a bonding
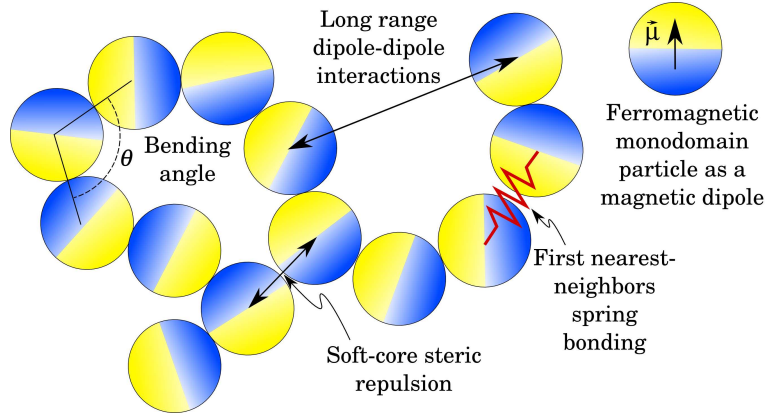
Figure 5.1: Representation of the coarse-grained model used to study the behavior of magnetic filaments.

interaction which includes two components: the first nearest neighbor attraction and the stiffness. For the first one, a finite extensible nonlinear elastic (FENE) potential provides a radial attraction between the said neighbors in the chain

$$U_{fene}(r) = \frac{-K_f \, r_{max}^2}{2} \ln\left[1 - \left(\frac{r}{r_{max}}\right)^2\right],$$
(5.3)

with $K_f = 30/\sigma^2$ and $r_{max} = 1.5\sigma$, being r again the distance between the center of the bonded particles[1]. Figure 5.2(a) shows the net profile resulting from such non-directional potentials, evidencing that in this model the bonds does not have a fixed length, but may have any length below the maximum value $r_{max} = 1.5\sigma$, led by the FENE potential, with the lower unbounded limit of the soft core repulsion.

On the other hand, the chain stiffness is represented by means of the following bending potential [254, 255]:

$$U_B = \sum_{\theta} \frac{\kappa}{2}(\cos\theta - \cos\theta_0)^2,$$
(5.4)

where θ is the bond angle determined by the positions of any three consecutive beads in the chain, θ_0 is the preferred angle —i.e., the angle that minimizes the bending energy of the chain— and κ is the bending constant. As is usual for coarse-grained models, the configuration of minimum bending energy has been assumed to be an straight rod, hence

---

[1]It should be noted that having the chain elastic bonding attraction as a function of the distance between the centers of the bonded beads, r, is a rough approximation to the actual experimental case, in which the linking molecules that constitute the semiflexible bond are fixed to points in the beads surface. Therefore, the contribution of the rotations of a bead to the stretching of its bonds are neglected.
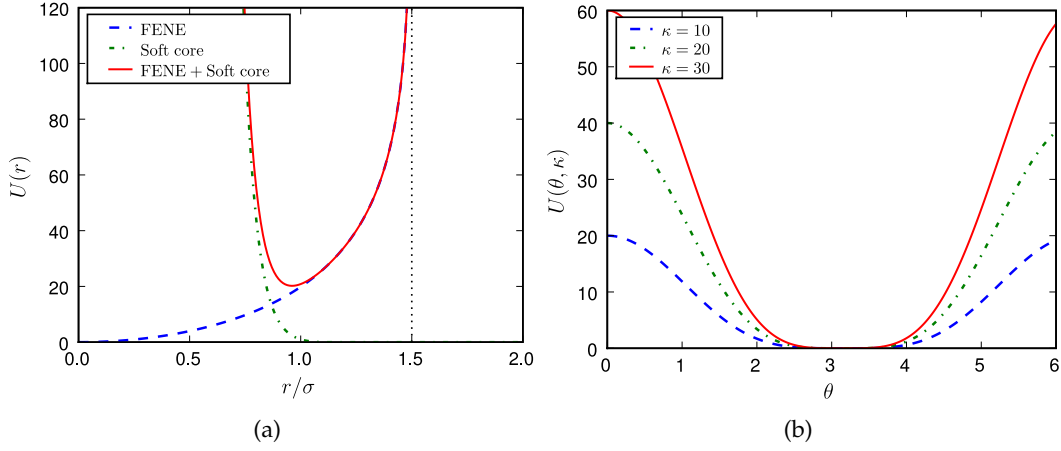
Figure 5.2: Terms of the bonding interactions of the chain beads: (a) radial terms; (b) bending potential.

the preferred angle has been taken to be $\theta_0 = \pi$. In the absence of magnetic interactions, the stiffness parameter κ is directly related to the chain persistence length, which can be experimentally measured by scattering techniques in real polymer chains [267–269]. This potential is depicted in Figure 5.2(b).

Since the magnetic nature of the filaments is represented by a point magnetic dipole at the center of each chain bead, the long range magnetic interactions between beads are given by the well known expression for magnetic dipole-dipole interactions:

$$U^{dip}(\mathbf{r}_{ij}) = \frac{\boldsymbol{\mu}_i \cdot \boldsymbol{\mu}_j}{|\mathbf{r}_{ij}|^3} - \frac{3[\boldsymbol{\mu}_i \cdot \mathbf{r}_{ij}][\boldsymbol{\mu}_j \cdot \mathbf{r}_{ij}]}{|\mathbf{r}_{ij}|^5}, \qquad (5.5)$$

where $\mathbf{r}_{ij} = \mathbf{r}_i - \mathbf{r}_j$ is the displacement vector between particles i and j, whereas $\boldsymbol{\mu}_i$ and $\boldsymbol{\mu}_j$ are their respective magnetic moments. As a first approach, the point dipole of each bead is allowed to freely rotate in any direction of the three-dimensional space, independently from the chain bonds. However, the behavior observed in ferrofluids makes reasonable to expected that magnetic interactions between first nearest neighbors will tend to align the dipoles with the chain backbone without imposing any explicit geometrical restriction to their orientations.

In this study each chain has been set to have all their dipoles with the same modulus, $|\boldsymbol{\mu}_i| = \mu$. The value of μ has been established from its squared expression, μ^2, which represents the total intensity of the dipolar pair interaction in reduced units. In fact, μ^2 is proportional to the maximum dipolar energy between two spherical dipoles and can be

related to the experimental parameters by $\mu^2 = \mu_e^2 / (\epsilon_e \, \sigma_e^3)$, where σ_e and ϵ_e are respectively the range and the strength of the interacting potential and μ_e is the experimental dipolar magnetic moment. Therefore, the value of μ^2 would depend in general on the composition and size of the magnetic particles. In particular, typical values for common magnetic minerals, such as magnetite, are found to be $\mu^2 < 10$, whereas more exotic magnetic materials, such as cobalt-based materials, can show higher values.

Since no attractive interaction between non-neighbor beads has been defined —apart from the effects of eventually favorable magnetic interactions— it is assumed that the background system is composed by a perfect solvent.

5.1.2 Surface interactions and dynamics

The simulation box consists in a three-dimensional constrained open space unbounded along the $x - y$ plane but limited in the z direction by two impenetrable, neutral and non-magnetic walls located at $z = 0$ and $z = 50\sigma$, respectively. The wall at $z = 0$ is an attractive surface which interacts with the filament beads by a truncated-shifted modified version of the Lennard-Jones potential:

$$U_s(z) = \begin{cases} U_{9-3}(z) - U_{9-3}(z_{cut}), & z < z_{cut} \\ 0, & z \geq z_{cut} \end{cases} \tag{5.6}$$

where

$$U_{9-3}(z) = 4\epsilon_s \left[\left(\frac{\sigma}{z} \right)^9 - \left(\frac{\sigma}{z} \right)^3 \right] \tag{5.7}$$

is the known 9–3 Lennard-Jones potential [270] expressed as a function of the distance between the wall and the center of the bead. This expression, obtained from the integration of the original Lennard-Jones potential over an infinite flat surface, is frequently used to represent the interactions of fluid particles with flat solid walls. In this case, the values $\epsilon_s = \epsilon_e = 1$ and $z_{cut} = 2.5\sigma$ have been taken.

The second wall, located at $z = 50\sigma$, has the purpose of preventing the filament to move too far away from the attractive wall. This is done to ensure that the the filaments will effectively interact with the adsorbing wall within a reasonable equilibration interval of time. Several tests have been performed for an adequate location of this repulsive wall in order to avoid any bias in the adsorption process. In this case, the repulsive interaction is represented by a potential equivalent to expression (5.1), with the same cutoff distance $r_{cut} = z_{cut} = 2^{1/6}\sigma$ and the change $r = 50\sigma - z$.

The main control parameter in the model is the system temperature. This parameter is defined in reduced units as $T \equiv k_B T_e/\epsilon_e$, where T_e is the experimental temperature and k_B the Boltzmann's constant. In simulations of other magnetic systems, a dimensionless dipolar coupling parameter λ is often defined to characterize the strength of the dipolar interaction. In general, λ is one half the ratio of the magnetic energy of two dipoles, separated by one particle diameter and oriented head to tail, to the thermal energy. In our reduced units this relation is $\lambda = \mu^2/T$.

The simulation of system dynamics is carried out by applying translational and rotational Langevin equations of motion, as discussed in Section 1.3.1, to any of the chain beads [30]:

$$M_i \frac{d\mathbf{v}_i}{dt} = \mathbf{F}_i - \gamma^T \mathbf{v}_i + \boldsymbol{\xi}_i^T \tag{5.8}$$

$$\boldsymbol{I}_i \cdot \frac{d\boldsymbol{\omega}_i}{dt} = \boldsymbol{\tau}_i - \gamma^R \boldsymbol{\omega}_i + \boldsymbol{\xi}_i^R \tag{5.9}$$

where $\mathbf{F}_i$, and $\boldsymbol{\tau}_i$ are respectively the total force and torque acting on the particle i, M_i and $\boldsymbol{I}_i$ are its mass and inertia tensor, γ^T and γ^R are the translational and rotational friction constants, whereas $\boldsymbol{\xi}_i^T$ and $\boldsymbol{\xi}_i^R$ are the gaussian random force and torque, respectively. The time is expressed in reduced units as $t = t_e \, [\epsilon_e/(M_e \, \sigma_e^2)]^{1/2}$, where M_e and t_e are the mass of the bead and the measured time, respectively.

For equilibrium simulations the values of the mass, the inertia tensor, as well as friction constants γ^T and γ^R are irrelevant. The bead mass has been chosen to be $M_i = 1$ and for the inertia tensor the identity matrix has been used in order to ensure isotropic rotations $\boldsymbol{I}_i = \mathbf{1}$. The values $\gamma^T = 1$ and $\gamma^R = 3/4$ have been taken from previous studies in which a conveniently fast relaxation to equilibrium was achieved [264,271]. Finally, the reduced time step has been set to be $\delta t = 5 \cdot 10^{-3}$.

In all the cases the simulation starts by placing the filament in the bulk region with its first bead located in the interval $z \in (\sigma, 5\sigma)$. This choice guarantees that the chain is sufficiently close to the attracting surface to avoid the unnecessary computational time that it would spend just diffusing in the bulk region. The remaining monomers are positioned using a self-avoiding random walk scheme with an overlap radius of 0.9σ. The system is pre-equilibrated for a period of $5 \cdot 10^5$ steps using a sequence of increasing time steps until the final value δt is reached. Subsequently, the chain is equilibrated for a period of $2 \cdot 10^6 \, \delta t$ to ensure that the results have lost memory of initial configuration. After the equilibration period, the system is sampled at intervals of $4 \cdot 10^3 \, \delta t$ for another

period of $2 \cdot 10^6 \, \delta t$. The equilibrium statistics heve been improved by averaging measures from 70 independent runs for each explored set of system parameters.

The results, presented in the next section, have been obtained using the simulation software ESPResSo [272], a package specifically intended for soft matter problems. Although the package includes advanced approaches for the evaluation of the long range interactions, such as Ewald summations [29] or approximate methods based on Fast Fourier Transforms [273], the simulation in open space of single chains with small lenghts performed in this study allows for the exact pair evaluation over all the chain particles.

5.2 Simulation results and calculations

The numerical experiments presented here have been performed for single magnetic chains with lengths varying in the range $N \in [20, \, 300]$ and strengths of the magnetic point dipole of the monomers within the range $\mu^2 \in [1, \, 10]$. Regarding the chain stiffness constant, values within the range $\kappa \in [0, 30]$ were explored but here, only the results obtained for $\kappa = 10$ will be presented in a complete form, because no qualitative difference was found for other values. In particular, the limit in which the persistence lengths is similar or larger than the chain contour length has not been considered. Finally, the range of inverse temperatures explored in the simulations has been $1/T \in [0.25, \, 4]$.

Figure 5.3 shows some examples of equilibrium conformations obtained for a chain with length $N = 100$. A first inspection of such equilibrium conformations clearly evidences that at high temperatures ($1/T \lesssim 0.25$) all chains are completely desorbed whereas at low temperatures ($1/T \to 4$) they are fully adsorbed. A more careful inspection evidences the existence of three possible different phases in the system. At high temperatures, the chain is desorbed and exhibits the shape of a self-avoiding random coil with little order in the orientation of their dipoles (Fig. 5.3(a)). As the temperature is lowered, the filament is adsorbed onto the surface and dipoles align with the chain backbone, which tends to adopt more stretched conformations (Fig. 5.3(b)). Except for the presence of the dipoles, this situation corresponds to the well known behavior observed for non-magnetic semiflexible polymers, whose adsorption process undergoes a continuum phase transition. Nonetheless, below a certain characteristic temperature that depends on the chain parameters, the tendency to stretch is reversed and the equilibrium chain conformations are characterized by the formation of closed structures in the adsorbed state, forming planar loops with a smooth curvature and an almost perfect alignment of the dipoles with
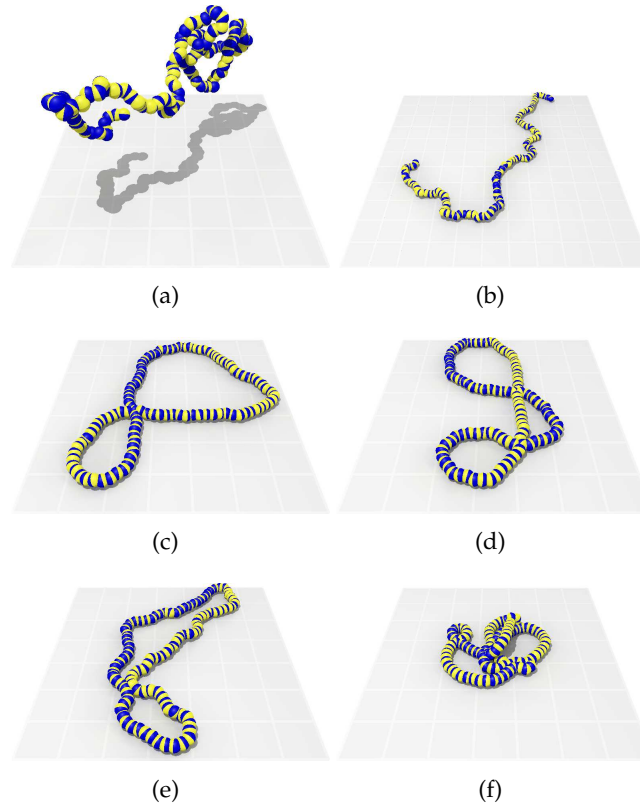
Figure 5.3: Snapshots of equilibrium conformations of a magnetic filament near a flat homogeneous attractive surface for $N = 100$, $\kappa = 10$ and $\mu^2 = 3$ at different temperature values. Filament beads are depicted as two-colored spheres with the two colors representing the magnetic dipole orientation. (a) $1/T = 0.5$, (b) $1/T = 1.0$, (c) $1/T = 3.0$, (d) $1/T = 4.0$. — Equilibrium chain conformations obtained at low temperatures ($1/T = 4.0$). (a) A fully flexible filament ($\kappa = 0$) for $N = 100$ and $\mu^2 = 3.0$ displays a more corrugated shape in comparison with Figs. 5.3(c) and 5.3(d); (b) Effect of high magnetization values ($\mu^2 = 10$) on the chain conformation ($N = 100$, $\kappa = 10$).

the chain backbone (Fig. 5.3(c) and Fig. 5.3(d)). This behavior suggests the existence of a second structural transition as a consequence of competing interactions in the system. A further reduction in temperature apparently leads to an increase in the number of loops (Fig. 5.3(d)).

For low temperatures and strengths of the magnetic interaction close to the upper limit of the thoroughly explored range, $\mu^2 \rightarrow 10$, there exist indications of a more complex behavior. Figure 5.3(f) depicts the shape of a typical filament structure obtained at $1/T = 4.0$ and $\mu^2 = 10$. It is reasonably identify such structure as corresponding to the result of a competition between the interaction with the adsorption surface, that tends

to flatten the adsorbed chain conformations, with secondary dipole-dipole interactions between beads which are far in the chain sequence but close in space, leading to an effective attraction between these beads which is strong enough to produce nonplanar compact adsorbed conformations. This behavior is similar to the one observed in non-magnetic polymer chains immersed in a poor solvent near an attractive surface, for which an adsorbed, non-flat collapsed phase is identified [245]. The role of the chain stiffness is illustrated in Figure 5.3(e), where a fully flexible chain ($\kappa = 0$) displays a more corrugated shape in comparison with the analogous semiflexible chain ($\kappa = 10$) shown in Figure 5.3(c).

As mentioned before, dipoles tend to align locally with the filament structure as the temperature is reduced. In order to quantify the degree of such local alignment, a bond-dipole local orientation parameter is defined as:

$$\langle A \rangle = \frac{1}{N-2} \left\langle \sum_{i=2}^{N-1} \left| \, \hat{\mathbf{r}}_{i-1,i+1} \cdot \hat{\boldsymbol{\mu}}_i \, \right| \, \right\rangle, \tag{5.10}$$

where $\langle \, ... \, \rangle$ stands for the thermal average of the different chain conformations collected from all runs at a given temperature T, $\hat{\mathbf{r}}_{i-1,i+1}$ is the unitary displacement vector between the center of particles $i-1$ and $i+1$, and $\hat{\boldsymbol{\mu}}_i$ is the unitary dipole moment associated to bead i. This definition for a mean local alignment parameter is not unique, but it is evident that in this case a perfect local alignment of the dipoles with the chain backbone will lead to $\langle A \rangle \rightarrow 1$, whereas a orientation distribution of the dipoles completely uncorrelated with the chain backbone will produce $\langle A \rangle \sim 1/2$. The behavior of this parameter with the inverse temperature is shown in Figure 5.4 for $N = 100$, $\kappa = 10$ and different values of the intensity of the magnetic interaction. It is evident that the local ordering tends to increase as the temperature is reduced until $\langle A \rangle$ reaches a plateau around $\langle A \rangle \sim 0.95$. The local alignment is never perfect due to the small but necessary curvature needed to form the closed structures that develop at small temperatures (see Fig.5.3). In general, the local alignment of the dipoles increases more abruptly and at a higher temperature as the dipolar strength is increased but, remarkably, for the highest values of μ^2 and very low temperatures $\langle A \rangle$ tends to slightly decrease again due to the growing ocurrences of the non-planar adsorbed conformations noted in the previous qualitative inspection.

The next two sections will be devoted to characterize the undergoing continuum phase transition of the magnetic filament towards the adsorbed state and the structural transition from open stretched chains to closed folded configurations led by magnetic interactions
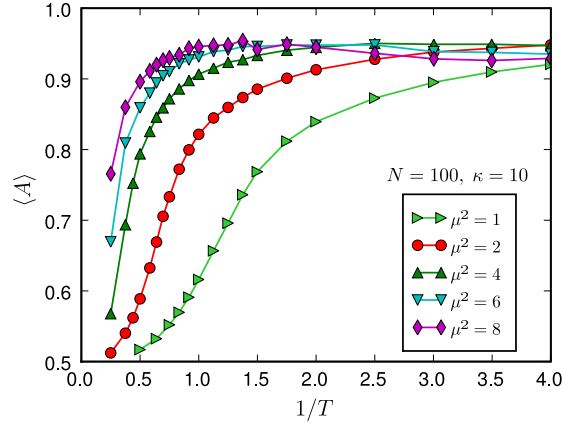
Figure 5.4: Bond-dipole local orientation parameter as a function of the inverse temperature for different values of the magnetization for the case $N = 100$ and $\kappa = 10$.

at low temperatures.

5.2.1 Adsorption transition

The adsorption transition in polymeric systems can be characterized using observables like the mean normalized adsorption energy, $\langle \Gamma \rangle$, and its associated specific heat at constant volume, C_V, which are defined as:

$$\Gamma = \left| \frac{U_{ads}}{U_{ads}^{(max)}} \right|, \tag{5.11}$$

$$\frac{C_V}{N} = \frac{\langle U_{ads}^2 \rangle - \langle U_{ads} \rangle^2}{NT^2}, \tag{5.12}$$

where

$$U_{ads} = \sum_{i=1}^{N} U_s(z_i) \tag{5.13}$$

is the total adsorption energy, obtained from equation (5.6), and $U_{ads}^{(max)}$ is the largest possible adsorption energy for the chain, obtained when all the monomers are located at the minimum of the potential (5.7) as defined by their assigned parameters: $U_{ads}^{(max)} = N U_s(z = 3^{1/6}\sigma)$.

Figure 5.5 presents the change of the mean normalized adsorption energy $\langle \Gamma \rangle$ as a function of the inverse temperature $1/T$ for different values of the dipolar interaction and for distinct chain lengths. The inset plots show the behavior of the associated specific
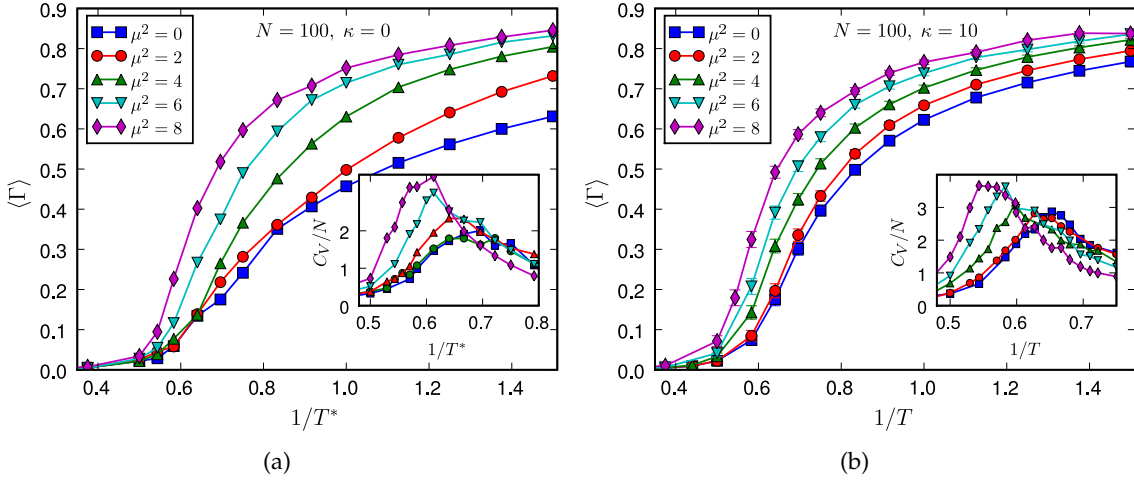
Figure 5.5: Mean normalized adsorption energy, $\langle \Gamma \rangle$, and its corresponding specific heat (inset figures), for a semiflexible chain with $\kappa = 10$ as a function of the inverse temperature $1/T$: (a) (b) for $N = 100$ and different values of the dipolar interaction μ^2.

heat derived from the energy fluctuations. In all cases the position of the C_V peak determines the characteristic adsorption temperature at which the filament adsorbs onto the surface. The results evidence that an increase of the dipolar interaction ($\mu^2 < 10$) favors the adsorption at higher temperatures as is commonly observed for an increasing chain stiffness (Figure 5.5(b)). The same effect, led exclusively by the magnetic interactions, can also be observed for a fully flexible magnetic filament ($\kappa = 0$). This result confirms the behavior expected from the existence of a configurational energy local minimum when the dipoles are aligned in a parallel head to tail orientation. Hence magnetic interactions favor more stretched configurations which, as occurs in non-magnetic polymers, tend to allow the adsorption of the chains at higher temperatures since stretched configurations lose much less entropy in such process than the coil-shaped ones. However, at lower temperatures and moderate values of the dipolar interaction, the tendency of the chains to stretch is reversed and the equilibrium chain conformations are characterized by the formation of ordered closed loops with smooth shapes. This behavior will be further analyzed in the next section.

The adsorption transition also exhibits an indication of criticality in its dependence with the system size: as shown in Figure 5.6, the adsorption takes place at higher temperatures as the chain length increases. Consequently, for a given chain stiffness the characteristic adsorption temperature depends on both the intensity of the magnetic interactions and
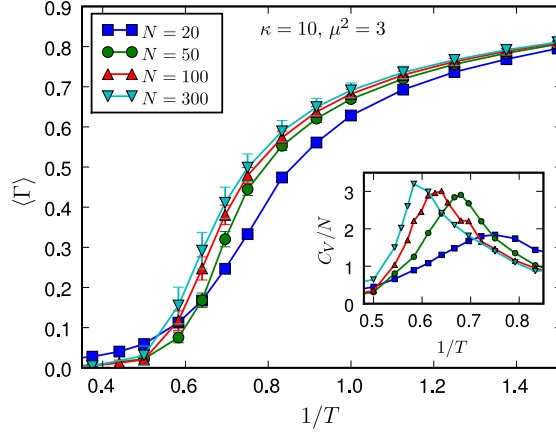
Figure 5.6: Same as Figure 5.5 for $\mu^2 = 3$ and $\kappa = 10$ for different values of the chain length N, illustrating the finite size effects.

the chain length: $T_c\left(N, \mu^2\right)$. The critical adsorption temperature, $T_c(N \to \infty, \mu^2)$, can be derived by extrapolation to the limit of infinite chain lengths from a least-square fitting of the assumed dependence for the critical temperature $T_c\left(N, \mu^2\right) \sim N^{-\phi}$, where ϕ is the critical crossover exponent. Figure 5.7(a) shows the result of this fitting for diverse values of the dipolar parameter, as well as the extrapolation to $N^{-\phi} = 0$ to obtain the corresponding critical temperatures. The data fits to the exponent $\phi = 0.59 \pm 0.04$, a value also obtained for the adsorption of non-magnetic homopolymers onto flat surfaces [225, 253].

Since the effects of the magnetic interactions on the adsorption transition of magnetic filaments appear to be essentially quantitative within the range of parameters explored, in order to examine the critical properties of such transition the known scaling *ansatz* for non-magnetic polymers, introduced in Section 4.3.3, has been adopted. Using the values of $T_c(\infty, \mu^2)$ previously obtained, the scaling relations (4.7) and (4.8) for the adsorption energy U_{ads} have been applied to the available data. The results of this rescaling of the adsorption energy for $\mu^2 = 3$ and different chain lengths are shown in Figure 5.7(b). The data reproduces reasonably well the conventional scaling relationship taking a value for the crossover exponent of $\phi = 0.59$. An analogous behavior has been observed for all the values of the dipolar interaction explored ($\mu^2 < 10$). This result confirms, for the range of parameters studied, the quantitative nature of the magnetic interaction effects on the adsorption transition.

A further insight on the chain morphology close to the adsorption transition point can
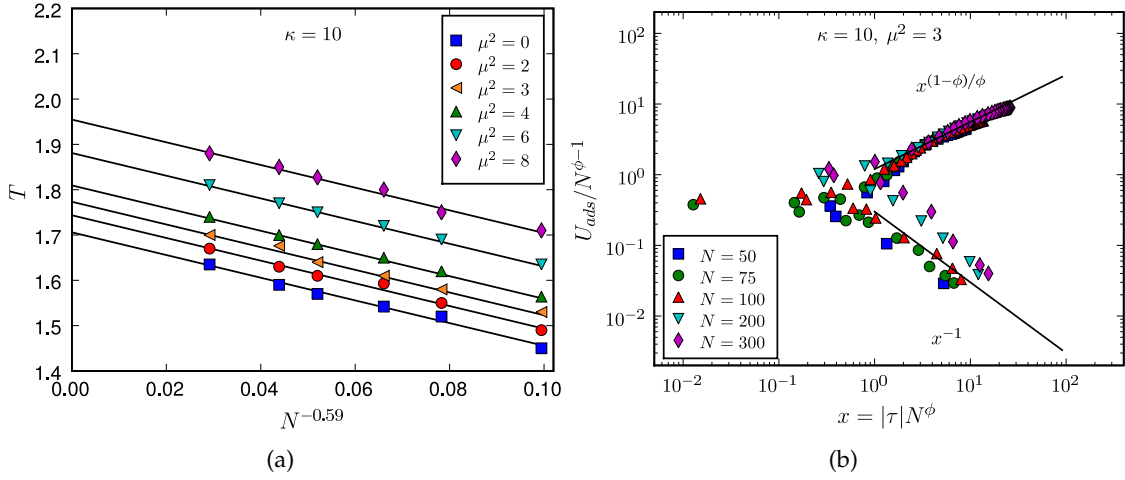
Figure 5.7: (a) Determination of the critical adsorption temperatures $T_c(N \to \infty, \mu^2)$ for different values of the dipolar interaction μ^2. The chain stiffness is set to $\kappa = 10$. The data fits to the known exponent $\phi = 0.59$ for the adsorption of homopolymers on flat surfaces. (b) The log-log plot of the scaling function $U_{ads}/N^{\phi-1}$ vs the scaling argument $|\tau|N^\phi$ for the case $\kappa = 10$ and $\mu^2 = 3$. The straight lines indicate the asymptotic limit.

be obtained from the study of the statistics of the three different types of structural motifs that may conform the filament during the adsorption process, namely: *loops, trains* and *tails*, as defined in Section 4.3.2. The results obtained for these motifs are summarized in Figure 5.8. In particular, Figure 5.8(a) shows an example of the averaged number of monomers belonging to loops, trains and tails, $\langle n \rangle$, as a function of the inverse temperature for $N = 100$, $\kappa = 10$ and $\mu^2 = 3$. In such representative case one can observe a monotonous increase in the averaged number of monomers in train segments as the temperature decreases, in an analogous way to the behavior observed for the adsorption energy, $\langle \Gamma \rangle$. This process is accompanied by a monotonous decrease of monomers in tails, as expected. On the other hand, the number of monomers involved in loops becomes only significant and reaches a maximum close to the characteristic adsorption transition temperature. This behavior is consistent with the idea that close to the transition point the adsorbed/unadsorbed fluctuations should be maximal. Nonetheless, the location of this maximum is slightly shifted to smaller temperatures with respect to the transition temperature derived from the position of the peak in the specific heat. But more interestingly, the temperature at which the curves corresponding to trains and tails intersect, namely T_{tt}, is found to be strongly correlated with the characteristic adsorption temperature $T_c(N, \mu^2)$ as shown in Figure 5.8(b). Within a precision of $\Delta T = \pm 0.04$ both temperatures coincide
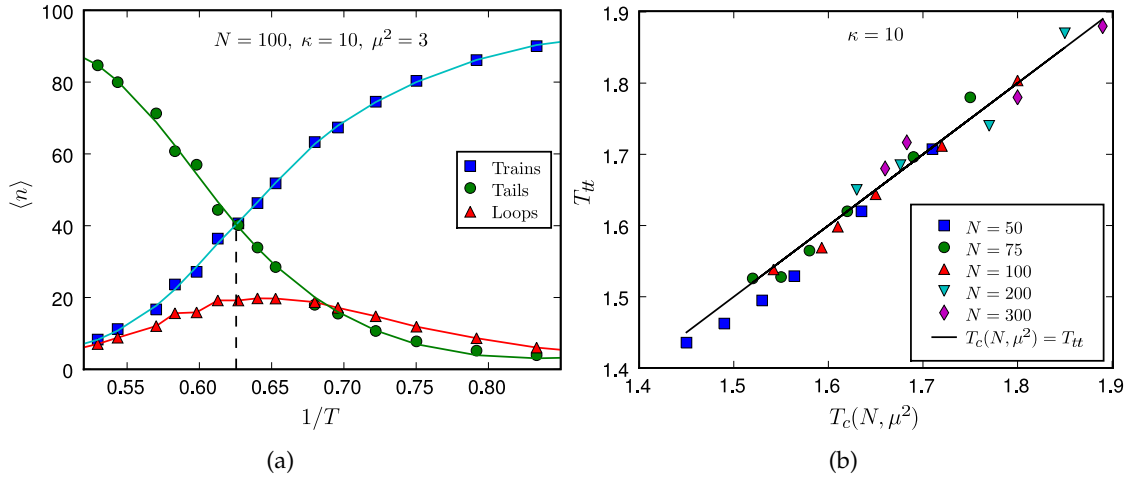
Figure 5.8: (a) Average number of monomers involved in train, tail and loop segments close to the adsorption transition point for $N = 100$, $\kappa = 10$ and $\mu^2 = 3$. The dashed line identifies the temperature at the train-tail crossing point, T_{tt}. (b) Correlation between the characteristic temperatures derived from the position of the peak in the specific heat data $T_c(N, \mu^2)$ and the intersection point between the averaged number of monomers in train and tail segments T_{tt} for $\kappa = 10$, $\mu^2 = 0, 2, 3, 4, 6, 8$ and different chain lengths N.

for all the cases studied. To date, this is the first time in which a technique based on the analysis of the train and tail statistics is used to determine the characteristic adsorption temperature. In addition, this technique has the advantage that good estimates can be obtained with much less numerical effort than the accurate determination of the specific heat maxima.

5.2.2 Structural open-closed transition

Once the critical behavior of the continuous phase transition led by the adsorption process has been characterized, the study is now focused on the structural change displayed by the adsorbed filament conformations at low temperatures. This behavior is particularly interesting since it has not known equivalence in non-magnetic systems.

As a first approach to such characterization, the behavior of the parallel, $\langle R^2_{g,\parallel} \rangle^{1/2}$, and perpendicular, $\langle R^2_{g,\perp} \rangle^{1/2}$, components of the root mean squared radius of gyration of the chains, as defined in the expressions (4.4), have been calculated. Figure 5.9 shows the results for these parameters as a function of $1/T$ for $N = 100$, $\kappa = 10$ and different values of the dipolar strength. At high temperatures, the perpendicular component drops to zero and the parallel component grows abruptly to a high value as soon as the chain becomes
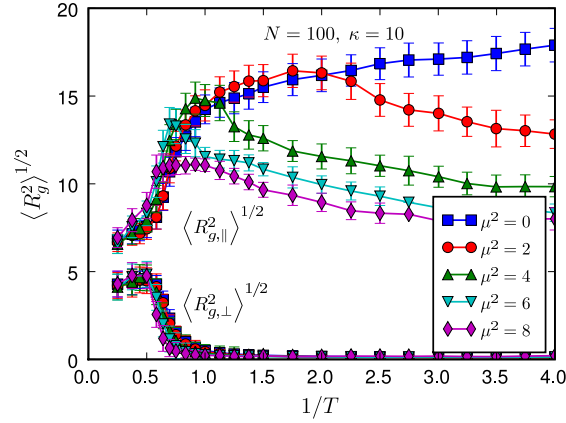
Figure 5.9: Parallel, $\langle R_{g,\parallel}^2 \rangle^{1/2}$, and perpendicular, $\langle R_{g,\perp}^2 \rangle^{1/2}$, components of the root mean squared radius of gyration as a function of $1/T$ for a magnetic filament with $N = 100$, $\kappa = 10$ and different values of the dipolar interaction μ^2.

adsorbed onto the surface, as previously observed in non-magnetic polymer chains [253]. In such non-magnetic systems the parallel component of the already adsorbed chain keeps growing smoothly as the temperature decreases due to the stretching of the chain structure, as illustrated by the case $\mu^2 = 0$. However, for non zero values of the dipolar interaction, the growth of the parallel component is reverted at a given temperature which increases with μ^2. Threfore, this particular behavior of the radius of gyration provides a numerical evidence of the new characteristic structures that would be observed in adsorbed magnetic filaments at low temperatures and moderate values of the dipolar interaction ($\mu^2 < 10$). This result strongly suggests the existence of a second structural transition that takes place at temperatures below the corresponding to the adsorption process, $T_c(\infty, \mu^2)$.

Considering its definition, provided in Equation (4.5), a more sensitive parameter to characterize the structural transition of magnetic filaments from a stretched to a closed planar structure as the temperature is decreased should be the root mean squared end-to-end distance, $\langle R_{ee}^2 \rangle^{1/2}$. In effect, the results obtained for this parameter, shown in Figure 5.10(a) for $N = 100$, $\kappa = 10$ and different values of the dipolar parameter, evidence more clearly the open-closed transition of the filament structures. As the temperature is reduced the mean end-to-end distance grows in a similar way as the parallel component of the radius of gyration, thus confirming the idea that moderated magnetic interactions tend to stretch the chain at relatively high temperatures, those at which the adsorption
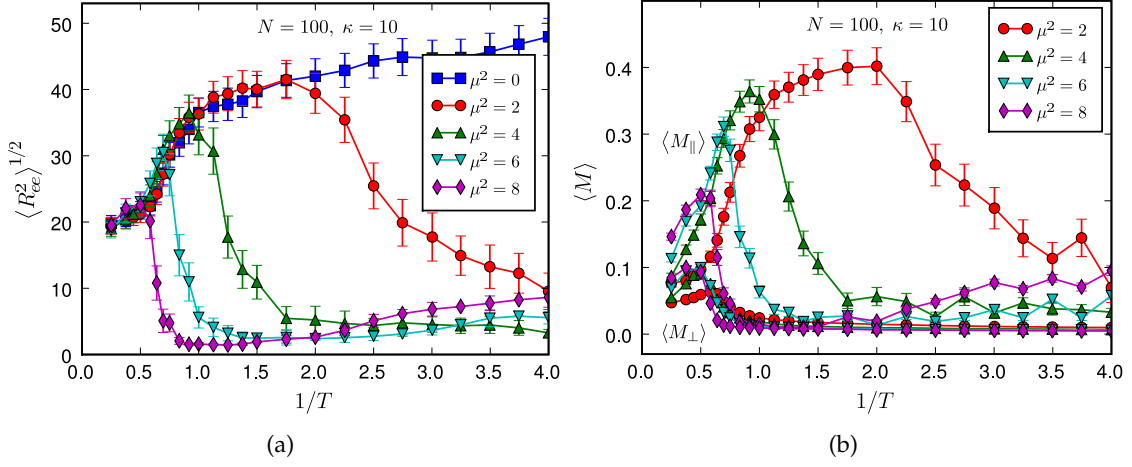
Figure 5.10: (a) Root mean squared end-to-end distance, $\langle R_{ee}^2 \rangle^{1/2}$, as a function of $1/T$ for $N = 100$, $\kappa = 10$ and different values of the dipolar interaction μ^2. (b) Parallel and perpendicular components with respect to the adsorbing surface of the total normalized magnetization $\langle M \rangle$ as a function of $1/T$ for $N = 100$, $\kappa = 10$ and non-zero values of the dipolar interaction μ^2.

process takes place. For non zero dipolar strengths, and after reaching a maximum value, $\langle R_{ee}^2 \rangle^{1/2}$ drops to almost zero values as a clear indication that a closed structure becomes the preferred equilibrium morphology. Again, this process operates at higher temperatures as the dipolar strength increases.

An analogous way to measure the structural change of the adsorbed magnetic filaments is by computing the normalized accumulated spontaneous magnetization of the chain, calculated as the modulus of the vector sum of all the dipoles, $M = \left| \sum_{i=1}^{N} \mu_i \right| / (N\mu)$. Figure 5.10(b) shows the mean parallel and perpendicular components of such parameter. Remarkably, the latter component has the same type of behavior observed for the end-to-end distance, with an evident correspondence between the curves obtained under the same system parameters. In fact, this correspondence is a direct consequence of having a good alignment between the dipoles and the backbones of the adsorbed chains: as long as such alignment increases, the end-to-end displacement vector, $\mathbf{R_{ee}}$, and the vector sum of the aligned dipoles, $\mathbf{M}$, will tend to differ only by a constant factor. The existence of a high alignment of the dipoles with the chain backbone for all the adsorbed states obtained at non zero dipole intensities can be deduced by observing the value of the local alignment parameter, presented in Figure 5.4, at temperatures below the adsorption transition point.

The presented structural parameters may provide further insights into the open-closed
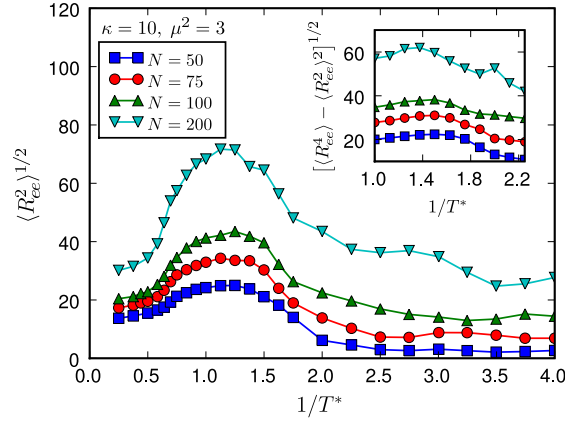
Figure 5.11: $\langle R_{ee}^2 \rangle^{1/2}$ vs. $1/T$ for $\kappa = 10$, $\mu^2 = 3$ and different values of the filament legth N. Inset: corresponding fluctuations of the same parameter.

transition. By analyzing their statistical fluctuations and their dependence with the system size in an analogous way to the adsorption transition analysis, the corresponding transition points and critical temperatures associated to each set of system parameters can be determined for this new transition. In this case, the end-to-end distance parameter, instead of a component of the system energy, has been chosen for the analysis due to the small differences in configurational energies exhibited by the open and closed adsorbed structures. Figure 5.11 shows the behavior of $\langle R_{ee}^2 \rangle^{1/2}$ and its fluctuations, in the inset figure, as a function of the inverse temperature for $\kappa = 10$, $\mu^2 = 3$ and different chain lengths. As was observed for the adsorption transition, a maximum in the parameter fluctuations that shifts towards higher temperatures as the chain length increases is obtained. Therefore, the dependence with the system size and the existence of the fluctuations maxima are again indications of a critical behavior associated to a continuous phase transition. Consequently, in order to estimate the critical temperatures for this new transition, $T_c(N \to \infty, \mu^2)$, the fluctuations maxima have been taken as finite size characteristic temperatures, $T_c(N, \mu^2)$, and an extrapolation to the limit of infinite chain lengths has been carried out. For this extrapolation, it has been assumed that the measured characteristic temperatures follow a power law dependence with the chain length defined by $T_c(N, \mu^2) = a - bN^{-\psi}$. A three parameters least-square fit to the data provides a new crossover exponent $\psi = 0.7 \pm 0.1$, though estimated temperatures are quite insensitive to the value of ψ within the error range.

Based on the results obtained for the adsorption and the structural transition tempera-
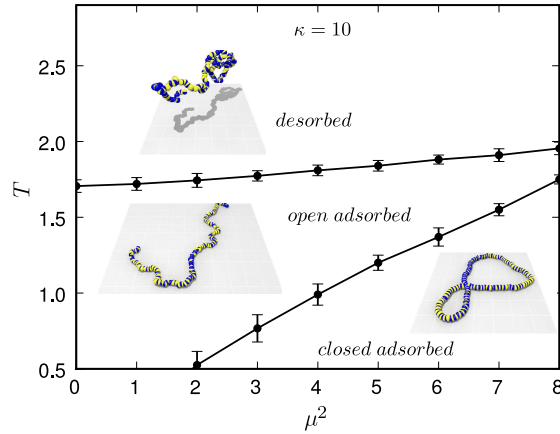
Figure 5.12: Representation of the phase diagram obtained for a single semiflexible magnetic filament ($\kappa = 10$) near an attractive flat surface for moderate values of the magnetization ($\mu^2 < 10$).

tures, Figure 5.12 shows a representation of the phase diagram for a semiflexible magnetic filament ($\kappa = 10$) near an attractive homogeneous surface with moderate values of the dipolar interaction ($\mu^2 < 10$). The diagram only includes temperatures as low as $T \geq 0.5$ due to the difficulties to obtain a good equilibration of the longest chains at the lowest temperatures and the excessive uncertainties associated with them. As anticipated by the inspection of the filament structures, the statistical analysis of the simulation results has confirmed the existence of three different phases for the range of parameters explored. At high temperatures the filaments remain in a unadsorbed state for any value of μ^2, displaying a self-avoiding random coil morphology. At intermediate temperatures there exist a region where the magnetic chains are adsorbed an exhibit preferentially open stretched structures. At low temperatures, beyond a minimal dipolar strength, another phase is observed in which planar closed loop structures are favored. This latter phase has not known equivalence in non magnetic systems.

The final point to be addressed in this study is the dependence of the structures found in the closed adsorbed phase with the dipole intensities. As already noted in the preliminary inspection of the filament conformations, the number of planar loops observed in such phase seems to increase with μ^2. In order to determine the mean number of loops in a given structure, a new characterization parameter is needed. A very simple parameter that contains information of the closed internal structures of the filament is the partial accumulated magnetization along the chain, $M(k)$, which is defined as the modulus of

(a)
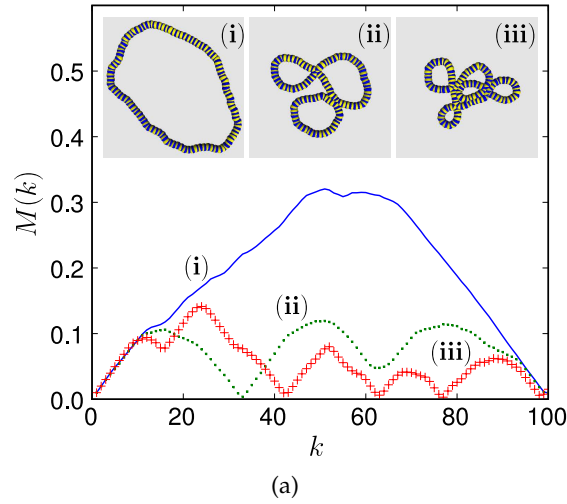
Figure 5.13: Behavior of the accumulated magnetization along the chain for three different filament conformations.

the vector sum of any k consecutive beads in the chain:

$$M(k) = \left| \sum_{i=1}^{k} \mu_i \right|, \quad k \leq N, \tag{5.14}$$

where the index $i = 1$ represents an arbitrary bead in the sequence of the closed chain and the sum is performed over consecutive neighbors in any of the two possible directions along the chain. Figure 5.13 shows the behavior of such parameter for three examples of filament structures formed by 1, 3 and 5 loops. It is notably evident the correspondence between the number of loops in the structure and the number of maxima, or *peaks*, in $M(k)$. Therefore, by simply counting the number of peaks in $M(k)$ along the whole domain of k, one obtains a rather good estimation of the number of loops present in the structure. The process can be easily automatized by using an adequate peak detection algorithm.

Figure 5.14 shows the smoothed normalized histograms of number of loops, $P(n)$, found in adsorbed structures with the previous method for some representative cases with $N = 100$ and $\kappa = 10$. On the one hand, Figure 5.14(a) corresponds to a fixed low temperature, $T = 0.25$, and three values of the dipole intensity. For $\mu^2 = 1$ the open structures ($P(n) = 0$) are still significant, but the most probable morphology is formed by a single closed loop. As the dipole intensity increases, the most probable structures have a higher number of loops. On the other hand, Figure 5.14(b) shows the same parameter for a fixed dipole intensity, $\mu^2 = 6$, and three values of temperature. In this case, the most
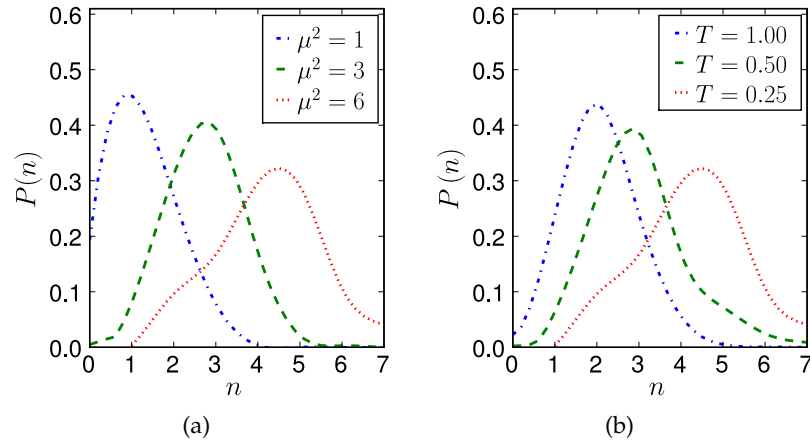
Figure 5.14: Normalized histograms for the mean number of loops calculated from the accumulated magnetization along the chain: (a) for $T = 0.25$ and different values of the dipolar constant; (b) for $\mu^2 = 6$ and different values of temperature.

probable number of loops clearly decreases with the increasing temperature. Therefore, it has been statistically confirmed that the number of loops in closed adsorbed structures tends to increase with the magnetic strength and decrease with temperature.

5.3 Discussion and concluding remarks

The equilibrium properties in the adsorption of stiff magnetic filaments close to an attractive flat surface has been studied thoroughly via extensive Langevin Dynamics simulations, with a particular attention to the effects of the magnetic interactions and the eventual differences that such interactions may lead with respect to analogous non magnetic systems. In general, common modeling strategies for the study of adsorption processes of non magnetic polymers have been adopted, introducing new specific characterization parameters only when needed.

A new coarse-grained model for magnetic filaments has been developed for this numerical study. In this model, magnetic filaments are represented by a bead-spring chain, with a point magnetic dipole of a given intensity located at the center of each bead. Excluded volume interactions are represented by a soft-core repulsive potential, whereas a radial, finitely extensible nonlinear elastic potential keeps bonded the first nearest neighbors in the chain and a bending potential models the bond stiffness. The dipoles are able to change their orientation independently from the bonds.

The numerical experiments evidence two main relevant phenomena within the range of parameters explored for the adsorption of a single filament onto the attractive surface: on the one hand, magnetic interactions have an additive effect on the adsorption continuous phase transition —extensively studied for magnetic polymers— which is analogous to the role played by the chain stiffness. On the other hand, the filaments already adsorbed may experience a structural transition between two very different morphologies as the system temperature is changed. This novel second transition, which is absent in non magnetic systems, also exhibits indications of criticality and allows the calculation of critical transition temperatures.

By combining the results obtained for both transitions, a representation of the structural phase diagram of a magnetic filament in a perfect solvent and close to an attractive surface has been presented for the first time. The phase diagram is limited to moderate values of temperatures, chain stiffness and dipole intensities.

The dominant mechanisms and resulting morphologies observed as the system temperature is changed can be summarized as follows. At relatively high temperatures, thermal fluctuations are the most significant mechanism in the system and the filaments remain unadsorbed, showing the shape of a self-avoiding random coil and a mostly random distribution of their dipoles orientations. In general, under this conditions the total magnetization of the chain is small but not zero.

As the temperature is decreased, the filament is more likely to have some segment adsorbed onto the attractive surface. The dipoles adopt soon a high alignment with the chain backbone, in a head to tail arrangement with their first nearest neighbors, by reducing their magnetic energy towards a local minimum. This behavior is consistent with such observed experimentally for the non bonded magnetic colloids that conform ferrofluids. In fact, the local arrangement of the dipoles, associated to a small reduction in the chain configurational entropy, necessarily modifies the self-avoiding random coil structures leading to more stretched morphologies. Therefore, the local ordering of the dipoles contributes to increase the effective chain stiffness and, consequently, to increase the radius of gyration, the end-to-end distance and the net chain magnetization.

As is well known for non magnetic polymers, the chain stiffness favors the adsorption process on a flat surface at higher temperatures due to the lower reduction in entropy needed to lay onto a plane by a stretched structure with respect to a random coil morphology. Consequently, the adsorption temperature increases with the dipole intensity, as well as with the chain stiffness. Interestingly, it has been reported for the first time the

existence of an unexpected strong correlation between the transition temperatures and the equilibrium point of two structural parameters, known as trains and tails, characteristic of the adsorption process of chains on flat surfaces. The nature of this correlation has not been formally established, but the following interpretation is suggested for future studies: under the simulation conditions of this study, the statistics for trains and tails is expected to capture the residence times of the chain into the adsorbed and the unadsorbed states, respectively. From the basis of such assumption, the identification bewteen the trains–tails equilibrium point and the transition temperature becomes evident. Finally, the asymptotic scaling behavior of the continuous adsorption transition has not been found to be essentially affected by the presence of the magnetic interactions.

At some temperature below the adsorption transition, dipoles are almost perfectly aligned with a very smooth and rather stretched chain backbone, thus they are not able to further reduce the configurational entropy by simple local rearrangements. Consequently, long range magnetic interactions become significant, leading to the closure transition of the chain and reducing the net magnetization to near zero. As pointed previously, this closure transition also exhibits indications of a critical behavior, for which a phenomenological characterization, based on the scaling properties of the end-to-end distance parameter, has been provided. The use of a structural parameter instead of any component of the system energy is justified by the fact that the differences between the configurational energies of the open and closed adsorbed structures is very small. This suggest that the nature of the closure transition could be essentially entropic.

The closure transition is also consistent with a presumably tendency expected from planar arrangements of magnetic dipoles to form single ring structures, which are known to be the ground state of two-dimensional ferrofluid systems. In this transition, the end-to-end distance shows an almost perfectly qualitative equivalence with the component of the magnetization parallel to the surface plane. However, as the temperature is reduced or the dipole intensity is increased, the closed adsorbed structure tends to be formed for an increasing number of closed loops which also minimize locally their net magnetization. Superficially, this could be understood as a contradictory result with respect to the previously noted behavior of formation of single rings expected from ferrofluids close to the ground state. However, magnetic filaments involve not only the magnetic interactions but the chain bonds, with a radial and an orientational components, as well as a given fixed chain length for every case. Therefore, the geometrical constrains imposed by different competing interactions and finite size effects in this system are expected to

be much more complex and is very hard to anticipate what could be its true ground state. Moreover, it seems quite reasonable to expect very different ground state conformations depending on the system parameters. In any case, the calculation of ground state conformations for this system falls outside the practical capabilities of simple Langevin Dynamics simulations.

Besides the range of parameters thoroughly explored, the system is also expected to exhibit even more interesting behaviors. For instance, at very low temperatures and high values of the dipole intensity, the numerical experiments show indications that magnetic interactions can become strong enough to compete with the chain stiffness and the adsorption potential to bring closer dipoles which are far away in the chain sequence, leading to nonplanar compact adsorbed structures. Thus, the phase diagram of magnetic filaments near an attractive flat surface is expected to be enriched with new phases, such as partially adsorbed globular structures.

6 Conclusions summary

In this Thesis, the relevant structural properties and transitions observed in two different clases of mesoscopic systems of interest in nanotechnological applications have been studied: thin solid films grown by physical vapor deposition and synthetic magnetic filaments. Both studies have been mainly carried out by means of extensive numerical simulations. In spite of the differences in the specific atomistic simulation models and techniques that have been used for each kind of system, both studies rely on the same basis of a common coarse-grained modeling perspective and a theoretical background based on the concepts of minimal physical modeling, criticality and phase transitions applied at the mesoscopic scale.

Effects of coordination on thin films mesoscopic morpholgy transitions

The non-equilibrium growth of thin films has been approached using the kinetic Monte Carlo simulation method with a novel coarse-grained atomistic simulation model. In particular, the model incorporates a novel flexible scheme for the arbitrary definition of the bonding symmetries led by the nature of the deposited material. In order to determine the effects of the microstructure maximum coordination number on the universal mesoscopic morphologies of thin solid films grown under simple deposition conditions, different (1+1) and (2+1)-dimensional abstract microstructures have been considered. The simplest Structure Zone Model, that describes qualitatively the mesoscopic morphologies of thin films obtained from simple physical vapor deposition processes, has been used as the main experimental refersence for the simulation results.

The simulation model and their approximations have been initially verified by analyzing the scaling behavior of the surface kinetic roughening of films grown under low adatom mobility conditions. As expected, the scaling behavior corresponding to the Ballistic Deposition model has been reproduced. As an additional result, it has been found that microstructure coordination number has no significant effects on the universal aspects of the Structure Zone Model.

The model of this Thesis also reproduces the essential experimental mechanisms of

selection of crystalline textures imposed by the substrate microstructure under epitaxial growth regimes, i.e., under relatively high adatom mobility conditions.

From the simulations, a strong evidence have been found for a behavior analogous to an equilibrium continuous phase transition of the changes in the thin film morfologies obtained in the steady, non-equilibrium growth regime as the deposition parameters are varied. Specifically, the equilibrium transition-like behavior has been evidenced for film characteristic morphologies at the border from structure Zone I to structure Zone II as the substrate temperature is increased. This analogy with equilibrium structural transitions has been used in general as the main analysis approach during this study.

The effects of the different microstructures have been characterized by means of an accurate statistical analysis of two non-extensive structural parameters, taken as order parameters for the continuous structural transition: the mean packing density and the mean coordination number. The simulation results show that the maximum coordination number of the microstructure has no significant effect on the transition point of the structural transition. This transition point is determined from the fluctuations maxima of the main packing density and is considered as the boundary between structure Zones I and II. This novel criterium for the determination of a structure zones boundary is suggested as a more consistent method than those proposed by previous studies.

The independence of the structure zones boundary with respect to the microstructure
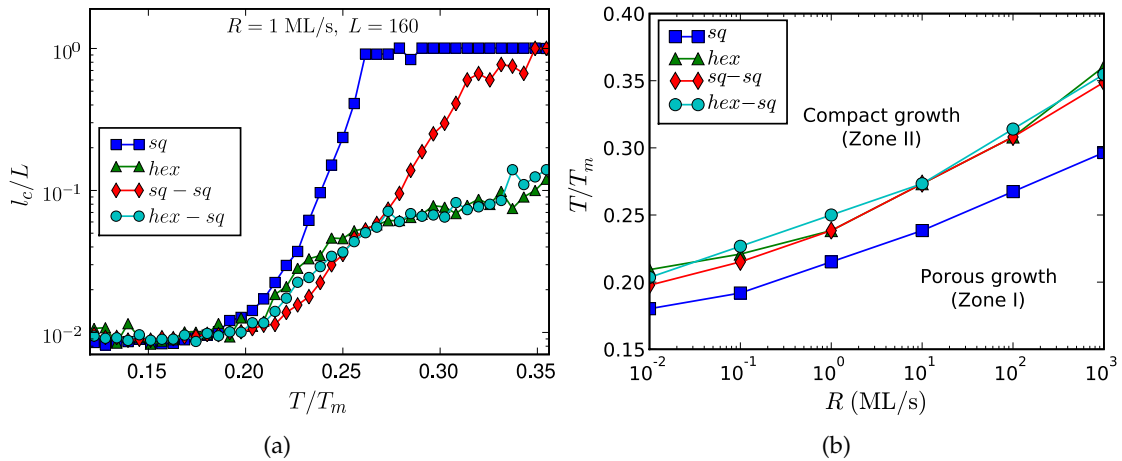
Figure 6.1: (a) Relative mean lateral width of the compact film structures as a function of the reduced substrate temperature for every (1+1)-dimensional bonding symmetry. (b) Phase diagram for the structure Zone I and Zone II for each (1+1)-dimensional microstructure.

is consistent with the experimental robustness observed in experiments for the Structure Zone models, specially with respect to the deposited materials. However, a quantitative dependence with the maximum coordination number is effectively observed in the vicinity of the boundary between structure zones, either for (1+1) and (2+1)-dimensional microstructures. In particular, this dependence is clearly observed in the behavior of the order parameters, as well as in the mean characteristic size of the compact, column-like crystalline substructures which conform the film for substrate temperatures close to the transition point, as illustrated in Figure 6.1(a): at high substrate temperatures —above the transition point— the size of such crystalline substructures tends to be larger for bonding symmetries with lower maximum coordination number, whereas at low substrate temperatures —below the transition point— the formation of crystalline substructures takes place at lower temperatures for the microstructures with a higher maximum coordination number.

On the other hand, the simulation results show that a non local change in the dynamic mechanisms of growth has a strong impact on the boundaries bewteen structure zones, as shown in Figure 6.1(b). More interestingly, the formation of non competing columnar structures has been observed in the simulated films without the inclusion of any explicit interlayer diffussion barrier in the model. Such behavior is explained by indirect dynamical constrains introduced by the interplay between the microstructure and epitaxial effects, and is found to be consistent with very recent experiments where the existence of implicit interlayer diffussion barriers induced by purely dynamical effects has been reported.

Altogether, these results provide a consistent picture of either the essential mechanisms of thin film growth and the relationship between the mesoscopic bulk morphologies and the deposition parameters, as well as an indication of the influence of the maximum coordination number of the system bonding symmetry on such morphologies. In particular, the growth regimes in which the microstructure of the deposited material can be highly significant for the resulting mesoscopic morphologies of the films have been characterized. Also, these results are expected to provide some useful coarse-grained modeling approaches to novel thin film systems.

Transitions of semiflexible magnetic filaments near an attratctive surface

In the second class of mesoscopic systems, the equilibrium structural behavior of synthetic magnetic filaments near to an attractive flat surface as the system temperature

is changed has been studied by means of extensive Langevin Dynamics simulations. The work constitutes the first study of equilibrium structural properties of this type of novel mesoscopic systems. For this purpose, a simple coarse-grained atomistic model —which includes long ranged magnetic dipolar interactions, excluded volume effects and stiffness— has been introduced. In general, the analysis of the simulation results has been based on an adaptation of well tested statistical analysis developed in the field of polymer physics.

The simulations have been performed for moderate values of the system parameters —the temperature, the chain length and the intensity of the magnetic dipoles— assuming the conditions of infinite dilution in a perfect solvent. Three phases with very different structural characteristics and two corresponding structural phase transitions have been identified at these moderate values of the parameters.

At high temperatures, the magnetic chain remains desorbed and exhibits the shape of a self-avoiding random coil, with the magnetic dipoles highly disordered. As the temperature is decreased, the adsorption of the filament onto the attractive surface begins to take place. At the same time, the dipoles tend to adopt a locally ordered head-to-tail conformation aligned with the chain backbone, increasing the total stiffness of the chain. As a consequence, the chain tends to globally adopt more stretched conformations, reducing its conformational entropy with respect to the non-magnetic case. Consequently, the adsorption process —which is the first equilibrium continous phase transition— is observed at higher temperatures as the intensity of the magnetic dipoles is increased and a higher local ordering of the dipoles is obtained.

The adsorption transition has been mainly characterized by a statistical analysis of the finite size and critical scaling behaviors of the adsorption energy. The simulations show that the same scaling exponents than the ones corresponding to non-magnetic, non-ideal homopolymers are obtained for the adsorption transition of magnetic filaments. This result reinforces the interpretation that, during the adsorption process, the magnetic interactions act just as a local stretching factor, leading to an effective enhancement of the chain stiffness. Another analysis based on the statistics of occurrences for the different types of chain structures found during the adsorption process —loops, trains and tails— has been also performed. This analysis shows a high correlation between the adsorption transition point and the temperature at which the mean numbers of trains and tails are the same. This alternative method for the estimation of the transition temperature has been found to require less statistics than the analysis of the adsorption energy fluctuations.

As the temperature is decreased below the adsorption transition point, the chain tends to remain adsorbed, displaying an increasing alignment of the dipoles with the chain backbone as well as smother and more stretched global conformations. However, at some characteristic low temperature —once the dipoles are almost perfectly aligned with the chain backbone— this tendency to stretch is reverted and the chain experiences a closure transition, leading to chain structures that tend to be formed by one or more closed two-dimensional smooth loops. This second structural transition is explained as a consequence of the long-ranged magnetic interactions that tend to minimize the magnetic energy globally, once the magnetic energy have been locally minimized by the alignment of the dipoles. The transition has been characterized by analyzing the finite size statistics of a structural parameter, the end-to-end distance, shown in Figure 6.2(a). Due to the high alignment of the dipoles with the chain backbone, such parameter has been found to be equivalent to the total magnetization of the chain. The analysis of the end-to-end distance has provided an estimation of the critical temperatures for this second transition, allowing the construction of an approximate phase diagram, shown in Figure 6.2(b), for the range of parameters explored.
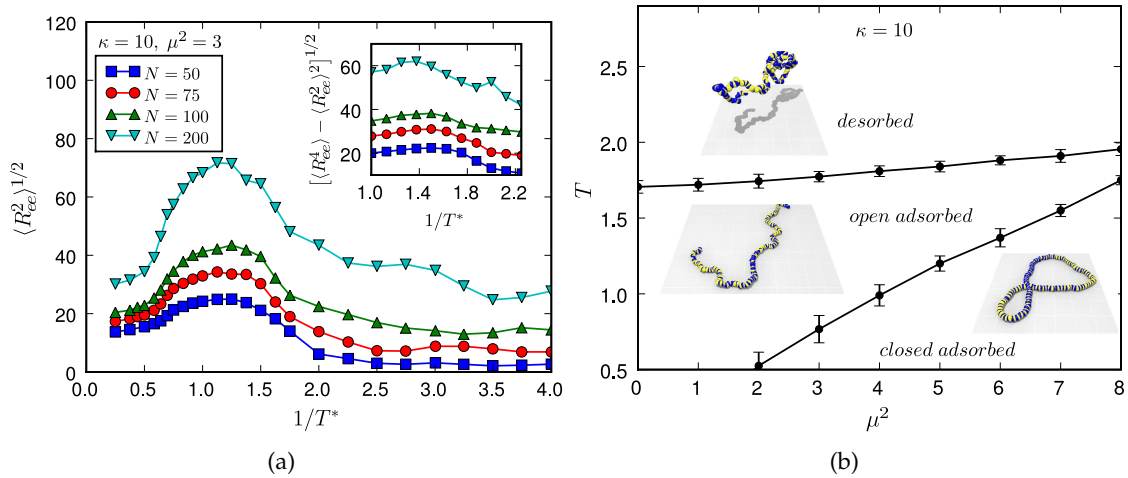
Figure 6.2: (a) Evolution of the end-to-end distance and its fluctuations (inset figure) of a magnetic filament with different lengths near to an attractive surface as a function of the system inverse temperature. (b) Representation of the corresponding configurational phase diagram obtained for moderate values of the magnetic dipoles.

As observed for the adsorption transition, the intensity of the magnetic dipoles favors the closure transition at higher temperatures. More interestingly, within the range of parameters studied, the number of closed loops forming the chain structure tends to

increase with the magnetic intensity and with the inverse temperature.

Even if it was not thoroughly studied in this Thesis, an indication of an even more complex behavior which may take place at higher values of the magnetic dipolar intensity has been obtained. In particular, for streghts of the magnetic interaction high enough compared to the stiffness and the adsorption potentials, the two-dimensional looped chain structure may collapse into a compact, partially desorbed globule structure in which dipoles far away in the chain sequence come into close contact. Moreover, further new phases are expected to arise from the interplay of extreme values of the parameters.

As a final concluding remark, this study has been intended to be a first step towards the adequate mesoscopic modeling and understanding of the behavior of magnetic filaments near attractive surfaces. Some interesting aspects of such novel systems have been determined from these numerical simulations but, as one can expect from any relevant early study on an almost unexplored system, many more new questions have arisen. Hopefully, such novel questions will be the central subject of future work.

Bibliography

[1] R. Feynman, There is plenty of room at the bottom, in *Miniaturization*, edited by H. D. Gilbert, New York, 1961, Reinhold Publishing Corp.

[2] N. Taniguchi, On the Basic Concept of 'Nano-Technology', in *Proc. Intl. Conf. Prod. London, Part II*, British Society of Precision Engineering, 1974.

[3] E. L. Wolf, *Nanophysics and Nanotechnology: An Introduction to Modern Concepts in Nanoscience*, John Wiley & Sons, 2004.

[4] P. Papon, J. Leblond, and P. H. E. Meijer, *The physics of phase transitions. Concepts and applications*, Springer, 2006.

[5] J. M. Lehn, J. M. Lehn, and B. Lehn, *Supramolecular Chemistry: Concepts And Perspectives*, VCH Verlag, 1996.

[6] P. Meakin, *Fractals, Scaling and Growth Far from Equilibrium*, Cambridge University Press, 1998.

[7] M. Kleman and O. D. Lavrentovich, *Soft Matter Physics: An Introduction*, Springer-Verlag, 2003.

[8] C. Bustamante, J. Liphardt, and F. Ritort, The Nonequilibrium Thermodynamics of Small Systems, Phys Today **58**(7), 43–48 (2005).

[9] R. A. L. Jones, *Soft Condensed Matter*, Oxford University Press, 2002.

[10] L. D. Landau and E. M. Lifshitz, *Statistical Physics*, volume 5 of *Course of Theoretical Physics*, Pergamon Press, 1980.

[11] C. Tsallis, *Introduction to Nonextensive Statistical Mechanics*, Springer, 2009.

[12] M. E. Fisher, The theory of equilibrium critical phenomena, Rep Prog Phys **30**(2), 615 (1967).

[13] E. H. Stanley, *Introduction to phase transitions and critical phenomena*, Oxford University Press, 1971.

[14] G. Lebon, D. Jou, and J. Casa-Vázquez, *Understading Non-equilibrium Thermodynamics*, Springer-Verlag, 2008.

[15] A.-L. Barabási and H. E. Stanley, *Fractal concepts in surface growth*, Cambridge University Press, 1995.

[16] G. Ódor, Universality classes in nonequilibrium lattice systems, Rev Mod Phys **76**(3), 663–724 (2004).

[17] M. Henkel, H. Hinrichsen, and S. Lübeck, *Non-equilibrium phase transitions*, Springer, 2008.

[18] K. A. Takeuchi, M. Kuroda, H. Chaté, and M. Sano, Experimental realization of directed percolation criticality in turbulent liquid crystals, Phys Rev E **80**(5), 051116 (Nov 2009).

[19] N. Metropolis, A. W. Rosenbluth, M. N. Rosenbluth, A. H. Teller, and E. Teller, Equation of state calculations by fast computing machines, J Chem Phys **21**(6), 1087–1092 (1953).

[20] E. Fermi, J. Pasta, and S. Ulam, Studies of nonlinear problems. I, Technical Report LA-1940, Los Alamos, 1955.

[21] B. J. Alder and T. E. Wainwright, Phase Transition for a Hard Sphere System, J Chem Phys **27**(5), 1208–1209 (1957).

[22] B. J. Alder and T. E. Wainwright, Studies in Molecular Dynamics. I. General Method, J Chem Phys **31**(2), 459–466 (1959).

[23] J. B. Gibson, A. N. Goland, M. Milgram, and G. H. Vineyard, Dynamics of Radiation Damage, Phys Rev **120**(4), 1229–1253 (1960).

[24] A. Rahman, Correlations in the Motion of Atoms in Liquid Argon, Phys Rev **136**(2A), A405–A411 (Oct 1964).

[25] L. Verlet, Computer "Experiments" on Classical Fluids. I. Thermodynamical Properties of Lennard-Jones Molecules, Phys Rev **159**(1), 98 (Jul 1967).

[26] D. C. Rapaport, *The art of molecular dynamics simulation*, Cambridge University Press, second edition, 2004.

[27] J. E. Jones, On the Determination of Molecular Fields. II. From the Equation of State of a Gas, Proc R Soc Lon Ser-A **106**(738), 463–477 (1924).

[28] D. Frenkel and B. Smit, *Understanding molecular simulation*, Academic Press, 2002.

[29] T. Schlick, *Molecular Modeling and Simulation*, Springer, 2nd edition, 2010.

[30] M. P. Allen and D. J. Tildesley, *Computer Simulation of Liquids*, Oxford Science Publications, Clarendon Press, Oxford, 1 edition, 1987.

[31] R. Kubo, The fluctuation-dissipation theorem, Reports on Progress in Physics **29**(1), 255 (1966).

[32] N. Metropolis, "The Beginning of Monte Carlo Method", Los Alamos Science **15**, 125–130 (1987).

[33] N. Metropolis and S. Ulam, The Monte Carlo method, J Am Stat Assoc **44**(247), 335—-341 (1949).

[34] D. Cox and H. Miller, *The Theory of Stochastic Processes*, Methuen, London, 1965.

[35] W. M. Young and E. W. Elcock, Monte Carlo studies of vacancy migration in binary ordered alloys: I, Proc Phys Soc **89**(3), 735 (1966).

[36] A. B. Bortz, M. H. Kalos, and J. L. Lebowitz, A new algorithm for Monte Carlo simulation of Ising spin systems, Journal of Computational Physics **17**(1), 10–18 (1975).

[37] D. T. Gillespie, A general method for numerically simulating the stochastic time evolution of coupled chemical reactions, J Comput Phys **22**(4), 403–434 (1976).

[38] A. F. Voter, Introduction to the Kinetic Monte Carlo Method, in *Radiation Effects in Solids*, edited by K. E. Sickafus, E. A. Kotomin, and B. P. Uberuaga, volume 235 of *NATO Science Series*, pages 1–23, Springer Netherlands, 2007.

[39] P. A. Maksym, Fast Monte Carlo simulation of MBE growth, Semicond Sci Tech **3**(6), 594 (1988).

[40] T. P. Schulze, Kinetic Monte Carlo simulations with minimal searching, Phys Rev E **65**(3), 036704 (Feb 2002).

[41] J. L. Blue, I. Beichl, and F. Sullivan, Faster Monte Carlo simulations, Phys Rev E **51**(2), R867–R868 (1995).

[42] K. N. Strafford, *Surface Engineering: processes and applications*, CRC Press, 1995.

[43] M. Ohring, *The Materials Science of Thin Films*, Academic Press, second edition, 2002.

[44] D. M. Mattox, *The foundations of vacuum coating technology*, Noyes / William Andrew Publishing, 2003.

[45] W. R. Grove, On the electro-chemical polarity of gases, Phil Trans R Soc Lond **142**, 87–101 (1852).

[46] M. Faraday, Experimental relations of gold (and other metals) to light, Phil Trans R Soc Lond **147**, 145–181 (1857).

[47] J. E. Greene, Transitioning from the art to the science of thin films: 1964 to 2003, Journal of Vacuum Science & Technology A: Vacuum, Surfaces, and Films **21**(5), S71–S73 (2003).

[48] B. A. Movchan and A. V. Demchishin, Study of structure and properties of thick vacuum condensates of Nickel, Titanium, Tungsten, aluminium oxide and Zirconium dioxide, Phys Met Metallogr+ **28**(4), 83–88 (1969).

[49] J. A. Thornton, Influence of apparatus geometry and deposition conditions on the structure and topography of thick sputtered coatings, J Vac Sci Technol **11**(4), 666–670 (1974).

[50] J. A. Thornton, High Rate Thick Film Growth, Annu Rev Mater Sci **7**(1), 239–260 (1977).

[51] G. H. Gilmer and P. Bennema, Simulation of Crystal Growth with Surface Diffusion, Journal of Applied Physics **43**(4), 1347–1360 (1972).

[52] D. Henderson, M. H. Brodsky, and P. Chaudhari, Simulation of structural anisotropy and void formation in amorphous thin films, Appl Phys Lett **25**(11), 641–643 (1974).

[53] A. G. Dirks and H. J. Leamy, Columnar microstructure in vapor-deposited thin films, Thin Solid Films **47**(3), 219–233 (1977).

[54] A. Elshabini-Riad and F. D. Barlow, *Thin Film Technology Handbook*, McGraw-Hill, 1998.

[55] *European White Book on Fundamental Research in Materials Science*, Max Planck Institute for Metals Research, 2001.

[56] K. Wasa, M. Kitabatake, and H. Adachi, *Thin Film Materials Technology: Sputtering of Compound Materials*, William Andrew Publishing, 2004.

[57] L. B. Freund and S. Suresh, *Thin Film Materials*, Cambridge University Press, 2004.

[58] R. Messier, A. P. Giri, and R. A. Roy, Revised structure zone model for thin film physical structure, J Vac Sci Technol A **2**(2), 500–503 (1984).

[59] P. B. Barna and M. Adamik, Fundamental structure forming phenomena of polycrystalline films and the structure zone models, Thin Solid Films **317**(1-2), 27–33 (1998).

[60] C. V. Thompson, Structure evolution during processing of polycrystalline films, Annu Rev Mater Sci **30**(1), 159–190 (2000).

[61] S. Mahieu, P. Ghekiere, D. Depla, and R. D. Gryse, Biaxial alignment in sputter deposited thin films, Thin Solid Films **515**(4), 1229–1249 (2006).

[62] T. Halpin-Healy and Y.-C. Zhang, Kinetic roughening phenomena, stochastic growth, directed polymers and all that. Aspects of multidisciplinary statistical mechanics, Phys Rep **254**(4–6), 215–414 (1995).

[63] P. J. Langley and J. Hulliger, Nanoporous and mesoporous organic structures: new openings for materials research, Chem Soc Rev **28**(5), 279–291 (1999).

[64] J. R. Levine, J. B. Cohen, Y. W. Chung, and P. Georgopoulos, Grazing-incidence small-angle X-ray scattering: new tool for studying thin film growth, Journal of Applied Crystallography **22**(6), 528–532 (Dec 1989).

[65] S. M. Rossnagel, Thin film deposition with physical vapor deposition and related technologies, J Vac Sci Technol A **21**(5), S74–S87 (2003).

[66] D. B. Chrisey, *Pulsed laser deposition of thin films*, John Wiley & Sons, 1994.

[67] I. G. Brown, Cathodic arc deposition of films, Annu Rev Mater Sci **28**, 243–269 (1998).

[68] D. M. Dobkin and M. K. Zuraw, *Principles of Chemical Vapor Deposition*, Springer, 2003.

[69] F. J. Arlinghaus, J. G. Gay, and J. R. Smith, Self-consistent local-orbital calculation of the surface electronic structure of Ni (100), Phys Rev B **21**(6), 2055–2059 (Mar 1980).

[70] E. Joos, H. D. Zeha, C. Kiefer, D. Giulini, J. Kupsch, and I.-O. Stamatescu, *Decoherence and the appearance of a classical world in quantum theory*, Springer, Berlin, 2003.

[71] L. Abelmann and C. Lodder, Oblique evaporation and surface diffusion, Thin Solid Films **305**, 1–21 (1997).

[72] K. Robbie and M. J. Brett, Sculptured thin films and glancing angle deposition: Growth mechanics and applications, J Vac Sci Technol A **15**(3), 1460–1465 (1997).

[73] R. Messier, V. C. Venugopal, and P. D. Sunal, Origin and evolution of sculptured thin films, J Vac Sci Technol A **18**(4), 1538–1545 (2000).

[74] A. Lakhtakia and R. F. Messier, *Sculptured Thin Films: Nanoengineered Morphology and Optics*, SPIE Press, 2005.

[75] D. Vick, T. Smy, and M. J. Brett, Growth behavior of evaporated porous thin films, J Mat Res **17**(11), 2904–2911 (2002).

[76] M. A. Morris, M. Bowker, and D. A. King, *Chemical kinetics*, volume 19, chapter 1, pages 1–163, Elsevier, 1984.

[77] H. J. Kreuzer, Theory of surface processes, Surf Sci **231**, 213–226 (1990).

[78] A. Fick, On liquid diffusion, Phil Mag **10**, 30 (1885).

[79] D. Llera-Hurlburt, A. S. Dalton, and E. G. Seebauer, Temperature-dependent surface diffusion parameters on amorphous materials, Surf Sci **504**, 244–252 (2002).

[80] R. G. Parr and W. Yang, *Density-functional theory of atoms and molecules*, Oxford University Press, 1994.

[81] K. Oura, V. Lifshits, A. Saranin, A. Zotov, and M. Katayama, *Surface Science: An Introduction*, Springer, Berlin, 2003.

[82] G. Antczak and G. Ehrlich, Jump processes in surface diffusion, Surf Sci Rep **62**(2), 39–61 (2007).

[83] A. Dalton and E. Seebauer, An improved theory for temperature-dependent Arrhenius parameters in mesoscale surface diffusion, Surf Sci **601**(3), 728–734 (2007).

[84] X. D. Zhu, A. Lee, A. Wong, and U. Linke, Surface diffusion of hydrogen on Ni(100): An experimental observation of quantum tunneling diffusion, Phys Rev Lett **68**(12), 1862–1865 (1992).

[85] J. A. Venables, G. D. T. Spiller, and M. Hanbucken, Nucleation and growth of thin films, Rep Prog Phys **47**(4), 399–459 (1984).

[86] C. Ratsch and J. A. Venables, Nucleation theory and the early stages of thin film growth, J Vac Sci Technol A **21**(5), S96–S109 (2003).

[87] M. C. Bartelt and J. W. Evans, Scaling analysis of diffusion-mediated island growth in surface adsorption processes, Phys Rev B **46**(19), 12675–12687 (1992).

[88] J. W. Evans and M. C. Bartelt, Nucleation, adatom capture, and island size distributions: Unified scaling analysis for submonolayer deposition, Phys Rev B **63**(23), 235408 (2001).

[89] J. W. Evans, P. A. Thiel, and M. C. Bartelt, Morphological evolution during epitaxial thin film growth: Formation of 2D islands and 3D mounds, Surf Sci Rep **61**(1–2), 1–128 (2006).

[90] T. Michely, M. Hohage, M. Bott, and G. Comsa, Inversion of growth speed anisotropy in two dimensions, Phys Rev Lett **70**(25), 3943–3946 (1993).

[91] G. Ehrlich and F. G. Hudda, Atomic View of Surface Self-Diffusion: Tungsten on Tungsten, J Chem Phys **44**(3), 1039–1049 (1966).

[92] R. L. Schwoebel, Step Motion on Crystal Surfaces. II, J Appl Phys **40**(2), 614–618 (1969).

[93] V. A. Shchukin, N. N. Ledentsov, and D. Bimberg, *Epitaxy of Nanostructures*, Springer, 2004.

[94] M. A. Herman, H. Sitter, and W. Richter, *Epitaxy: Physical Principles and Technical Implementation*, Springer, 2004.

[95] E. Bauer, Phänomenologische Theorie der Kristallabscheidung an Oberflächen. I, Z Kristallogr **110**, 372–394 (1958).

[96] C.-h. Chiu, Z. Huang, and C. T. Poh, Formation of Nanostructures by the Activated Stranski-Krastanow Transition Method, Phys Rev Lett **93**(13), 136105 (Sep 2004).

[97] H. J. Leamy, G. H. Gilmer, and A. G. Dirks, The Microstructure of Vapor-Deposited Thin Films, in *Current Topics in Materials Science*, volume 6, pages 309–344, North Holland Publishing Company, 1981.

[98] P. Politi, G. Grenet, A. Marty, A. Ponchet, and J. Villain, Instabilities in crystal growth by atomic or molecular beams, Physics Reports **324**(5-6), 271 – 404 (2000).

[99] R. Messier and J. E. Yehoda, Geometry of thin-film morphology, J Appl Phys **58**(10), 3739–3746 (1985).

[100] J. A. Thornton, Influence of substrate temperature and deposition rate on structure of thick sputtered Cu coatings, J Vac Sci Technol **12**(4), 830–835 (1975).

[101] R. Messier, Toward quantification of thin film morphology, J Vac Sci Technol A **4**(3), 490–495 (1986).

[102] I. Petrov, P. B. Barna, L. Hultman, and J. E. Greene, Microstructural evolution during film growth, J Vac Sci Technol A **21**(5), S117–S128 (2003).

[103] M. Haïdopoulos, F. Mirabella, M. Horgnies, C. Volcke, P. Thiry, P. Rouxhet, and J.-J. Pireaux, Morphology of polystyrene films deposited by RF plasma, Journal of Microscopy **228**(2), 227–239 (2007).

[104] J. H. E. Cartwright, B. Escribano, O. Piro, C. I. Sainz-Diaz, P. A. Sanchez, and T. Sintes, Ice Film Morphologies and the Structure Zone Model, in *Complex Systems: 5th International Workshop on Complex Systems*, edited by M. Tokuyama, I. Oppenheim, and H. Nishiyama, volume 982 of *AIP Conference Progceedings*, pages 696–701, AIP, 2008.

[105] F. Family and T. Vicsek, Scaling of the active zone in the Eden process on percolation networks and the ballistic deposition model, J Phys A-Mat Gen **18**(2), L75–L81 (1985).

[106] J. Krug, Origins of scale invariance in growth processes, Adv Phys **46**(2), 139–282 (1997).

[107] W. E. Hagston and H. Ketterl, Growth models and the question of universality classes, Phys Rev E **59**(3), 2699–2706 (Mar 1999).

[108] S.-C. Park and J.-M. Park, Universality classification of restricted solid-on-solid type surface growth models, Phys Rev E **67**(1), 010103 (2003).

[109] A. Mazor, D. J. Srolovitz, P. S. Hagan, and B. G. Bukiet, Columnar growth in thin films, Phys Rev Lett **60**(5), 424–427 (Feb 1988).

[110] J. G. Amar and F. Family, Phase transition in a restricted solid-on-solid surface-growth model in 2+1 dimensions, Phys Rev Lett **64**(5), 543–546 (Jan 1990).

[111] C. Roland and H. Guo, Interface growth with a shadow instability, Phys Rev Lett **66**(16), 2104–2107 (Apr 1991).

[112] R. Cuerno and L. Vazquez, Universality issues in surface kinetic roughening of thin solid films, in *Advances in Condensed Matter and Statistical Mechanics*, edited by E. Korutcheva and R. Cuerno, Nova Science Publishers, New York, 2004.

[113] R. Cuerno, M. Castro, J. Munoz-García, R. Gago, and L. Vázquez, Universal non-equilibrium phenomena at submicrometric surfaces and interfaces, Eur Phys J-Spec Top **146**, 427–441 (2007).

[114] J. D. Weeks and G. H. Gilmer, *Dynamics of crystal Growth*, volume 40 of *Advances in Chemical Physics*, chapter 4, pages 157–228, Wiley, 1979.

[115] J. S. Langer, Instabilities and pattern formation in crystal growth, Rev Mod Phys **52**(1), 1–28 (1980).

[116] M. Kotrla, Numerical simulations in the theory of crystal growth, Comput Phys Commun **97**(1-2), 82–100 (1996).

[117] H. N. G. Wadley, X. Zhou, R. A. Johnson, and M. Neurock, Mechanisms, models and methods of vapor deposition, Prog Mater Sci **46**(3-4), 329–377 (2001).

[118] K.-H. Müller, Ion-beam-induced epitaxial vapor-phase growth: A molecular-dynamics study, Phys Rev B **35**(15), 7906–7913 (1987).

[119] M. Schneider, A. Rahman, and I. K. Schuller, Epitaxial growth of thin films studied by molecular dynamics simulation, Superlattice Microst **7**(1), 39–46 (1990).

[120] R. W. Smith and D. J. Srolovitz, Void formation during film growth: A molecular dynamics simulation study, J Appl Phys **79**(3), 1448–1457 (1996).

[121] T.-H. Fang, W.-J. Chang, C.-M. Lin, and W.-C. Lien, Molecular dynamics and experimental studies on deposition mechanisms of ion beam sputtering, Appl Surf Sci **254**(11), 3436–3441 (2008).

[122] A. C. Levi and M. Kotrla, Theory and simulation of crystal growth, J Phys-Condens Mat **9**(2), 299–344 (1997).

[123] M. Eden, A Two-dimensional Growth Process, in *Proceedings of the Fourth Berkeley Symposium on Mathematical Statistics and Probability*, volume 4, pages 223–239, University of California Press, 1961.

[124] T. A. Witten and L. M. Sander, Diffusion-Limited Aggregation, a Kinetic Critical Phenomenon, Phys Rev Lett **47**(19), 1400–1403 (1981).

[125] J. W. Evans, Random-deposition models for thin-film epitaxial growth, Phys Rev B **39**(9), 5655–5664 (Mar 1989).

[126] R. P. U. Karunasiri, R. Bruinsma, and J. Rudnick, Thin-Film Growth and the Shadow Instability, Phys Rev Lett **62**(7), 788–791 (Feb 1989).

[127] M. R. W. and, Scaling in a solid-on-solid model of epitaxial growth, Phys Rev B **46**(19), 12896 (1992).

[128] M. J. Vold, A numerical approach to the problem of sediment volume, J Coll Sci **14**(2), 168–174 (1959).

[129] M. J. Vold, Sediment Volume and Structure in Dispersions of Anisometric Particles, The Journal of Physical Chemistry **63**(10), 1608–1612 (1959).

[130] P. Meakin, P. Ramanlal, L. M. Sander, and R. C. Ball, Ballistic deposition on surfaces, Phys Rev A **34**(6), 5091–5103 (Dec 1986).

[131] R. Baiod, D. Kessler, P. Ramanlal, L. Sander, and R. Savit, Dynamical scaling of the surface of finite-density ballistic aggregation, Phys Rev A **38**(7), 3672–3679 (Oct 1988).

[132] J. Krug and P. Meakin, Microstructure and surface scaling in ballistic deposition at oblique incidence, Phys Rev A **40**(4), 2064–2077 (Aug 1989).

[133] R. A. Outlaw and J. H. Heinbockel, A potential energy scaling Monte Carlo simulation of thin film nucleation and growth, Thin Solid Films **108**(1), 79–86 (1983).

[134] H. Huang and G. Gilmer, Multi-lattice Monte Carlo model of thin films, J Comput-Aided Mater **6**, 117–127 (1999), 10.1023/A:1008722515055.

[135] H. Huang and G. H. Gilmer, Atomistic simulation of texture competition during thin film deposition, J Comput-Aided Mater **7**(3), 203–216 (2001).

[136] W. Cavalcanti, M. Santos, and W. Figueiredo, Random deposition model of particles with discrete orientations, Physica A **322**, 467–476 (2003).

[137] R. Hrach, Simulation of thin film growth, International Journal of Electronics **69**(1), 55–64 (1990).

[138] G. S. Bales and D. C. Chrzan, Dynamics of irreversible island growth during submonolayer epitaxy, Phys Rev B **50**(9), 6057–6067 (1994).

[139] R. Messier, The nano-world of thin films, J Nanophotonics **2**, 021995 (2008).

[140] S. F. Edwards and D. R. Wilkinson, The Surface Statistics of a Granular Aggregate, Proc Roy Soc London A **381**(1780), 17–31 (1982).

[141] M. Kardar, G. Parisi, and Y.-C. Zhang, Dynamic Scaling of Growing Interfaces, Phys Rev Lettedward **56**(9), 889–892 (1986).

[142] M. Plischke, Z. Rácz, and D. Liu, Time-reversal invariance and universality of two-dimensional growth models, Phys Rev B **35**(7), 3485–3495 (1987).

[143] J. M. Kim and J. M. Kosterlitz, Growth in a restricted solid-on-solid model, Phys Rev Lett **62**(19), 2289–2292 (1989).

[144] Z. Racz, M. Siegert, and M. Plischke, Surface-Diffusion Induced Instabilities, in *Surface Disordering: Growth, Roughening and Phase Transitions*, edited by R. JUllien, J. Kertész, P. Meakin, and D. Wolf, pages 39–44, Nova Science, 1992.

[145] D. D. Vvedensky, A. Zangwill, C. N. Luse, and M. R. Wilby, Stochastic equations of motion for epitaxial growth, Phys Rev E **48**(2), 852–862 (Aug 1993).

[146] E. Katzav, S. F. Edwards, and M. Schwartz, Structure below the growing surface, Europhys Lett **75**(1), 29–35 (2006).

[147] F. A. Silveira and F. D. A. A. Reis, Surface and bulk properties of deposits grown with a bidisperse ballistic deposition model, Phys Rev E **75**, 061608 (2007).

[148] G. Hu, J. Huang, G. Orkoulas, and P. D. Christofides, Investigation of film surface roughness and porosity dependence on lattice size in a porous thin film deposition process, Phys Rev E **80**(4), 041122 (Oct 2009).

[149] G. H. Gilmer, H. Huang, T. D. de la Rubia, J. D. Torre, and F. Baumann, Lattice Monte Carlo models of thin film deposition, Thin Solid Films **365**(2), 189–200 (April 2000).

[150] H. Huang and L. Zhou, Atomistic simulator of polycrystalline thin film deposition in three dimensions, J Comput-Aided Mater **11**, 59–74 (2005).

[151] K.-H. Müller, Dependence of thin-film microstructure on deposition rate by means of a computer simulation, J Appl Phys **58**(7), 2573–2576 (1985).

[152] K.-H. Müller, A computer model for postdeposition annealing of porous thin films, J Vac Sci Technol A **3**(6), 2089–2092 (1985).

[153] Y. G. Yang, R. A. Johnson, and H. N. G. Wadley, A Monte Carlo simulation of the physical vapor deposition of nickel, Acta Mater **45**(4), 1455–1468 (1997).

[154] H. Savaloni and M. G. Shahraki, A computer model for the growth of thin films in a structure zone model, Nanotechnology **15**(3), 311–319 (2004).

[155] J. Cho, S. G. Terry, R. LeSar, and C. Levi, A kinetic Monte Carlo simulation of film growth by physical vapor deposition on rotating substrates, Mater Sci Eng A **391**(1-2), 390–401 (January 2005).

[156] M. G. Shahraki and H. Savaloni, Thin-film-growth characteristics by computer simulation: Nanostructural changes as a function of deposition conditions, Phys Stat Sol B **244**(9), 3115–3136 (2007).

[157] G. Neumann and W. Hirschwald, Mechanisms of surface self-diffusion, Z Phys Chem B **81**, 163 (1972).

[158] Y. Shim and J. G. Amar, Rigorous synchronous relaxation algorithm for parallel kinetic Monte Carlo simulations of thin film growth, Phys Rev B **71**(11), 115436 (Mar 2005).

[159] Y. Shim and J. G. Amar, Semirigorous synchronous sublattice algorithm for parallel kinetic Monte Carlo simulations of thin film growth, Phys Rev B **71**(12), 125432 (Mar 2005).

[160] Y. Shim and J. G. Amar, Hybrid asynchronous algorithm for parallel kinetic Monte Carlo simulations of thin film growth, J Comput Phys **212**(1), 305–317 (2006).

[161] M. de Berg, O. Cheong, M. van Kreveld, and M. Overmars, *Computational Geometry: Algorithms and Applications*, Springer, 3rd edition, 2008.

[162] B. Stroustrup, *The C++ Programming Language*, Addison-Wesley, 1997.

[163] R. Ganapathy, M. R. Buckley, S. J. Gerbode, and I. Cohen, Direct Measurements of Island Growth and Step-Edge Barriers in Colloidal Epitaxy, Science **327**(5964), 445–448 (2010).

[164] S. Bellini, Su di un particolare comportamento di batteri d'acqua dolce, Technical report, Istituto di Microbiologia dell'Universitá di Pavia, 1963.

[165] S. Bellini, Ulteriori studi sui 'batteri magnetosensibili', Technical report, Istituto di Microbiologia dell'Universitá di Pavia, 1963.

[166] R. P. Blakemore, Magnetotactic bacteria, Science **190**(4212), 377–379 (1975).

[167] D. Schüler, The biomineralization of magnetosomes in 'Magnetospirillum gryphiswaldense', Int Microbiol **5**, 209–214 (2002).

[168] A. Kobayashi, J. L. Kirschvink, C. Z. Nash, R. E. Kopp, D. A. Sauer, L. E. Bertani, W. F. Voorhout, and T. Taguchi, Experimental observation of magnetosome chain collapse in magnetotactic bacteria: Sedimentological, paleomagnetic, and evolutionary implications, Earth and Planetary Science Letters **245**(3-4), 538–550 (2006).

[169] A. Komeili, Z. Li, D. K. Newman, and G. J. Jensen, Magnetosomes Are Cell Membrane Invaginations Organized by the Actin-Like Protein MamK, Science **311**(5758), 242–245 (2006).

[170] R. B. Frankel, R. P. Blakemore, and R. S. Wolfe, Magnetite in Freshwater Magnetic Bacteria, Science **203**, 1355–1357 (1979).

[171] J. J. Benkoski, S. E. Bowles, R. L. Jones, J. F. Douglas, J. Pyun, and A. Karim, Self-assembly of polymer-coated ferromagnetic nanoparticles into mesoscopic polymer chains, J Polym Sci, Part B: Polym Phy **46**(20), 2267–2277 (2008).

[172] E. F. DeLong, R. B. Frankel, and D. A. Bazylinski, Multiple Evolutionary Origins of Magnetotaxis in Bacteria, Science **259**, 803–806 (1993).

[173] C. P. McKay, E. I. Friedmann, R. B. Frankel, and D. A. Bazylinski, Magnetotactic bacteria on Earth and Mars, Astrobiology **3**, 263–270 (2003).

[174] D. A. Bazylinski and R. B. Frankel, Magnetic iron oxide and iron sulfide minerals within microorganisms: potential biomarkers, in *Biomineralization*, edited by E. Baeuerlein, pages 17–43, Weinheim, Germany, 2004, Wiley-VCH.

[175] M. Kamachi, Magnetic polymers, J Macromol Sci-Pol R **C42**(4), 541–561 (2002).

[176] S. J. Blundell and F. L. Pratt, Organic and molecular magnets, J Phys-Condens Mat **16**, R771–R828 (2004).

[177] M. Cavallini, M. Facchini, C. Albonetti, and F. Biscarini, Single molecule magnets: from thin films to nano-patterns, Phys Chem Chem Phys **10**(6), 784–793 (2008).

[178] C. Lang and D. Schüler, Biomineralization of magnetosomes in bacteria: Nanoparticles with potential applications, in *Microbial bionanotechnology: Biological self-assembly systems and biopolymer-based nanostructures*, edited by B. H. A. Rehm, pages 107–124, Wymondham, 2006, Horizon Bioscience.

[179] A.-H. Lu, E. Salabas, and F. Schüth, Magnetic Nanoparticles: Synthesis, Protection, Functionalization, and Application, Angew Chem Int Edit **46**(8), 1222–1244 (2007).

[180] M. A. Vergés, R. Costo, A. G. Roca, J. F. Marco, G. F. Goya, C. J. Serna, and M. P. Morales, Uniform and water stable magnetite nanoparticles with diameters around the monodomain–multidomain limit, J Phys D Appl Phys **41**(13), 134003 (2008).

[181] A. G. Roca, R. Costo, A. F. Rebolledo, S. Veintemillas-Verdaguer, P. Tartaj, T. González-Carreño, M. P. Morales, and C. J. Serna, Progress in the preparation of magnetic nanoparticles for applications in biomedicine, J Phys D Appl Phys **42**(22), 224002 (2009).

[182] J. Liu, Ferromagnetic nanoparticles: Synthesis, processing, and characterization, JOM-J Min Met Mat S **62**, 56–61 (2010).

[183] B. D. Cullity and C. D. Graham, *Introduction to magnetic materials*, Wiley/IEEE Press, 2nd edition, 2009.

[184] E. M. Furst, C. Suzuki, M. Fermigier, and A. P. Gast, Permanently Linked Monodisperse Paramagnetic Chains, Langmuir **14**(26), 7334–7336 (1998).

[185] E. M. Furst and A. P. Gast, Micromechanics of Dipolar Chains Using Optical Tweezers, Phys Rev Lett **82**(20), 4130–4133 (May 1999).

[186] R. Dreyfus, J. Baudry, M. L. Roper, M. Fermigier, H. A. Stone, and J. Bibette, Microscopic artificial swimmers, Nature **437**(7060), 862–865 (2005).

[187] O. Tabata, H. Kojima, T. Kasatani, Y. Isono, and R. Yoshida, Chemo-mechanical actuator using self-oscillating gel for artificial cilia, in *Proceedings IEEE Sixteenth Annual International Conference on Micro Electro Mechanical Systems*, pages 12–15, jan. 2003.

[188] H. Singh, P. E. Laibinis, and T. A. Hatton, Synthesis of Flexible Magnetic Nanowires of Permanently Linked Core–Shell Magnetic Beads Tethered to a Glass Surface Patterned by Microcontact Printing, Nano Lett **5**(11), 2149–2154 (2005).

[189] H. Singh, P. E. Laibinis, and T. A. Hatton, Rigid, Superparamagnetic Chains of Permanently Linked Beads Coated with Magnetic Nanoparticles. Synthesis and Rotational Dynamics under Applied Magnetic Fields, Langmuir **21**(24), 11500–11509 (2005).

[190] J. J. Benkoski, H. Hu, and A. Karim, Generation of Hierarchical Topologies from Photocrosslinkable, Particle-Stabilized Emulsions, Macromol Rapid Commun **27**(15), 1212–1216 (2006).

[191] B. Y. Geng, J. Z. Ma, X. W. Liu, Q. B. Du, M. G. Kong, and L. D. Zhang, Hydrophilic polymer assisted synthesis of room-temperature ferromagnetic Fe[sub 3]O[sub 4] nanochains, Appl Phys Lett **90**(4), 043120 (2007).

[192] P. Y. Keng, I. Shim, B. D. Korth, J. F. Douglas, and J. Pyun, Synthesis and Self-Assembly of Polymer-Coated Ferromagnetic Nanoparticles, ACS Nano **1**(4), 279–292 (2007).

[193] S. E. Bowles, W. Wu, T. Kowalewski, M. C. Schalnat, R. J. Davis, J. E. Pemberton, I. Shim, B. D. Korth, and J. Pyun, Magnetic Assembly and Pyrolysis of Functional Ferromagnetic Colloids into One-Dimensional Carbon Nanostructures, J Am Chem Soc **129**(28), 8694–8695 (2007).

[194] J. J. Benkoski, S. E. Bowles, B. D. Korth, R. L. Jones, J. F. Douglas, A. Karim, and J. Pyun, Field Induced Formation of Mesoscopic Polymer Chains from Functional Ferromagnetic Colloids, J Am Chem Soc **129**(19), 6291–6297 (May 2007).

[195] J. J. Benkoski, R. L. Jones, J. F. Douglas, and A. Karim, Photocurable Oil/Water Interfaces as a Universal Platform for 2-D Self-Assembly, Langmuir **23**(7), 3530–3537 (Mar. 2007).

[196] Z. Zhou, G. Liu, and D. Han, Coating and Structural Locking of Dipolar Chains of Cobalt Nanoparticles, ACS Nano **3**(1), 165–172 (2009).

[197] J. J. Benkoski, R. M. Deacon, H. B. Land, L. M. Baird, J. L. Breidenich, R. Srinivasan, G. V. Clatterbaugh, P. Y. Keng, and J. Pyun, Dipolar assembly of ferromagnetic nanoparticles into magnetically driven artificial cilia, Soft Matter **6**, 602–609 (2010).

[198] Y. Wang, A. E. DePrince, S. K. Gray, X.-M. Lin, and M. Pelton, Solvent-Mediated End-to-End Assembly of Gold Nanorods, The Journal of Physical Chemistry Letters **1**(18), 2692–2698 (2010).

[199] T. Garel, H. Orland, and E. Orlandini, Phase diagram of magnetic polymers, Eur Phys J B **12**(2), 261–268 (1999).

[200] S. L. Biswal and A. P. Gast, Mechanics of semiflexible chains formed by poly(ethylene glycol)-linked paramagnetic particles, Phys Rev E **68**(2), 021402 (Aug 2003).

[201] M.-B. Luo, Finite-size scaling analysis on the phase transition of a ferromagnetic polymer chain model, J Chem Phys **124**(3), 034903 (2006).

[202] M.-B. Luo and C. Qian, Short-time Monte Carlo study on the phase transition of a ferromagnetic polymer chain model, Polymer **47**(4), 1451–1455 (2006).

[203] K. Ērglis, D. Zhulenkovs, A. Sharipo, and A. Cēbers, Elastic properties of DNA linked flexible magnetic filaments, J Phys-Condens Mat **20**(20), 204107 (2008).

[204] K. Ērglis, L. Alberte, and A. Cēbers, Thermal fluctuations of non-motile magnetotactic bacteria in AC magnetic fields, Magnetohydrodynamics **44**(3), 223–236 (2008).

[205] A. Cēbers and I. Javaitis, Dynamics of a flexible magnetic chain in a rotating magnetic field, Phys Rev E **69**(2), 021404 (Feb 2004).

[206] A. Cēbers, Flexible magnetic filaments, Curr Opin Colloid Interface Sci **10**(3-4), 167–175 (2005).

[207] M. Belovs and A. Cēbers, Ferromagnetic microswimmer, Phys Rev E **79**(5), 051503 (May 2009).

[208] M. Belovs, T. Cīrulis, and A. Cēbers, Equilibrium shapes of twisted magnetic filaments, J Phys A: Math Theor **42**(23), 235206 (2009).

[209] G. Kirchhoff, Über das Gleichgewicht und die Bewegungen eines unendlichdünnen Stabes, J Reine Angew Math **56**, 285–313 (1859).

[210] P. Villaggio, *Mathematical models for elastic structures*, Cambridge University Press, 1997.

[211] M. Doi, *Introduction to Polymer Physics*, Oxford University Press, 1996.

[212] A. Y. Grosberg and A. R. Khokhlov, *Statistical Physics of Macromolecules*, AIP Press, 1994.

[213] M. A. Moore, Theory of the polymer coil-globule transition, J Phys A-Math Gen **10**(2), 305 (1977).

[214] B. M. Baysal and F. E. Karasz, Coil-Globule Collapse in Flexible Macromolecules, Macromol Theor Simul **12**(9), 627–646 (2003).

[215] P.-G. de Gennes, *Scaling Concepts in Polymer Physics*, Cornell University Press, 1979.

[216] M. Rubinstein and R. H. Colby, *Polymer Physics*, Oxford University Press, 2003.

[217] P. Debye, The Intrinsic Viscosity of Polymer Solutions, J Chem Phys **14**(10), 636–639 (1946).

[218] E. Eisenriegler, *Polymers near surfaces*, World Scientific, 1993.

[219] C. A. Croxton, The development of loops, trains, and tails in a self-avoiding polymer sequence at a rigid boundary as a function of solvent composition, Macromolecules **21**(1), 244–249 (1988).

[220] A. N. Semenov, Adsorption of a semiflexible wormlike chain, Eur Phys J E **9**(4), 353–363 (2002).

[221] S. Bhattacharya, V. G. Rostiashvili, A. Milchev, and T. A. Vilgis, Forced-Induced Desorption of a Polymer Chain Adsorbed on an Attractive Surface: Theory and Computer Experiment, Macromolecules **42**(6), 2236–2250 (2009).

[222] P. G. de Gennes, Scaling theory of polymer adsorption, J Phys France **37**(12), 1445–1452 (1976).

[223] P. G. de Gennes, Conformations of Polymers Attached to an Interface, Macromolecules **13**(5), 1069–1075 (Sept. 1980).

[224] H. W. Diehl and S. Dietrich, Field-theoretical approach to multicritical behavior near free surfaces, Phys Rev B **24**(5), 2878–2880 (Sep 1981).

[225] E. Eisenriegler, K. Kremer, and K. Binder, Adsorption of polymer chains at surfaces: Scaling and Monte Carlo analyses, J Chem Phys **77**(12), 6296–6320 (1982).

[226] H. Meirovitch and S. Livne, Computer simulation of long polymers adsorbed on a surface. II. Critical behavior of a single self-avoiding walk, J Chem Phys **88**(7), 4507–4515 (1988).

[227] R. Hegger and P. Grassberger, Chain polymers near an adsorbing surface, J Phys A-Math Gen **27**(12), 4069 (1994).

[228] P.-Y. Lai, Statics and dynamics of a polymer chain adsorbed on a surface: Monte Carlo simulation using the bond-fluctuation model, Phys Rev E **49**(6), 5420–5430 (Jun 1994).

[229] E. Y. Kramarenko, R. G. Winkler, P. G. Khalatur, A. R. Khokhlov, and P. Reineker, Molecular dynamics simulation study of adsorption of polymer chains with variable degree of rigidity. I. Static properties, J Chem Phys **104**(12), 4806–4813 (1996).

[230] J. de Joannis, C.-W. Park, J. Thomatos, and I. A. Bitsanis, Homopolymer Physisorption: A Monte Carlo Study, Langmuir **17**(1), 69–77 (Jan. 2001).

[231] J. de Joannis, R. K. Ballamudi, C.-W. Park, J. Thomatos, and I. A. Bitsanis, Scaling of homopolymers next to adsorbing surfaces: A Monte Carlo study, Europhys Lett **56**(2), 200–206 (oct 2001).

[232] S. Metzger, M. Müller, K. Binder, and J. Baschnagel, Adsorption Transition of a Polymer Chain at a Weakly Attractive Surface: Monte Carlo Simulation of Off-Lattice Models, Macromol Theor Simul **11**(9), 985–995 (2002).

[233] S. Metzger, M. Müller, K. Binder, and J. Baschnagel, Surface excess in dilute polymer solutions and the adsorption transition versus wetting phenomena, J Chem Phys **118**(9), 8489—-8499 (2003).

[234] R. Descas, J.-U. Sommer, and A. Blumen, Static and dynamic properties of tethered chains at adsorbing surfaces: A Monte Carlo study, J Chem Phys **120**, 8831 (2004).

[235] J. Bonet Avalos, A. D. Mackie, and S. Diez-Orrite, Comparison of the Importance Sampling Single Chain Mean Field Theory with Monte Carlo Simulation and Self-Consistent Field Calculations for Polymer Adsorption onto a Flat Wall, Macromolecules **37**(3), 1143–1151 (Feb. 2004).

[236] N. Källrot and P. Linse, Dynamic Study of Single-Chain Adsorption and Desorption, Macromolecules **40**(13), 4669–4679 (June 2007).

[237] E. J. J. van Rensburg and A. R. Rechnitzer, Multiple Markov chain Monte Carlo study of adsorbing self-avoiding walks in two and in three dimensions, J Phys A-Math Gen **37**(27), 6875 (2004).

[238] A. Chremos, E. Glynos, V. Koutsos, and P. J. Camp, Adsorption and self-assembly of linear polymers on surfaces: a computer simulation study, Soft Matter **5**, 637–645 (2009).

[239] A. Johner and J. F. Joanny, Polymer adsorption in a poor solvent, J Phys II France **1**(2), 181–194 (feb 1991).

[240] H. Liu and A. Chakrabarti, Molecular dynamics study of adsorption and spreading of a polymer chain onto a flat surface, Polymer **40**(26), 7285–7293 (1999).

[241] T. Vrbová and S. G. Whittington, Adsorption and collapse of self-avoiding walks and polygons in three dimensions, J Phys A-Math Gen **29**(19), 6253 (1996).

[242] T. Vrbová and S. G. Whittington, Adsorption and collapse of self-avoiding walks at a defect plane, J Phys A-Math Gen **31**(34), 7031 (1998).

[243] T. Vrbová and K. Procházka, Adsorption of self-avoiding walks at an impenetrable plane in the expanded phase: a Monte Carlo study, J Phys A-Math Gen **32**(29), 5469 (1999).

[244] Y. Singh, D. Giri, and S. Kumar, Crossover of a polymer chain from bulk to surface states, J Phys A-Math Gen **34**(8), L67–L74 (2001).

[245] R. Rajesh, D. Dhar, D. Giri, S. Kumar, and Y. Singh, Adsorption and collapse transitions in a linear polymer chain near an attractive wall, Phys Rev E **65**(5), 056124 (May 2002).

[246] P. K. Mishra, D. Giri, S. Kumar, and Y. Singh, Does a surface attached globule phase exist?, Physica A **318**(1-2), 171–178 (2003).

[247] J. Krawczyk, A. L. Owczarek, T. Prellberg, and A. Rechnitzer, Layering transitions for adsorbing polymers in poor solvents, Europhys Lett **70**(6), 726–732 (jun 2005).

[248] A. L. Owczarek, A. Rechnitzer, J. Krawczyk, and T. Prellberg, On the location of the surface-attached globule phase in collapsing polymers, J Phys A: Math Theor **40**(44), 13257 (2007).

[249] M. Bachmann and W. Janke, Conformational Transitions of Nongrafted Polymers near an Absorbing Substrate, Phys Rev Lett **95**(5), 058102 (Jul 2005).

[250] M. Bachmann and W. Janke, Substrate adhesion of a nongrafted flexible polymer in a cavity, Phys Rev E **73**(4), 041802 (Apr 2006).

[251] K. Sumithra, M. Brandau, and E. Straube, Adsorption and pinning of multiblock copolymers on chemically heterogeneous patterned surfaces, J Chem Phys **130**(23), 234901 (2009).

[252] A. R. Khokhlov, F. F. Ternovsky, and E. A. Zheligovskaya, Statistics of stiff polymer chains near an adsorbing surface, Makromol Chem-Theor **2**(2), 151–168 (1993).

[253] T. Sintes, K. Sumithra, and E. Straube, Adsorption of Semiflexible Polymers on Flat, Homogeneous Surfaces, Macromolecules **34**(5), 1352–1357 (Feb. 2001).

[254] J. J. Cerdà, T. Sintes, and K. Sumithra, Adsorption of semiflexible block copolymers on homogeneous surfaces, J Chem Phys **123**, 204703 (2005).

[255] J. J. Cerdà and T. Sintes, Stiff polymer adsorption. Onset to pattern recognition, Biophys Chem **115**(2-3), 277–283 (2005).

[256] J. Luettmer-Strathmann, F. Rampf, W. Paul, and K. Binder, Transitions of tethered polymer chains: A simulation study with the bond fluctuation lattice model, J Chem Phys **128**(6), 064903 (2008).

[257] V. A. Ivanov and J. A. Martemyanova, Monte Carlo Computer Simulation of a Single Semi-Flexible Macromolecule at a Plane Surface, Macromol Symp **252**(1), 12–23 (2007).

[258] V. A. Ivanov, J. A. Martemyanova, M. Müller, W. Paul, and K. Binder, Conformational Changes of a Single Semiflexible Macromolecule Near an Adsorbing Surface: A Monte Carlo Simulation†, J Phys Chem B **113**(12), 3653–3668 (Mar. 2009).

[259] M. Möddel, M. Bachmann, and W. Janke, Conformational Mechanics of Polymer Adsorption Transitions at Attractive Substrates, J Phys Chem B **113**(11), 3314–3323 (Mar. 2009).

[260] T. Vogel, M. Bachmann, and W. Janke, Freezing and collapse of flexible polymers on regular lattices in three dimensions, Phys Rev E **76**(6), 061803 (Dec 2007).

[261] A. V. Dobrynin, Theory and simulations of charged polymers: From solution properties to polymeric nanomaterials, Curr Opin Colloid Interface Sci **13**(6), 376–388 (2008).

[262] A. N. Rissanou, S. H. Anastasiadis, and I. A. Bitsanis, A Monte Carlo study of the coil-to-globule transition of model polymer chains near an attractive surface, J Polym Sci, Part B: Polym Phy **47**(24), 2462–2476 (2009).

[263] J. S. Klos, D. Romeis, and J.-U. Sommer, Adsorption of random copolymers from a melt onto a solid surface: Monte Carlo studies, J Chem Phys **132**(2), 024907 (2010).

[264] S. Kantorovich, J. J. Cerdà, and C. Holm, Microstructure analyisis of monodisperse ferrofluid monolayers: theory and simulation, Phys Chem Chem Phys **10**(14), 1883–1895 (2008).

[265] T. A. Prokopieva, V. A. Danilov, S. S. Kantorovich, and C. Holm, Ground state structures in ferrofluid monolayers, Phys Rev E **80**(3), 031404 (Sep 2009).

[266] J. D. Weeks, D. Chandler, and H. C. Andersen, Role of Repulsive Forces in Determining the Equilibrium Structure of Simple Liquids, J Chem Phys **54**(12), 5237–5247 (1971).

[267] A. Brulet, F. Boue, and J. Cotton, About the experimental determination of the persistence length of wormlike chains of polystyrene, J Phys II France **6**(6), 885–891 (June 1996).

[268] G. Beaucage, S. Rane, S. Sukumaran, M. Satkowski, L. Schechtman, and Y. Doi, Persistence length of isotactic poly(hydroxy butyrate), Macromolecules **30**(14), 4158–4162 (July 1997).

[269] E. Buhler and F. Boue, Persistence length for a model semirigid polyelectrolyte as seen by small angle neutron scattering: a relevant variation of the lower bound with ionic strength, Eur Phys J E **10**(2), 89–92 (Feb. 2003).

[270] F. F. Abraham and Y. Singh, The structure of a hard-sphere fluid in contact with a soft repulsive wall, J Chem Phys **67**(5), 2384–2385 (1977).

[271] J. J. Cerdà, S. Kantorovich, and C. Holm, Aggregate formation in ferrofluid monolayers: simulations and theory, J Phys-Condens Mat **20**, 204125 (2008).

[272] H. J. Limbach, A. Arnold, B. A. Mann, and C. Holm, ESPResSo – An Extensible Simulation Package for Research on Soft Matter Systems, Comput Phys Commun **174**(9), 704–727 (May 2006).

[273] J. J. Cerdà, V. Ballenegger, O. Lenz, and C. Holm, P3M algorithm for dipolar interactions, J Chem Phys **129**, 234104 (2008).

List of Figures

Curriculum Vitae

PERSONAL INFORMATION

Surnames	Sánchez Romero
Name	Pedro Antonio
ID number	43059274P
Date of birth	10/04/1973
Postal address	C/. Nuredduna 1, 6º A 07006 Palma de Mallorca (Spain)
Email address	pedroasr@gmail.com

CURRENT POSITION

Position	PhD student at the Instituto de Física Interdisciplinar y Sistemas Complejos, IFISC (UIB-CSIC). Beginning date: 01/01/2006.
Address	Campus UIB, Ctra. Valldemossa km 7,5 Ed. Instituts Universitaris, Office S07-5 07122 Palma de Mallorca (Spain)
Phone	(+34) 971 25 98 82
Fax	(+34) 971 17 32 48
Email address	pedro@ifisc.uib-csic.es

EDUCATION

15/10/2007	Master en Física (M.Sc in Physics), UIB.
12/07/2007	Especialista Universitari en Bioinformàtica (University Especialist in Bioinformatics), UIB.
08/04/2005	Curs d'Aptitud Pedagògica (Postgraduate Certificate in Education), UIB.
20/02/2004	Llicenciat en Física (spanish 5 years degree in Physics), UIB.

SCIENTIFIC AND TEACHING ACTIVITIES

2007–2010	Professor ajudant (graduate teaching assistant) at the Physics Department of the Universitat de les Illes Balears (UIB).
2006–2007	Research Formation Fellowship, HIELOCRIS project (CSIC), IMEDEA/UFI (UIB-CSIC).

PUBLICATIONS RELATED TO THIS THESIS

Journal Papers

1. P. A. Sánchez, T. Sintes, O. Piro, and J. H. E. Cartwright, Effects of microstructures on mesoscopic morphological transitions in deposition growth models, *Proc R Soc A-Math Phys Eng Sci* **465**(2112), 3875–3884 (2009).

2. P. A. Sánchez, T. Sintes, O. Piro, and J. H. E. Cartwright, Influence of microstructure on the transitions between mesoscopic thin-film morphologies in ballistic-diffusive models, *Phys Rev E* **81**, 011140 (2010).

3. P. A. Sánchez, J. J. Cerdà, V. Ballenegger, T. Sintes, O. Piro and C. Holm, Semiflexible magnetic filaments near attractive flat surfaces: a Langevin dynamics study, Accepted for publication in *Soft Matter* (2011). DOI: 10.1039/C0SM00772B

Proceedings

1. J. H. E. Cartwright, B. Escribano, O. Piro, C. I. Sainz-Diaz, P. A. Sanchez, and T. Sintes, Ice Film Morphologies and the Structure Zone Model, in *Complex Systems: 5th International Workshop on Complex Systems*, edited by M. Tokuyama, I. Oppenheim, and H. Nishiyama, volume 982 of *AIP Conference Progceedings*, pages 696–701, AIP, 2008.

OTHER PUBLICATIONS

Journal Papers

1. F. Marino, G. Catalán, P. Sánchez, S. Balle, and O. Piro, Thermo-Optical "Canard Orbits" and Excitable Limit Cycles, *Phys Rev Lett* **92**(7), 073901 (2004).

CONFERENCE CONTRIBUTIONS

1. Dynamical basis of the Structure Zone Model of thin solid films growth.
   XIV Congreso de Física Estadística FISES2006,
   Granada (Spain), September 2006.
   Poster.

2. Effects of microstructural symmetries on the morphology of thin solid films
   International Conference on Crystal Growth and Chemistry of Ice Thin Films under Extreme Conditions HIELOCRIS-2007.
   Maó (Spain), April 2007.
   Oral presentation.

3. Non-equilibrium phase transition between bulk structures in ballistic-diffusive stochastic models of thin film growth.
   XV Congreso de Física Estadística FisEs08.
   Salamanca (Spain), March 2008.
   Poster.

4. Two dimensional glassy water: searching for minimal models of LDA-HDA transitions.
XVI Congreso de Física Estadística FisEs09.
Huelva (Spain), September 2009.
Poster.

5. Adsorption and self-organization properties of stiff magnetic filaments.
Jülich Soft Matter Days 2009.
Bonn (Germany), November 2009.
Poster.

6. Effects of external magnetic fields on equilibrium properties of magnetic filaments.
International Soft Matter Conference 2010.
Granada (Spain), July 2010.
Poster.

RESEARCH STAYS ABROAD

17/06–17/07/2009   Institut für Computerphysik, ICP (Universität Stuttgart), Stuttgart (Germany). Under the supervision of Dr. Joan J. Cerdà and Dr. Christian Holm.

ORGANIZATION OF R&D ACTIVITIES

International conference on crystal growth and chemistry of ice thin films under extreme conditions HIELOCRIS 2007. Organization Committee.

OTHER PROFESSIONAL ACTIVITIES

2001–2005   Freelance software developer/IT consultant.

2000–2001   Computer programmer.

1992–2000   Services sector worker.